University of Stavanger

Faculty of Science and Technology

MASTER'S THESIS

Study program/ Specialization: Petroleum Geosciences Engineering	Spring semester, 2015 Open
Writer: Mona Wetrhus Minde	…… (Writer's signature)
Faculty supervisor: Dr Udo Zimmerman Co-supervisor(s): Prof Merete Vadla Madland	
Thesis title: Micro- and nano-applications to monitor the rock-fluid interaction in fractured chalk	
Credits (ECTS): 30	
Key words: Chalk Clay minerals Carbonate, Mg-rich carbonate Liège Fracture Scanning electron microscopy, FE-SEM Mineral Liberation Analyzer, MLA Secondary ion mass spectrometry, nanoSIMS	Pages: …… + enclosure: …… Stavanger, …….. Date/year

Micro- and nano-applications to monitor the rock-fluid interaction in fractured chalk

by

Mona Wetrhus Minde

MSc Thesis
Petroleum Geosciences Engineering
Presented to the Faculty of Science and Technology
The University of Stavanger
Norway

The University of Stavanger
June 2015

Acknowledgement

First, I would like to thank my two supervisors Dr Udo Zimmermann and Prof Merete Vadla Madland for guidance, encouragement, and inspiring and fruitful discussions. I am forever grateful for the recognition and opportunities I have been given and for faith they have had in me.

In need of acknowledgment is also Dr Megawati Megawati for performing the flooding experiment on this core, and for letting me use this chalk core for my thesis. Dr Tania Hildebrand-Habel has contributed to this work through supporting imaging of the core by FE-SEM and being a great teacher and support in SEM analyses together with Ingunn C. Oddsen.

Dr. Zimmermann has arranged for the possibility to go to Freiberg and Luxembourg for MLA and nanoSIMS studies. Without this, this thesis could not have been completed and I would like to thank Prof Bernhard Schultz at TU Bergakademie in Freiberg and Jean-Nicolas Audinot at the Luxembourg Institute of Science and Technology (LIST) for welcoming me so warmly and helping me with the analyses. In Freiberg, I received great help from Sabine Haser and Kai Bachmann, and in Luxembourg Patrick Grysan and Ester Lentzen were constantly at my side.

I would also like to extend thanks to Dr Reidar Inge Korsnes, Dr Anders Nermoen, and Prof Aksel Hiorth for valuable input, help and inspiring discussions on the subject.

I would like to recognize COREC and the national IOR centre of Stavanger for their support to this project.

At last, I would like to thank my family and friends, as well as IRIS AS for the support they have all given me.

Table of contents

List of figures

List of commonly used abbreviations

IOR – Improved Oil Recovery

EOR – Enhanced oil Recovery

OLM – Optical Light Microscopy

SEM – Scanning Electron Microscopy

SE – Secondary Electrons

BSE – Backscattered Electrons

EDS – Energy Dispersive system

MLA – Mineral Liberation Analyzer

SIMS – Secondary Ion Mass Spectrometry

AAN – Average Atomic Number

SSW – Synthetic Seawater

wt.% – Weight percent

Abstract

The aim of this project is to contribute to the research of improved oil recovery (IOR) through studying the formation of new mineral phases in a fractured Cretaceous onshore chalk core, flooded with synthetic seawater (SSW). An important aspect is to identify minerals present after flooding and to understand how the composition of the rock influences the fluid-flow inside the core, hence affecting the mechanical properties and compaction of chalk. To achieve this goal, a variety of state – of – the – art methods has been applied, which has contributed with different data sets. Two types of fractures have been produced in the core; a) an artificial fracture perpendicular to fluid-flow and b) an natural fracture parallel to fluid-flow. This study will discuss both of these.

The use of Mineral Liberation Analyzer (MLA) and Nano Secondary Ion Mass Spectrometry (NanoSIMS) shows that the texture of the chalk influences the fluid-flow throughout the core and manipulates fluid flow along the fractures.

Micro and nano-sized silicates and minute grains of Mg-rich carbonates most likely grow on larger micron-sized calcite crystals as well as precipitate in pore-space. The carbonates in the fracture show higher Mg and Si concentrations than those of the surrounding matrix. Remarkable is the observation that shell fragments from macrofossils, which are orientated perpendicular to the fluid flow, influences the rock-fluid interaction. In those areas, the chemo-mechanical reactions are disturbed and lead to a less homogeneous fluid character. This shows that fluid flow and flooding movements are, even in seemingly homogeneous rocks like chalk, strongly dependent on the texture, which reflects in this case the environmental conditions during deposition of the carbonate. This has, in turn, a significant effect on the distribution of mineral alteration, which happen during flooding, beyond doubt at micro-scale. If these effects are possible to upscale is out of the scope of this study, but should be an

important research goal for EOR investigation activities. Furthermore, the gain of knowledge of chemical and textural alterations, which occur during flooding with non-equilibrium brines, is important input when designing new experiments, in EOR-simulations, and further understanding of the geo-mechanical behaviour of chalk.

1 Introduction

1.1 Enhanced Oil Recovery (EOR)

According to the Norwegian Petroleum Directorate (NPD) the recovery factor for oil fields on the Norwegian Continental Shelf (NCS) was 46% at the end of 2014. A large amount of resources cannot be produced with the current technology or strategies, and the potential is enormous for creating large values through improving the recovery from these fields (Figure 1).

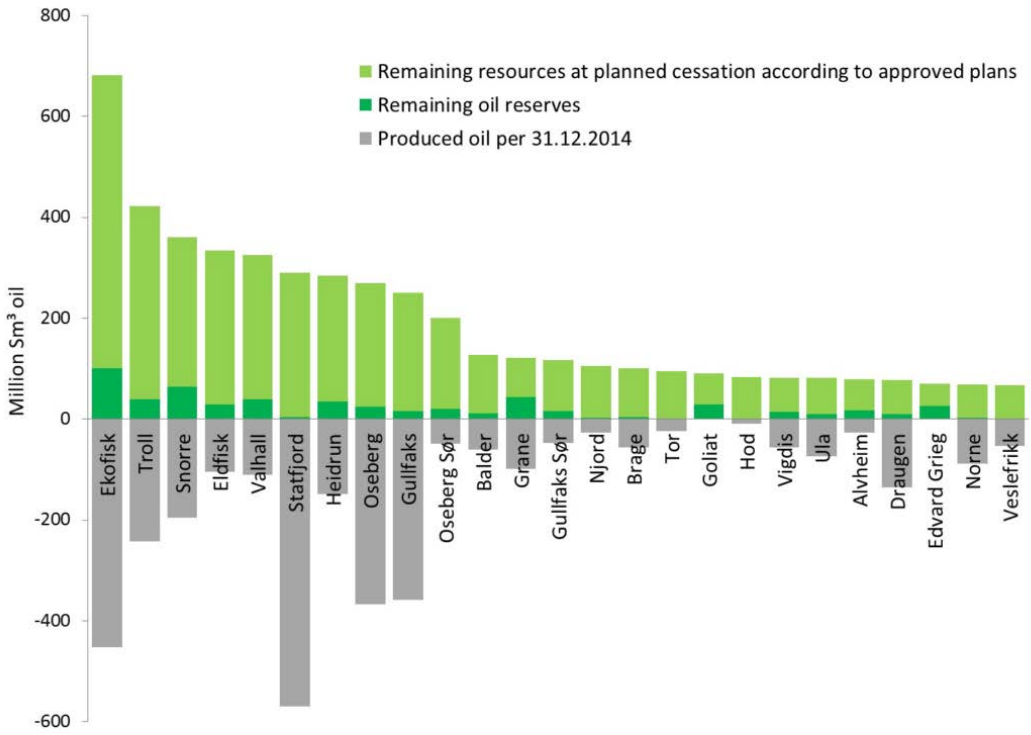

Figure 1. Produced oil and remaining reserves and resources in the NCS according to NPD at the end of 2014 (from www.npd.no)

The amount of oil which is possible to produce from a field varies depending on a number of factors, such as geological conditions and how the field is developed and produced. Improved Oil Recovery (IOR) is a process, which stimulates the production of oil from a reservoir through e.g. injection of water or gas. The definition of IOR has come to include any process that increases the recovery rate, including upgrades in production technology and Enhanced Oil Recovery (EOR).

EOR is, on the other hand, related to mobilization of what is categorized as immobile oil (Figure 2). This is oil which is trapped in the pores of reservoir rock and not possible to produce with conventional methods. Examples of EOR-methods are injection of fluids with specialized composition, polymers, surfactants and microbial EOR.

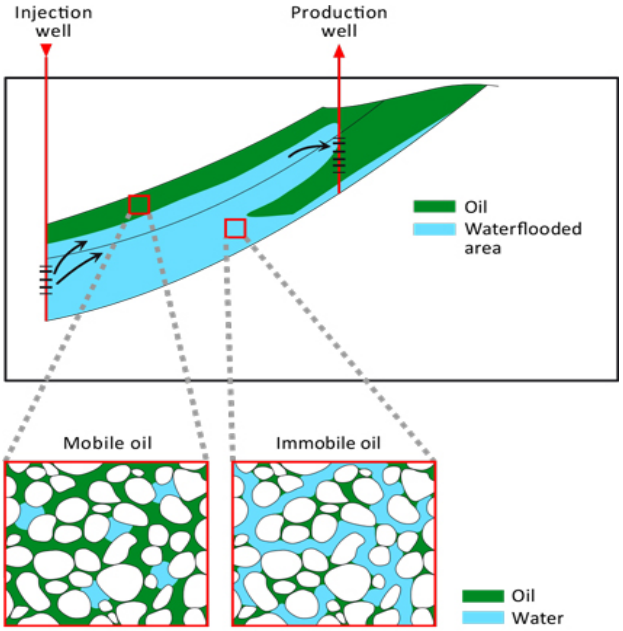

Figure 2. Mobile and immobile oil in a reservoir (from www.npd.no)

Water-injection is one of the methods used with great success to increase the recovery rate and maintain formation-pressure in the North Sea, where some of the major reservoirs are chalk-reservoirs. The composition of this water together with temperature seems to have an effect on oil recovery through chemical and mineralogical alteration as well as changes in mineral surface complexes, thus surface-charge and -potential of the rock ((Madland, et al., 2011); (Megawati, et al., 2012); (Hiorth, et al., 2013)). The composition of the rock has an influence on this interaction, but it might not be the most critical factor, though studies have shown that the silica-content may play an important role (Halleux, et al., 1985). The process of alteration is not clear, as there is no single model that precisely describes how much of this alteration is due to precipitation and dissolution, ion exchange, or changes in surface-charge; however, textural changes are observed ((Hiorth, et al., 2013); (Wang, In press)). Chemical

and textural alterations have shown to affect the mechanical strength of the rock, hence the compaction of chalk ((Risnes, 2001); (Risnes, et al., 2003); (Heggheim, et al., 2005); (Madland, 2005); (Korsnes, 2007); (Austad, et al., 2008); (Omdal, 2010); (Madland, et al., 2011); (Andersen, et al., 2012)). These changes also seem to affect the wetting properties of the rock, and as a consequence the production of oil.

In order to understand the processes of textural and chemical alteration, it is important to perform basic experiments to study the alteration in the rock due to fluid injection. This is an important part of a research field where characterization of reservoir chalk and analogue onshore chalks are essential steps. One of the main objectives of this research is to study in detail how the available onshore chalk is altered due to fluid injection and apply this knowledge to reservoir chalk. To be able to understand the changes on core- and field-scale, it is important to understand these alterations at pore-scale. The knowledge and data gathered in these experiments are used as input for models and computer simulations, which aim to predict how reservoirs may be produced to retrieve the maximum amount of oil (Evje & Hiorth, 2011). In addition, findings from flooding experiments may help designing new and better experiments as well as optimizing the water chemistry of the injected brine. In this way the study of mineralogical alterations due to flooding experiments are closely linked to EOR.

1.2 Objective

A large variety of experiments carried out on flooded chalk cores has led to a large dataset (e.g. (Risnes, et al., 2003); (Madland, 2005); (Heggheim, et al., 2005); (Austad, et al., 2008); (Puntervold & Austad, 2008); (Madland, et al., 2011); (Korsnes, et al., 2008)), and reveals an extraordinary complexity of reactions even though the mineralogy of the rock itself is rather simple. Previous projects have shown bulk alteration in flooded cores from nearly pure calcite chalk towards a magnesium-rich carbonate and precipitation of magnesite (e.g. (Madland, et al., 2011); (Zimmermann, et al., 2015); (Wang, In press); (Nermoen, et al., 2015)).

The objective of this study is to identify the different mineral phases formed during flooding and their location, at pore-scale, in fractured rock material. Do new minerals precipitate in all areas of the core, or are certain locations, such as the fractures, more favoured than others? This goes in hand with the thorough textural studies by the proposed applications to observe and understand the rock-fluid interaction and the fluid movements in chalk. In addition, the author aims to investigate how well the methods applied are suitable to resolve the objectives of this study. It should be noted that the flooding experiment itself is not performed by the author and is not considered to be part of this thesis.

The data is based on the following analytical methods: optical petrography, field emission scanning electron microscope (FE-SEM), energy-dispersive X-ray spectroscopy (EDS), mineral liberation analyzer (MLA) and nano secondary ion mass spectrometry (nanoSIMS). The use of MLA and nanoSIMS on chalk has only to a small extent been applied to chalk earlier, and the results of this study may therefore give new insight on how these methods may be used at best.

2 Theory

2.1 Chalk

Chalk is by definition a fine-grained, carbonate sedimentary rock, a pelagic sediment of mostly biogenic and authigenic character. Chalk is coloured white to grey and beige and has at large scale commonly a layered homogenous nature, due to its low-energy depositional environment. However, reworking of sediments is common. Syn- and post-depositional gravitational movement often give the chalk a more heterogeneous brecciated form, when tectonic movements allow for large faulted blocks where the chalk can be destabilized and move towards deeper basin (Kennedy, 1985).

The rock consists mainly of the remains from calcareous organisms, which thrive under warm climatic conditions. In chalk, these organisms include high abundances of coccolithophores, a planktonic algae, and foraminifera, an amoeba-like organism. Figure 3 shows a scanning electron microscopy (SEM) micrograph of typical chalk structure.

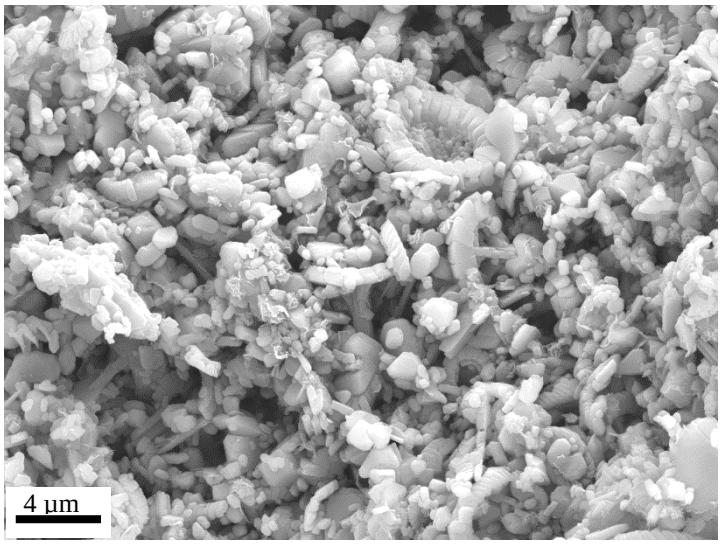

Figure 3. SEM micrograph of chalk sampled from Liège, Belgium

Coccolithophores often dismantle into their individual skeletal plates, coccoliths. The size of the coccolithophores is in the area of 10 µm and above, while individual coccolith rings range

between 0.3 and 5 µm (Hjuler & Fabricius, 2009), or even larger (Kennedy, 1985). Coccolith rings are built up of platelets or grains with sizes of one µm and below, and as coccolith rings degrade these platelets are often found in their individual forms (Figure 3). Foraminifera are much larger, ranging in size between 20 and 100s of µm. In addition, chalk often contains large amounts of shells and fragments from larger fossils like bivalves and gastropods. As the hard shells and skeletal debris from these organisms fall to the seafloor, they form calcareous ooze.

As oozes accumulates slowly, 1 to 6 cm per thousand year (Garrison, 2010), the deposition of the hundreds of meter thick layers of chalk, as found in the North Sea, takes millions of years. The rate is not only related to the accumulation of sediments, but also to the dissolution rate of calcareous material in the ocean water. Oozes rarely form below the carbon compensation depth (CCD), which is the depth where the dissolution rate equals or higher than the sedimentation rate. This depth usually lies around 4500 meters, depending on e.g. pH, temperature, and CO_2-concentration of the seawater (Garrison, 2010). As the micro-and nano-organisms are to a large extent preserved, the depositional depth of the chalk cannot be too deep. After deposition, burial and de-fluidization leads to compaction and lithification of the ooze, forming the fine-grained sedimentary rock chalk. During burial, the ooze is mechanically compacted leading to a porosity reduction from 60 – 80% to values usually between 35 – 50% (Hjuler & Fabricius, 2009).

Calcareous organisms prefer high temperatures, a lot of light and clean water. In colder climate, one often sees a shift to higher abundances of siliceous microorganisms. In calcareous ooze there is, however, a certain concentration of siliceous organisms. These may later due to diagenesis form nodules or layers of chert, microcrystalline quartz (Madsen, et al., 2010). In addition, clay-minerals are one of the major constituents of the non-carbonate

content of chalk, either from detrital origin during deposition or as an alteration product due to diagenesis.

During sedimentation, not only the skeletal remains of the organisms are deposited. In addition, organic material of the countless dead organisms accumulate, and may be preserved if anoxic conditions are present. During burial, diagenesis, and catagenesis, hydrocarbons may be generated from organic material.

The grain-size of the chalk is very small and permeability is low, often in the range between 1 to 5 mD (Sulak & Danielsen, 1989). The porosity is however, surprisingly high for such a fine-grained rock. This is possibly due to overpressure in the reservoir during burial or by early oil emplacement ((Risnes, 2001); (Monzurul Alam, et al., 2012)). Early oil emplacement also plays a role reducing diagenetic processes in the rock. The commonly high porosity of chalk enables accumulation of substantial amounts of hydrocarbons.

The Cretaceous was a period of exceptionally high sea level and temperatures and had the perfect climate for deposition of carbonates and chalk. In relation to the breakup of the supercontinent Pangea, continental spreading formed several intra-cratonic basins. During the Late Cretaceous, large areas of Northern Europe had been covered by a shallow sea, where the Central North Sea Graben formed a deeper marine environment (Molenaar & Zijlstra, 1997). This epi-continental sea had structural highs and lows. Coarser-grained carbonates were produced at shallower depth, while fine-grain coccolithic mudstones (chalk) were deposited in deeper areas (Molenaar & Zijlstra, 1997). Many large oil fields in the North Sea, such as the Ekofisk and Valhall fields, are chalk-reservoirs, where the main oil-bearing formations are of Late Cretaceous to Palaeocene age.

2.2 Fractures in chalk

Due to the exceptionally low permeability in high porosity chalk, fractures play an important role in fluid flow. Matrix permeability in the Ekofisk field lies in the range of 1 to 5 mD (Sulak & Danielsen, 1989). In addition, matrix permeability may be even further diminished by pore collapse due to increase in effective stress during depletion of the reservoir. This means that well production depends on a certain concentration of fractures to increase the effective permeability (Snow & Brownlee, 1989). The effective permeability in the Ekofisk field ranges between 1 to 100 mD (Sulak & Danielsen, 1989).

When injecting water into a chalk reservoir, the main fluid flow of the injected water will follow the fracture system, and not necessarily flow into the matrix itself. Most of the oil in chalk reservoirs is, however, trapped in the matrix (Korsnes, 2007). In fractured carbonate reservoirs, displacement of oil is mostly related to spontaneous imbibition of water into the matrix (Zhang, et al., 2007). Hence, it is important to understand how fractures in the reservoir behave during flooding and how to fully utilize the injected water to mobilize oil from the matrix and creating a more effective sweep.

2.3 Chalk and EOR

Why is EOR such an important issue for chalk? Because of the fine-grained nature of chalk, permeability is commonly low. Even though the porosity is high, grain-size, pores and pore-throats are small (Risnes, 2001). These factors increase the amount of immobile oil, and reduce the recovery from the reservoir. This leaves a huge potential for EOR.

Production from the chalk reservoir at the Ekofisk field started in 1971. Injection of seawater was introduced to maintain formation-pressure in the late the 1980s and to reduce compaction and subsidence of the seabed. The compaction-rate was reduced, but further compaction could

not be completely eliminated. This indicates, together with decades of experimental work, that the interplay between injected fluids and the chalk itself plays an important role in the mechanical behaviour of chalk ((Risnes, et al., 2003); (Madland, 2005); (Korsnes, 2007); (Madland, et al., 2008); (Omdal, 2010); (Madland, et al., 2011); (Hiorth, et al., 2013)). This is referred to as water weakening of chalk and this weakening or compaction has in chalk a positive impact on the production of oil through pressure depletion and oil mobilisation. As chalk has a high specific surface area, up to 10 times the value of sandstones, the injected water will interact with the rock over a much higher area, increasing the effect of the fluid-rock interaction and the fluid sensitivity of the rock (Heggheim, et al., 2005).

Spontaneous imbibition is an important IOR process in chalk, but may only take place if the chalk is water-wet (Yu, et al., 2009). The chemistry of the injected water is an important, if not a paramount factor, which influences the wetting condition of the chalk. An initially oil-wet chalk surface may alter wetting state to become more water-wet due to the injection of sulphate ions in the injected brine (Strand, et al., 2006). Due to normally high concentrations of Ca^{2+} cations in reservoir brine, the surface of chalk becomes positively charged, attracting negatively charged carboxylic materials present in crude oil with high acid number, hence chalk is often neutral to preferential oil-wet. The surface charge is strongly dependent on pH of the brine and the adsorbed ions (Megawati, et al., 2013). By injecting negatively charges sulphate ions, in favourable concentrations compared to Ca^{2+} cations and at elevated temperatures, it is possible to alter the positively charged chalk surface, "reversing the wetting conditions by desorption of carboxylic material" (Strand, et al., 2006, p. 2) towards preferential water-wet conditions, thus increasing the amount of recoverable oil.

Zhang et al. (2007) shows that Mg^{2+} ions also plays an important role in the surface charge of onshore chalk. It is therefore important to understand if, and then possibly, how these ions in turn alter the chalk with respects to mineralogy and texture. Processes such as dissolution and

precipitation of minerals and possible mobilization of fine-grained clay-minerals would also affect the equilibrium between the brine and the solid, thus affecting the surface charge of the rock. It is commonly found that through interaction with the injected water, calcite is dissolved. If this calcite is oil wet, such a process may also liberate the oil from the rock (Hiorth, et al., 2008). Another important aspect when discussing surface charge is how negatively charged sulphate ions may create a negatively charged chalk surface, which may exert a disjoining pressure between the calcite grains, leading to repulsive forces between the grains, hence reducing the mechanical strength of the chalk (Megawati, et al., 2013).

2.4 Geologic background of the chalk core

The chalk core, which has been the subject of this experiment, is from the Gulpen Formation taken from an outcrop near Liège in Belgium. The chalk is of Upper Cretaceous age, namely Late Campanian to Early Maastrichtian. In particular, this core is from the Zevenwegen Member, which is the lowermost member of the Gulpen Formation and of Late Campanian to early Maastrichtian age (Molenaar & Zijlstra, 1997).

The Gulpen Formation lies conformably on top of the Vaals Formation, which was formed in a coastal environment; hence, the transition from coastal to deeper marine facies may have been caused by transgressive processes. Covering the Gulpen Formation is the Maastrichtian Formation consisting of silt- and fine-sand-sized grainstones of bioclastic origin (Felder, 1975).

The chalk from the Liège outcrop has a very clean nature. The non-carbonate content is approximately 5 wt.% and consists of quartz, smectite/mixed smectite-illite layer, mica and clinoptilolite as well as apatite, feldspar, pyroxene and titanium oxide (Hjuler & Fabricius, 2009). The preservation of coccoliths and pore-space is medium and good, respectively. No

calcite cementation is observed, however contact cement is commonly found in studies on this type of chalk (Hjuler & Fabricius, 2009), pointing to a low degree of diagenesis.

As reservoir-chalk is very difficult and expensive to acquire, equivalents of onshore chalk is commonly used as analogues. Chalk from Liège has been found to resemble reservoir chalk with respect to composition and mechanical properties.

2.5 Mechanical properties of the chalk core

Before testing, porosity was measured to 40.1% and permeability 5 mD in the core. A fractured core was created to be used as study object. The core measures approximately 7 cm long and has a diameter near 3.8 cm (Figure 4). The core was fractured in two directions. About one third from the inlet of the core, the core was cut in two with a saw, perpendicular to the flooding direction, creating an artificial fracture.

In a Brazilian cell, where the core is subjected to uniaxial stress from top and bottom (Claesson & Bohloli, 2002), another fracture was mechanically induced in the second half of the core, downstream in the flooding direction. This enables us to study both an artificial fracture orthogonal to flow and a close to natural fracture parallel to flow (Figure 4).

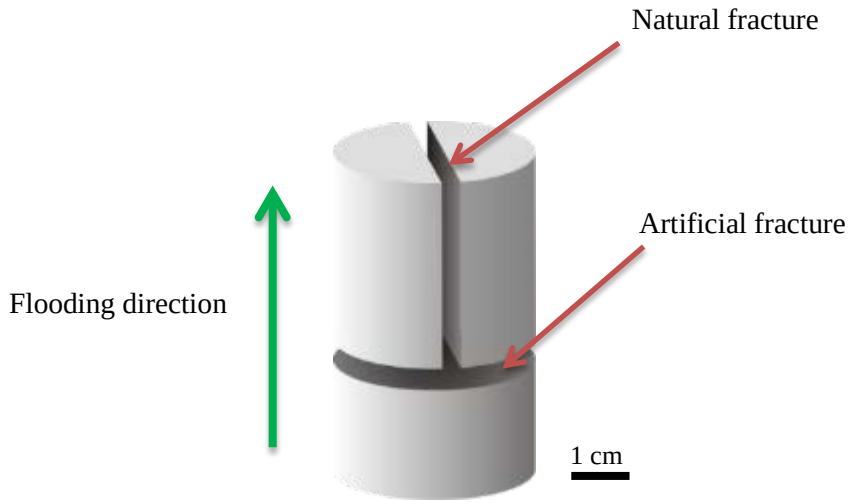

Figure 4. Sketch of the chalk core of how it was cut before flooding. (Courtesy of Tania Hildebrand-Habel).

Both fractures were mechanically produced in the lab. However, the nature of the fracture induced in the Brazilian cell is more like fractures expected to be found in naturally fractured chalk, spilt in the weakest bonds and not as destructive as in the fracture cut by a saw. This fracture is therefore, in this study considered a natural fracture.

2.6 Background and previous work

Vast amounts of experiments have been carried out on this subject, and this study only touches on a small part of this research. It may however be an important contribution to the research field, testing out new approaches on how to analyse chalk related to EOR.

With respect to mechanical properties and fluid-rock interaction studies on chalk have a long history and a lot of the background for this experiment has come as a result of decades of work at UiS and other laboratories. Mechanical testing of chalk started as a research theme several years ago (e.g. (Sarda, 1985); (Halleux, et al., 1985)). At UiS, hundreds, if not thousands, of flooding experiments have been performed, starting from basic mechanical testing and chalk characterization (e.g. (Risnes, 2001); (Madland, 2005); (Omdal, 2010)) to studies of how brine composition influences the mechanical properties of chalk and

mobilization of oil for EOR purposes, (e.g. (Korsnes, 2007); (Zhang, et al., 2007); (Austad, et al., 2008); (Yu, et al., 2009)).

Cores are flooded with various brines with different chemical composition. Injection rate, temperature, confining and pore pressures are controlled to resemble in-situ reservoir conditions or repeatable simplified conditions specially designed to test parameters believed to affect the recovery of hydrocarbons or the mechanical strength of the rock. In addition, ion-chromatography on the effluent brine measures the ion composition of the produced water from the core. Changes in the ion composition may be attributed to chemical changes in the rock mineralogy. During flooding, the axial strain in the flooding direction may be continuously measured. The core is studied with regard to density, porosity, and permeability before and after flooding.

Work by Korsnes (2007), Madland et al. (2011), Wang (In press) and Nermoen et al. (2015) amongst others show that chemical and textural alterations do happen during flooding. Numerous minerals have been identified as results of these experiments, depending on which type of brine the chalk has been exposed to. When flooding with SSW, typically clay-minerals have been found to precipitate (Megawati, 2015) together with anhydrite or gypsum and magnesium-bearing carbonates, while in cores flooded with $MgCl_2$ precipitation of magnesite ($MgCO_3$) and/or magnesium-rich carbonates is common.

Studies of flooded chalk by the methods applied in this research have before been utilized by Zimmermann et al. (2015).

3 Methodology

Several methods were applied to be able to conduct an investigation which is thorough, where the analyses complement each other, and has a certain redundancy. As a preliminary tool, optical light microscopy was used for "navigation" and to find the areas interesting for further analyses. After this, SEM imaging was used to study these areas in more detail before further preparation of samples was carried out for MLA and nanoSIMS analyses. Even though the flooding experiment itself is not part of the thesis, the process of flooding is included here to further help understanding of the investigated material and the textural and chemical changes in the core.

3.1 Experimental setup of the flooding experiment

To simulate alteration processes when injecting non-equilibrium brines into reservoir rock, cores of onshore outcrop chalk is flooded in hydraulically operated tri-axial cells (Figure 5) (for detailed information see Madland et al. (2011)).

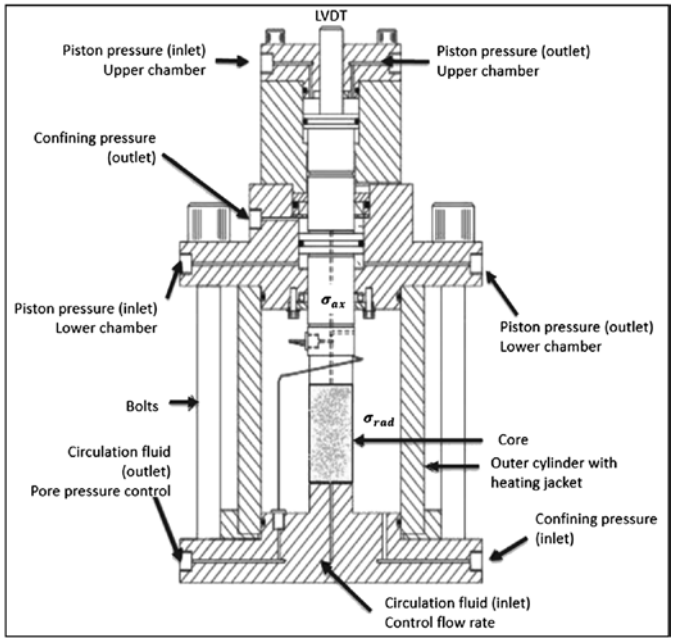

Figure 5. Sketch of the setup of a tri-axial cell in use at UiS. Courtesy of Ola Kjetil Siqveland, UiS

The core for this project was flooded in the chalk lab at UiS. Synthetic seawater (SSW) was flooded through the core in a tri-axial cell at the rate of one pore-volume (PV) a day at a temperature of 130°C. For the composition of the SSW, please see Appendix A

After an initial flooding of the core with NaCl, the flow-through experiment with SSW lasted for 34 days. After this phase, the core clogged and was bypassed with SSW for another 24 days. Even though water in the plug at this stage was locked in, one cannot assume total equilibrium of the pore water, as constant flow of SSW around the plug could induce ion exchange through solid-state diffusion. The axial stress after loading was 11.4 MPa while pore pressure was set to be constant at 0.7 MPa. This value is comparable to the effective stress of Ekofisk reservoir rock initially upon discovery (Johnson, et al., 1989), and is equal to overburden pressure minus the pore pressure. In a reservoir, the pore pressure carries some of the load of the overburden rocks, and is formulated through the effective stress relation first introduced by Terzaghi (1923):

$$\sigma'_p = \sigma_p - \alpha\sigma_f$$

where σ'_p is the effective stress, σ_p is the overburden stress, σ_f is the pore pressure, and α is the Biot-coefficient, here set as $\alpha = 1$. In hydrostatic tests, the side stress equals the axial stress. In a hydrostatic experiment performed in the tri-axial cells σ_p is simply given by the pressure in the confining pressure chamber surrounding the plug. The Biot-coefficient was introduced by Maurice Biot to account for the observation that the externally imposed stress (σ_p) is reduced by a fraction (α between 0 and 1) of the pore pressure (Biot, 1941). The fraction has been interpreted to be a measure of the fluid to solid contact area and how well grains in the rock are connected to each other.

The temperature of the experiment is set to 130°C to match the temperature of the major chalk reservoir of the Norwegian Continental Shelf, Ekofisk and Valhall. The flooding rate does not

match the injection rate of water into the reservoir, but has been set to 1 PV a day to speed up the processes within the core.

After flooding and mechanical compaction, the core was dried and cut in seven slices and given the author for further preparation and analyses (Figure 6).

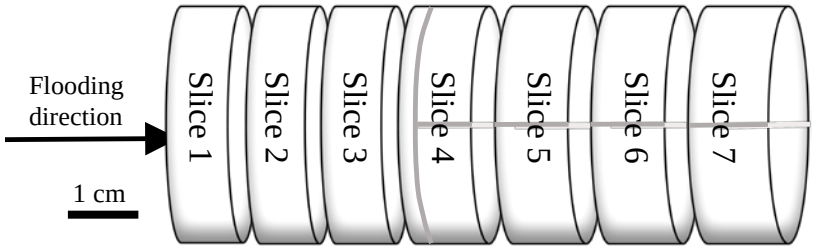

Figure 6. Sketch of how the chalk core was sliced after flooding

This experiment was not set up to mimic reservoir conditions as such, but rather to emphasize the textural and chemical alteration in a flooded chalk-core as simple and repeatable experiments. We know that dissolution and precipitation of minerals are highly dependent on temperature, pH, and stress, and that the composition of the flooding brine is an important factor for chemical and mechanical interplay ((Heggheim, et al., 2005); (Korsnes, 2007)). The value of the effective stress used in this experiment is comparable to the effective stress initially measured at the Ekofisk field, 13.8 MPa at discovery (Johnson, et al., 1989). However, the use of 11.4 MPa effective stress is in the experiment a result of increasing the confining and pore pressures though isotropic loading until the core plug reaches yield, i.e. the moment the material reaches the point of transition from elastic to plastic strain phase (Figure 7). In this test yield was reached at 9 MPa (the point where the linear curves for elastic strain, first phase, and plastic strain, second phase, cross in Figure 7). Bulk modulus was calculated to 0.52 GPa, given by the slope of the curve in the elastic region. The hydrostatic loading was done during flooding with NaCl. After 5.7 days, the flooding fluid was changed to SSW and accelerated creep can be observed (Figure 8).

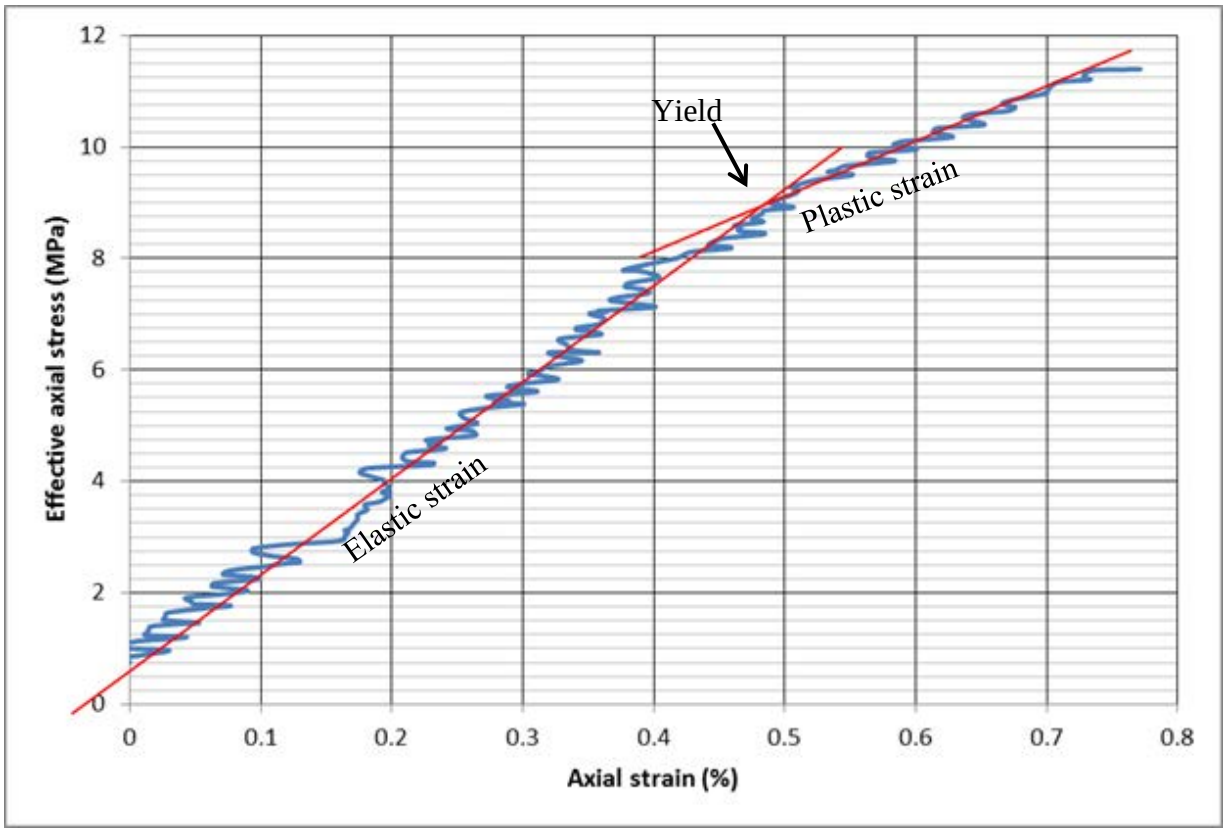

Figure 7. The hydrostatic loading phase of the experiment showing strain vs effective stress for the flooded chalk core. Yield = 9 MPa defined by the crossing of the slope of the two regimes; elastic (from 0 to 0.49% Axial strain) to plastic strain (last part of the curve) (Courtesy of Megawati Megawati)

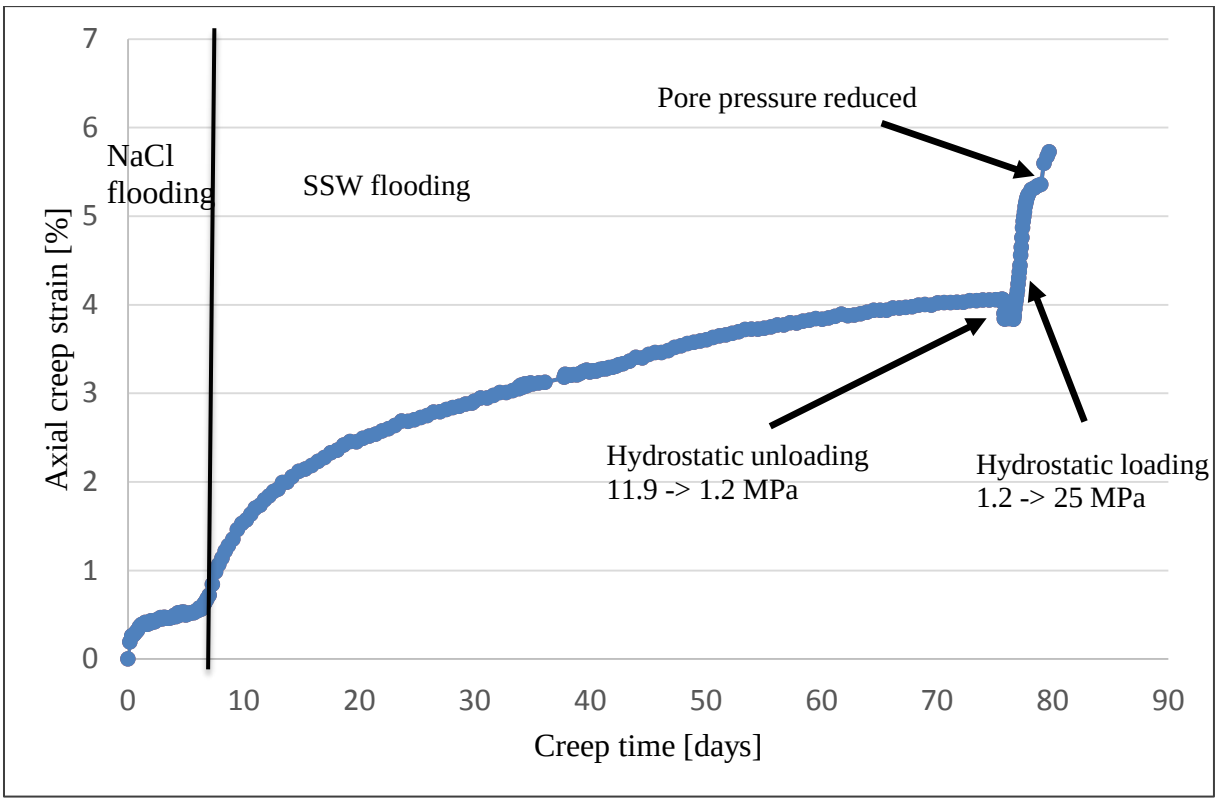

Figure 8. Plot showing the creep curve for the experiment on the chalk core, indicating creep strain versus time

After yield was reached, the confining pressure was increased by another 2.4 MPa, to 11.4 MPa, and the core was left to creep, i.e. deform at this constant stress level. After clogging of the core at 34 days of flooding with SSW, a bypassed phase followed. During this phase, the core was subjected to unloading of the confining pressure and a second isotropic loading phase up to approximately 25 MPa effective stress.

3.2 Sample preparation

After the untreated slices of the core had been studied preliminary in an optical light microscope and FE-SEM, they were polished for further analyses. As the objectives of the analyses are to scan the fractured areas, and their surroundings for differences in chemical, hence mineralogical composition, the samples had to be polished to obtain a completely flat surface, enabling analyses by MLA and nanoSIMS.

Samples were first set in epoxy shaped as small disks with diameter of 1 inch with fractures facing down. The disks were later polished using grinding paper to remove excessive epoxy on the fractured surface. To create a smooth flat surface, MD-Dac paper and DiaPro Nap B with DiaPro Dac lubricant was used.

For FE-SEM analyses of the polished surfaces and the exterior of the core, samples were coated with carbon. For secondary FE-SEM analyses of freshly broken surface, palladium was the coating agent.

3.3 Optical light microscopy (OLM)

Optical light microscopy was done by a Zeiss Stemi 2000-C optical microscope. This microscope works at magnification up to 20 times and is based of transmission and reflection

of visual light through the lenses of the microscope. At this level of magnification, we are able to identify macrofossils in chalk, such as foraminifera and shells from bivalves and gastropods. We are not able to image coccolithophores and coccoliths with this method of investigation, as their size is below the resolution of the microscope.

3.4 Field emission scanning electron microscopy (FE-SEM)

A Zeiss Supra 35VP FE-SEM at the University of Stavanger (UiS) was used for this project (Figure 9). By the use of scanning electron microscopy (SEM) we do not look at the samples with visual light, but image how electrons interact with the surface of the sample. This allows for magnifications up to 100 000 times, which is not possible in a normal light microscope which is limited by the wavelength of visual light. In many cases, one wish to study a broken surface of the sample and compared to OLM the depth of field is much higher. This is of high importance when the surface is not completely flat.

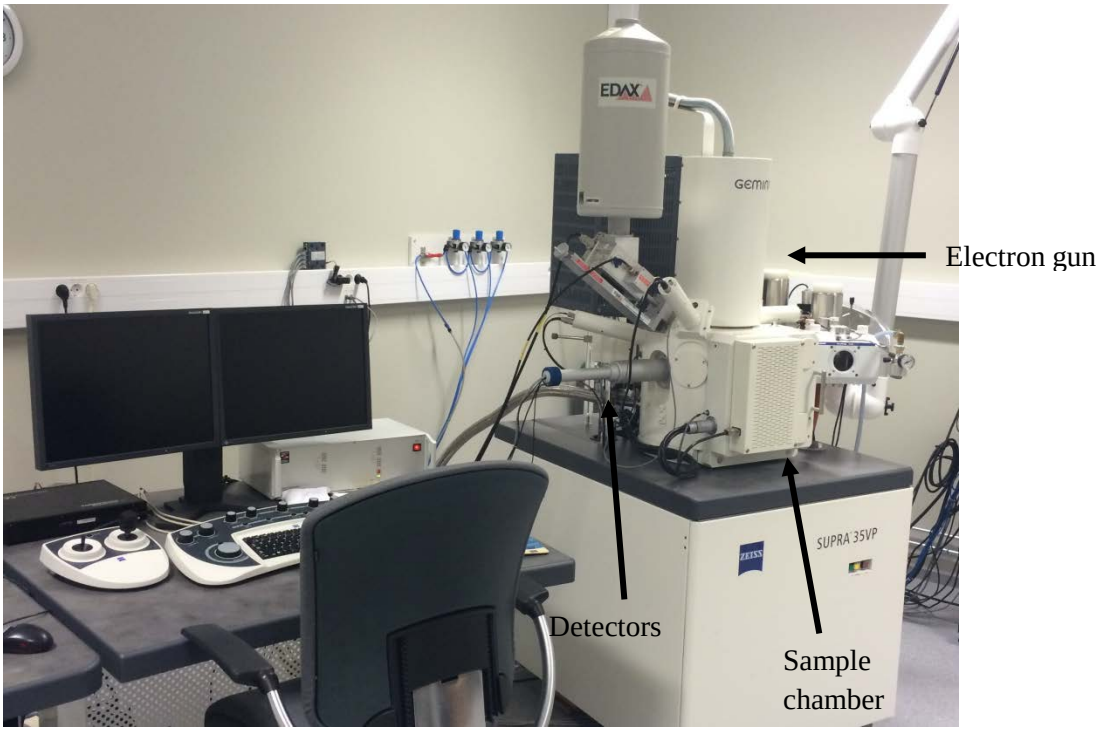

Figure 9. Zeiss Supra 35-VP FE-SEM at the University of Stavanger

Electrons are accelerated in an electron gun to create a focused beam of electrons scanning the sample. The FE-SEM has, instead of a wolfram- or LaB6-filament, a field-emission gun. This creates a much smaller beam-diameter with a higher intensity of electrons; hence, the resolution of this type of SEM is much higher. Through electromagnetic lenses, the beam is focused and adjusted to produce an as small as possible spot of electrons at the sample surface.

Samples have to be coated with an electrically conductive material, such as carbon, palladium, or gold, to allow a steady electron flux and avoid charging. When the beam hits the surface of the sample, various energy signals reflect or produce from the surface, which are collected by different detectors. These are back-scattered electrons (BSE), secondary electrons (SE), X-rays (energy dispersive system, EDS) and light (cathodoluminescence detector, CL). The emission of secondary electrons will vary as a function of the topography and composition of the sample surface, enabling imaging of the surface (Figure 10). As an atom is bombarded with primary electrons, electrons initially in the shells of the atom may be excited and emitted from the sample as secondary electrons. These are inelastic scattered and have a much lower energy than the primary electrons. It is not only the upper part of the surface that produces secondary electrons, the primary electrons penetrates a certain distance into the sample, depending on which type of material is studied and how high the acceleration voltage is. The higher the voltage, the further into the sample electrons penetrate. As the secondary electrons have a lower energy-value, only electrons from the upper 5λ (wavelength of the primary electrons) will escape the sample (Hjelen, 1989). The secondary electrons are gathered in a SE-detector through a scanning sequence to create SEM-micrographs.

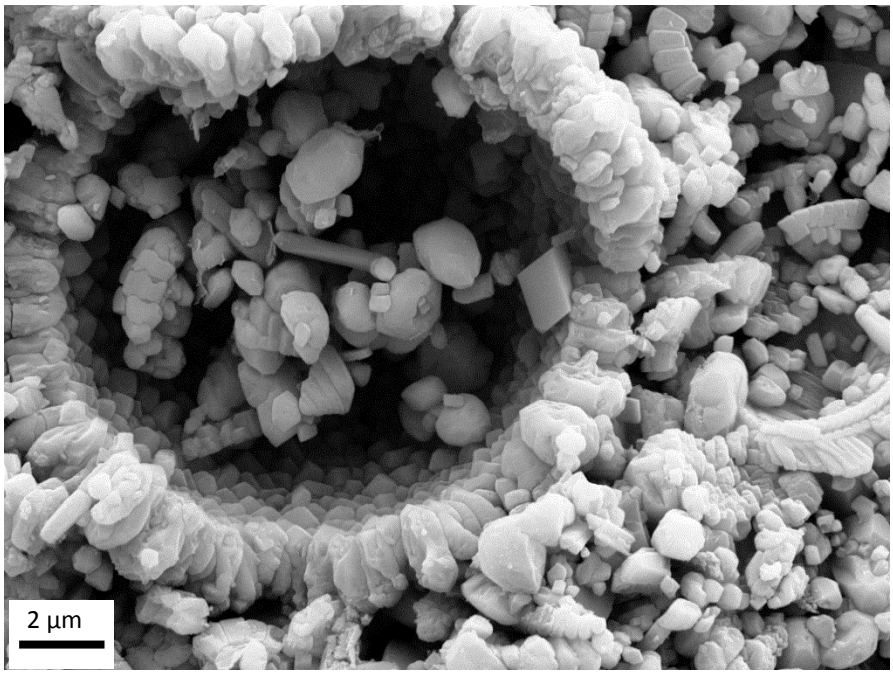

Figure 10. SE-SEM-micrograph of chalk. Coccoliths, grains and precipitated crystals in a pore of a foraminifera. (Courtesy of Wenxia Wang)

A BSE detector collects the reflected, or backscattered, primary electrons, which are a result of elastic scattering. The backscattered electrons change direction, while the energy is more or less conserved. The fraction of backscattered electrons is related to the atomic number of the element scanned. With this method, mapping of elements on the surface is possible. As the backscattered electrons keep their high energy level, the emission-volume of BSE is much larger than for SE. This means that electrons from deeper into the sample may be emitted from the sample and detected.

In the SEM at UiS there is also mounted an EDAX Energy-dispersive X-ray spectroscopy system (EDS-detector) which analyses the chemical composition of a point defined by an approximately 2µm wide beam or a larger scanned area on a semi-quantitative level. As electrons from the inner shells of atoms excite they enable an electron from an outer shell to jump to the inner shell, releasing energy in form of a characteristic X-ray. Because of the difference in atomic structure, the energy level of the released X-ray from each element will differ. The x-ray is detected by a silicon crystal doped with lithium and creates a spectrum

where the elements present in a sample may be identified (Figure 11). Semi-quantification of the weight (wt.%) and atomic percent (at.%) for each element is also possible. The accuracy varies based on many factors, and lighter elements such as carbon and oxygen are especially difficult to measure precisely. However, use of standards allow for a quantification based of the spectrum produced.

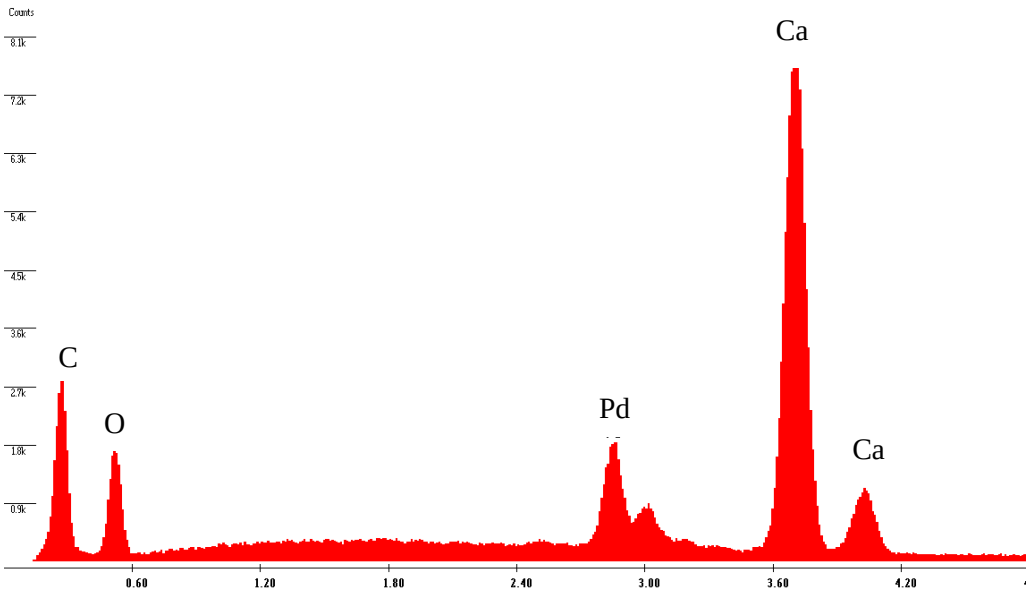

Figure 11. EDS-spectrum from a calcite crystal. Peaks from the main elements in $CaCO_3$, Ca, C, and O. The sample is coated with palladium (Pd)

Images and spectra were collected with 15 kV acceleration voltage, 30-µm aperture and working distance between 10 and 11 mm.

In addition to the signals discussed above, samples bombarded with accelerated electrons also emit light, Auger and continuous X-rays. These will not be used for this project and therefore not discussed here.

3.5 Mineral liberation analyzer (MLA)

MLA is a way of combining imaging by SEM-BSE analyses and X-ray mineral identification by EDS. A high-resolution BSE image where the elemental constituents of crystals and grains may be measured may accurately identify the minerals present in a sample. This is a semi-quantitative measurement, automated to be repetitive, cost effective, and absent of user bias.

The analyses were carried out at Technische Universität Bergakademie Freiberg (TU Bergakademie Freiberg) in Germany. The SEM in use is a FEI Quanta 650 FEG together with an EDS system (Figure 12). The software controlling the MLA is Quantix Esprit 1.8. Images and analyses were acquired using 25 kV acceleration voltage.

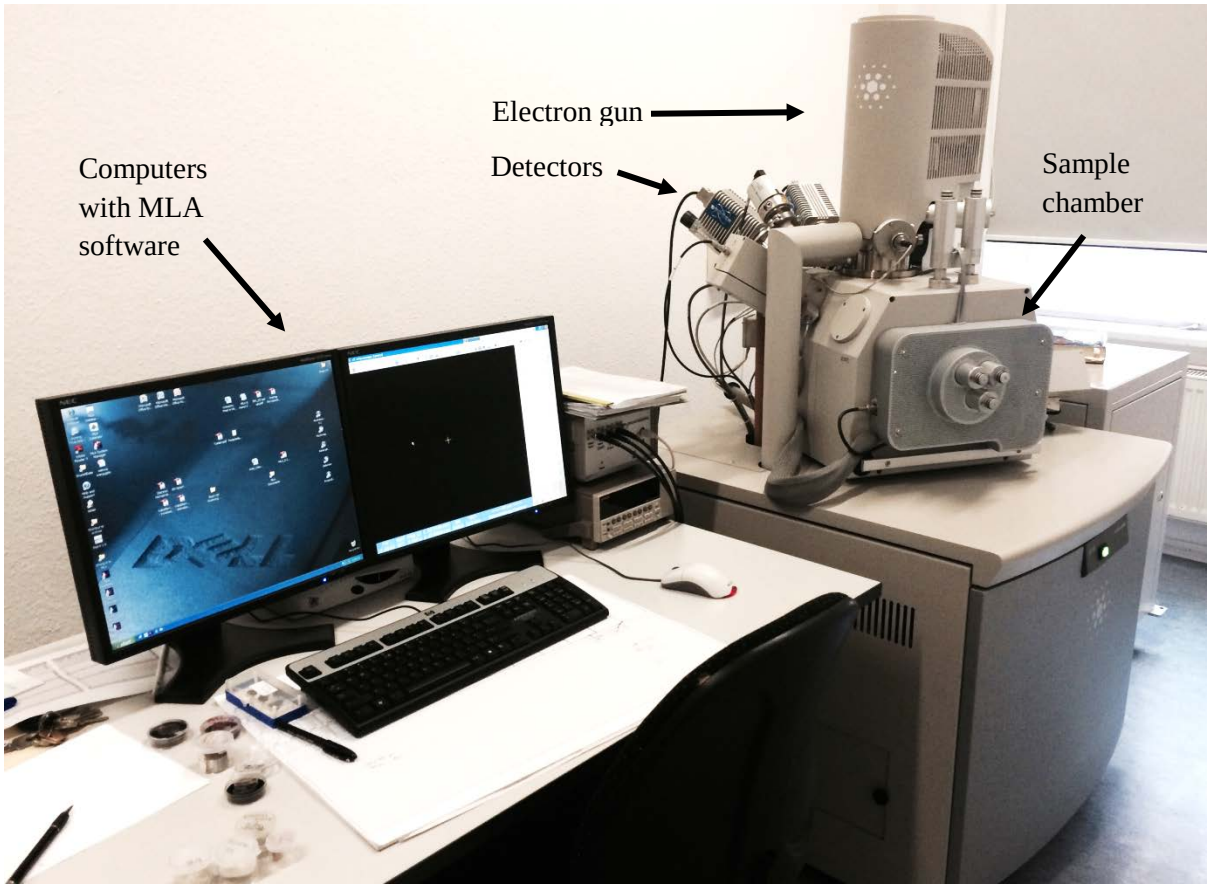

Figure 12. FEI Quanta 650 FEG at the TU Bergakademie in Freiberg used for MLA anlayses

The prepared samples are analysed on a polished surface, coated with carbon. Scanning selected grains, matrix, or crystals with an EDS detector, produces a spectrum of the elements

present. Each spectrum is then classified as a certain mineral or mix of minerals, assigned a colour, and added to a database. This mineral is in the end coupled to the average grayscale value of the BSE image. As the average atomic number of each mineral phase corresponds to the number of backscattered electrons from a sample, the average grayscale-value is therefore unique to this mineral (Fandrich, et al., 2006). The greyscale for each mineral will naturally vary slightly. Therefore, a certain variance in greyscale-values is allowed for. To ensure good measurements, the grayscale is calibrated with a copper-standard. In this way, the greyscale-value in the BSE-image corresponds to a collected EDS-spectrum in the database and larger areas may be mapped based on the greyscale in the BSE-image.

Processing the images has a certain order when using the MLA technique. After creating a database of spectra for classification, the selected area is scanned over a period of time by the use of a BSE-detector. After the image is scanned, the first step is particulation, removal of background based on a minimum BSE greyscale level. Anything below this threshold, in this case the epoxy resin or air bubbles, is removed from the image. The second step is segmentation, where grain boundaries and internal structures are defined based on BSE characteristics. Cracks and preparation artefacts are removed. In this process different particles within each grain is identified. After segmentation is finished, classification of the minerals present in the area of interest starts. There are several methods in use for mapping. For simpler use, basic BSE mode is an option. In this mode, each particle, i.e. mineral, is measured based on the grayscale of the BSE-image already linked to an EDS spectrum. The mode used for this project is GXMAP mode. This mode is based on identification of particles through BSE imaging, then x-ray mapping of each particle in a pre-defined grid, collecting the spectra of characteristic x-rays at each point. This allows for high special resolution scanning and avoids limitation by poorly defined grain boundaries in BSE images caused by similar average atomic number of minerals (Fandrich, et al., 2006). The scanned area is

coupled to the EDS-spectra database for classification of minerals in the sample. In this way, we may produce color-coded maps imaging the mineralogical distribution of the surface (Figure 13), enabling evaluation of spatial textural and chemical composition in one process.

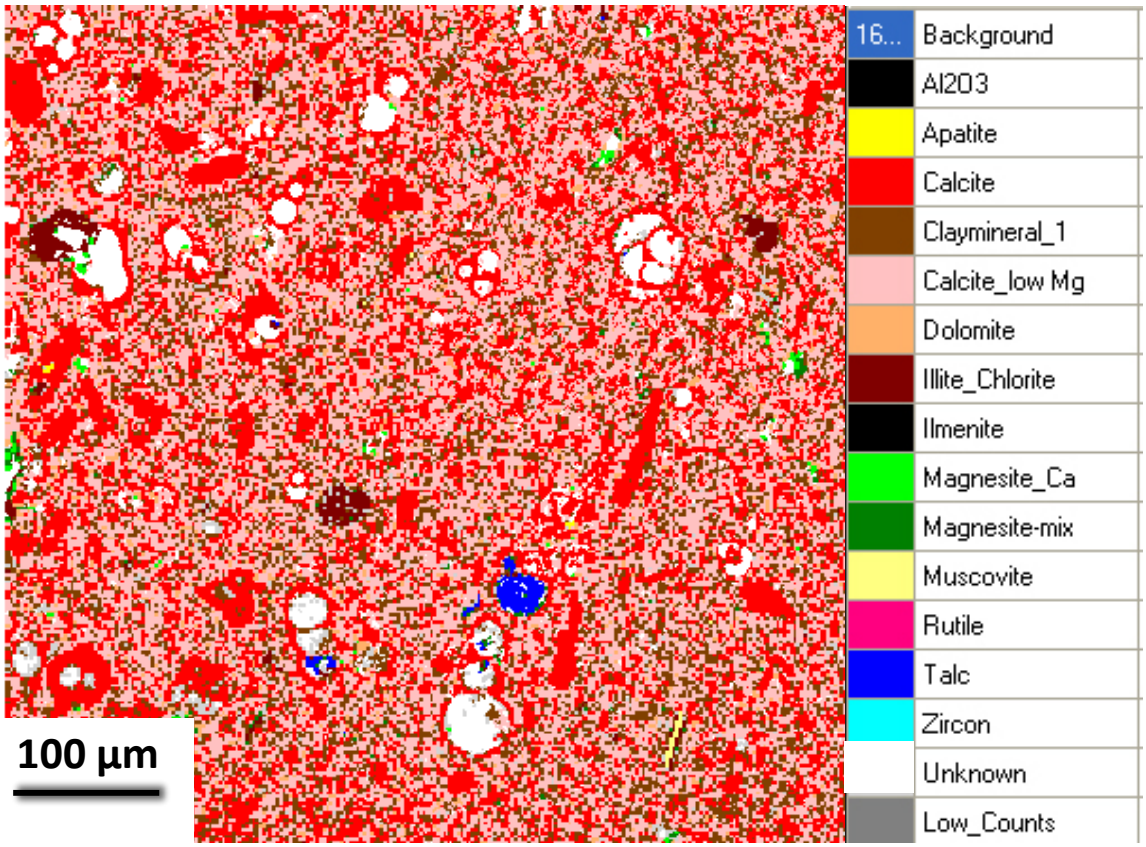

Figure 13. Example of color-coded MLA map of a thin section of chalk. (Courtesy by Dr. Udo Zimmermann)

The resolution of the MLA scanning depends on the size of the area scanned and time used, but may be set as high as to less than one micrometer per pixel. A certain number of grains or crystals will still not be identified based on the mineral database used, and be counted as "unknown".

An important part of analysing samples by the use of MLA is to work with the produced data after scanning. Often it is possible to produce additional information through different groupings and filtering of minerals or mineral-mixes. Of particular interest for this project, are the concentrations of silicon, magnesium, and aluminium and their distribution in the samples with regard to the fractures and the texture of the rock. As the grain-size of chalk is so minute,

the size of the mineral-particles may be beyond the resolution of the MLA and it may not be possible to classify these particles as separate minerals, but rather as mixed spectra with variable amounts of minerals present. To attain better use of the data gathered, one may therefore group these mixed spectra according to the concentration of exactly these minerals to study their distribution in the sample.

By the use of MLA software one may also quantify the mineral distribution and manipulate data to investigate other properties of the sample, such as groups of minerals, grain distribution, or grain shapes.

3.6 Nano Secondary Ion Mass Spectrometry (nanoSIMS)

Secondary ion mass spectrometry is based on the fact that when a primary ion beam hits a surface, secondary ions are produced which may provide us with information about chemical composition and structures of the surface (Hirata, et al., 2011).

The same samples already scanned by MLA was also studied with a Cameca NanoSIMS50 application (Figure 14) at the “Centre de Recherce Public Gabriel Lippmann” in Luxembourg (now Luxembourg Institute of Science and Technology, LIST). As discussed in the chapter 3.5, the particle size in chalk may be too small to be sufficiently recognized by MLA. Therefore, the need for further sub-micron studies is present and this may be supplied by nanoSIMS.

NanoSIMS scans the surface with a focused Cs^+ ion beam. The beam is expected to be smaller than 100 nm in diameter (lateral resolution) (Zimmermann, et al., 2015). For this project, the area scanned varies between 55 and 10 µm. As the image have 256 x 256 pixels, this results in a resolution between approximately 200 and 40 nm per pixel.

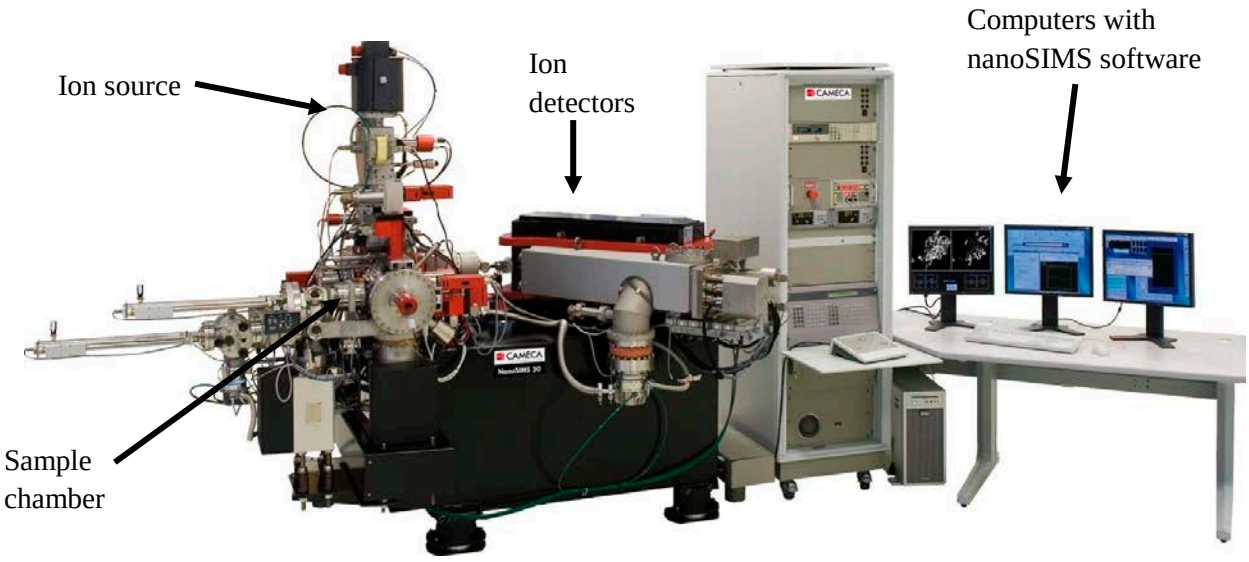

Figure 14. The Cameca nanoSIMS 50 as used in Luxembourg (from www.cameca.com)

The impact of the primary beam produces a secondary ion beam, known as “sputtering”. The particles produced from the surface may be positive, negative, or neutral, depending on the primary ions identity (Griffiths, 2008). The ion-yield varies with respect to the type of beam used, e.g. cesium or oxygen, and the ionization energy of the element and sample matrix (Handley, 2002). To be able to detect neutral particles, a laser ionizes the secondary beam. The ions are accelerated and directed into a mass spectrometer by an electric field. In the Cameca NanoSIMS50 both a time-of-flight (TOF) and a magnetic sector analyser are installed. By the use of TOF-detector, one may measure several ions at one time. By this multiple scanning of a fragile surface is avoided (Griffiths, 2008). The same surface was in this project, however, scanned twice to collect in all ten different masses; ^{16}O, ^{28}Si, $^{24}Mg^{16}O$, $^{40}Ca^{16}O$, $^{56}Fe^{16}O$, ^{32}S, ^{35}Cl, $^{23}Na^{16}O$, $^{27}Al^{16}O$, and $^{31}P^{16}O_2$. This may enable identification of which elements are present in one certain grain or crystal down to a resolution of 40 nm (Figure 15). In Figure 15 we see how in the encircled grain, only magnesium, together with oxygen and carbon, is present, while it is clearly lacking both silicon (Si) and calcium (CaO). This leads to the conclusion that this grain is magnesite.

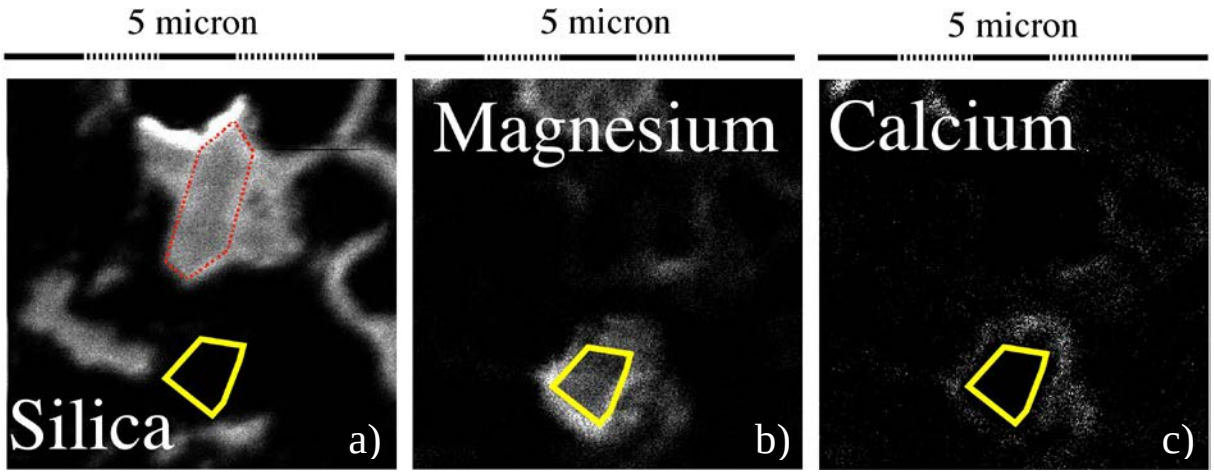

Figure 15. NanoSIMS identification of minerals based on elements present in grain. Elements: a) Si, b) MgO and c) CaO. A grain (marked in yellow) with no Si and Ca, but containing Mg together with C and O is most likely magnesite (Zimmermann, et al., 2015)

Another application of the NanoSIMS is to make depth profiles and to create 3D-images, scanning a 10 x 10 µm area repeatedly to measure the composition of a specific area, grain, or crystal, to a depth of approximately 1µm.

The scanning results in an image for each mass displays the intensity of the ions produced from each area. The value of the intensity between two images of e.g. calcium and magnesium is not comparable, meaning that the method is not quantitative as such. One may study the images of an element to identify where a certain element is present and say something about the relative difference within the area.

To identify the areas to be studied in the sample, the nanoSIMS is coupled to an optical camera. Navigation on polished surfaces of chalk is challenging because of the lack of topography and colours, and this method very time consuming.

After scanning, “ImageJ” software is used for analysing the data. It may be very useful to compare the presence of selected ions. In all, ten images were obtained for each area and these may be compared and enhanced to produce the best understanding of the grains and particles in question and the elemental distribution in the sample. ImageJ allows for

adjustment of colours and contrast of the images as well as merging images for selected ions, enabling mapping of elements or minerals (Figure 16).

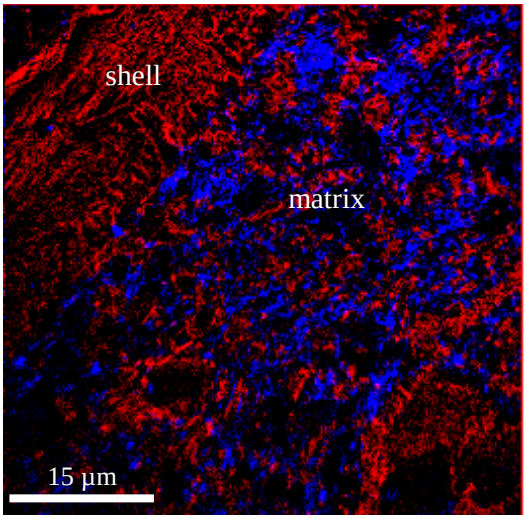

Figure 16. Merged images from nanoSIMS scanning. Red; CaO, blue; Si. Part of a bivalve shell (left) with surrounded matrix in a flooded chalk core.

4 Results

4.1 Optical light microscopy (OLM)

By the use of OLM the two fractures were identified in the sample, the artificial fracture in slice 4 and the natural fracture in slice 5 (Figure 17 and Figure 18, respectively). As seen from the images in Figure 17 and Figure 18, the artificial fracture is much easier to identify. It has a much more pronounced relief on the surface of the core and runs as a clean cut through the rock, perpendicular to the fluid flow.

Figure 17. The artificial fracture in slice 4 at the core exterior imaged with OLM (arrow pointing to fracture)

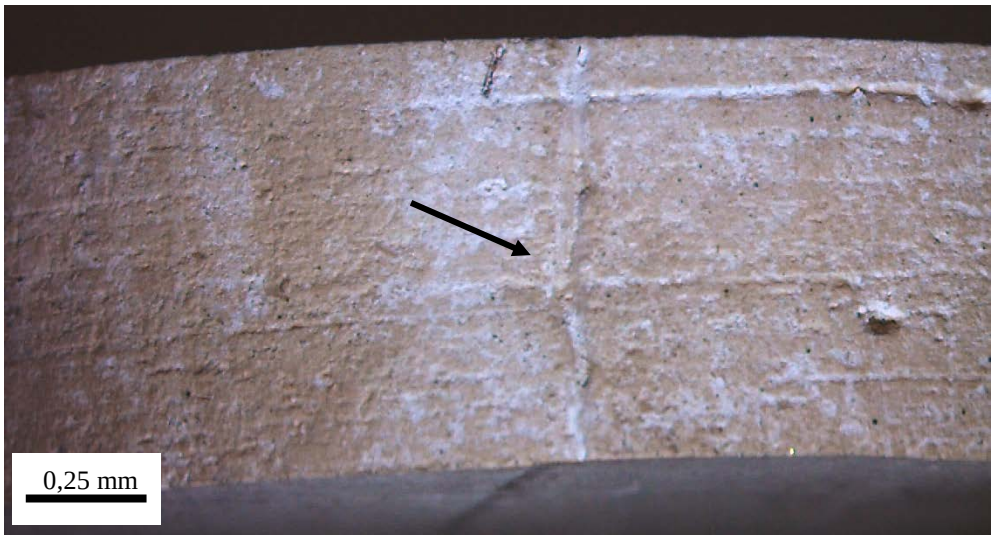

Figure 18. The natural fracture in slice 5 identified on the core exterior imaged with OLM (arrow pointing to fracture)

The natural fracture runs in harmony with the texture of the rock, looks to have a filling material and to have healed in a more complete manner than the artificial fracture. Based on these observations, parts of these two slices, 4 and 5, was chosen for further analyses.

The two slices were polished at UiS to be prepared for analyses by MLA and nanoSIMS. To ease localization of the two fractures in the polished surface, the epoxy was constantly marked with a needle at each end of the fractures during polishing. Figure 19 shows the two polished samples, with their markings and labelled study zones.

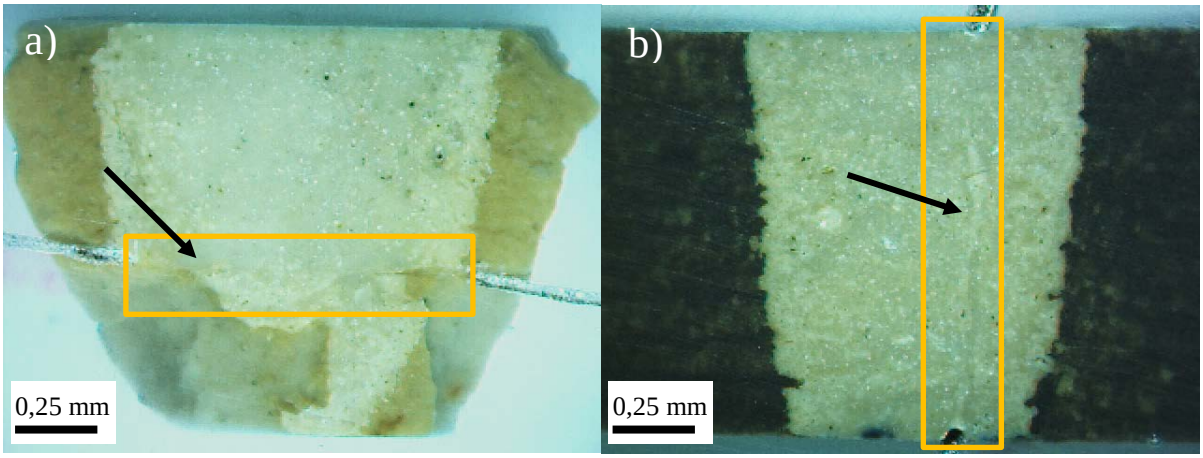

Figure 19. The artificial fracture in slice 4 (a) and the natural fracture in slice 5 (b) after polishing imaged with OLM. Study zones marked in yellow

Both fractures in Figure 19 have a denser and brighter appearance than the surrounding matrix.

For more detailed OLM images of the two slices, see appendix B

4.2 Field emission scanning electron microscope – Secondary electron images and EDS measurements

Before and after polishing, both samples were studied by the use of FE-SEM at UiS. The aim was to identify new mineral phases possibly formed in the fractures and to investigate the morphology of the fractures before further preparation.

4.2.1 Artificial fracture

The FE-SEM work on the artificial fracture in slice 4 has been done by Dr Megawati Megawati as part of a Petromaks project led by UiS (Megawati, 2015). The work was done together with Dr Hildebrand-Habel, and is included here to provide additional information to this study. Analyses were carried out both on polished surface and on freshly broken pieces of the core. As seen in Figure 20, the fracture is much more compact than the surrounding matrix. The denser area is approximately 30 µm in thickness, with an open line running through the centre. In some parts of the fracture, this open space is not present.

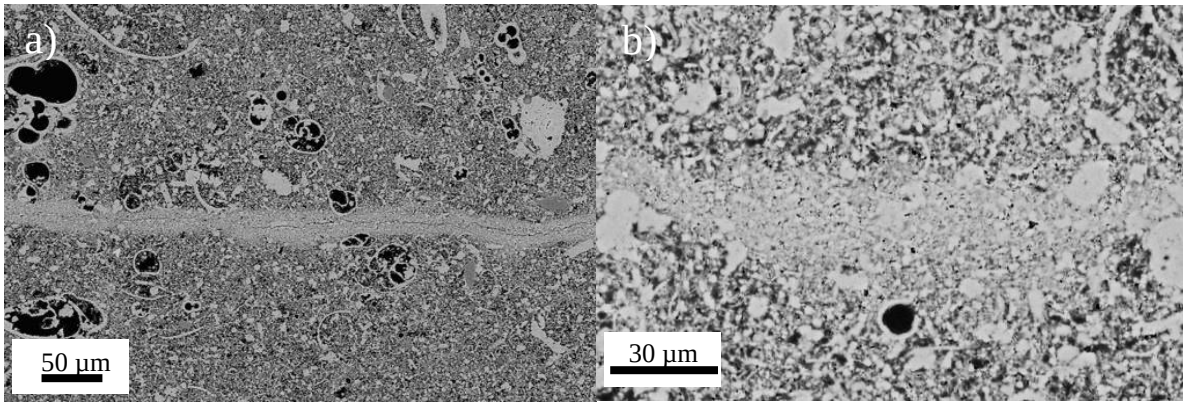

Figure 20. SE-SEM micrographs of the artificial fracture in slice 4 taken on a polished surface at different magnifications

By studies of a freshly broken surface of the fractured slice 4, textural and chemical differences are observable. No new mineral phases can be identified as such. However, there is a clear visual difference between the area of the fracture and the surrounding matrix (Figure 21). The denser area of the fracture shows a high concentration of minute clay-minerals in the

pore space, while the area below the fracture is rather clean, with low amounts of clay minerals.

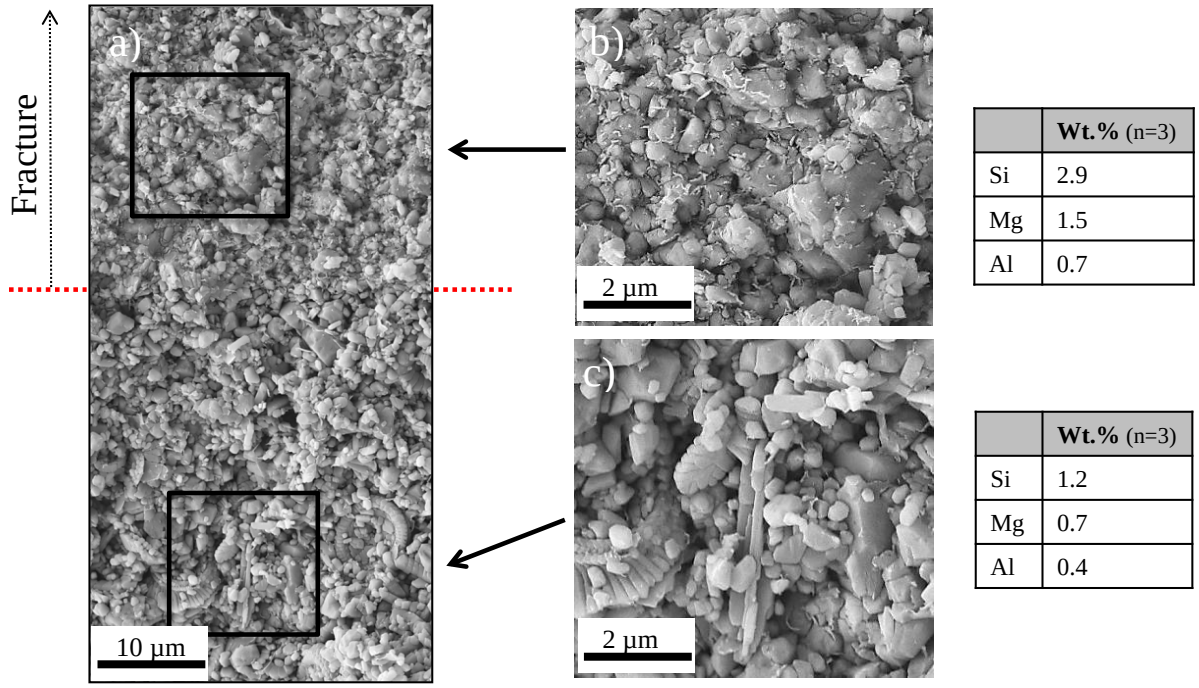

	Wt.% (n=3)
Si	2.9
Mg	1.5
Al	0.7

	Wt.% (n=3)
Si	1.2
Mg	0.7
Al	0.4

Figure 21. Textural and chemical difference between the fractured area (above the red line) and the surrounding matrix. Image b and c displaying parts of a, at higher magnifications. Note the increase in clay-minerals and Si-, Mg- and Al-content in image b

Three repetitive EDS-measurements were done on each of the two areas shown in squares to the right of Figure 21. As seen in the boxes to the right, the wt.% of silicon (Si) and magnesium (Mg) is increased considerably inside the fracture. Both of these values are more than doubled, increased by 142% and 114% for silicon and magnesium, respectively. Aluminium does also show a comparable increase, but as the wt.% of aluminium is below 1%, the margin of error increases significantly. One of the strengths of the use of FE-SEM together with EDS-measurements is the ability to visually investigate the SEM micrographs for explanations of deviations in chemical composition. In this case, it is clear that the abundance of clay minerals correlates to the increase in the amount of silicon, magnesium and aluminium in the sampled area.

In the fractured area, we cannot observe any fossil structures. Most grains seem to be of a precipitated origin, larger and more crystalline than grains usually found in high porosity chalk.

4.2.2 Natural fracture

Identification of the natural fracture inside the flooded core was attempted using both OLM and FE-SEM. This was not successful, underlining the smooth nature of this fracture. As a result, the fracture was firstly studied on the exterior of the core.

The complete fracture in slice 5 was imaged and when studying the surface by FE-SEM-imaging, the fracture itself seems to consist of a harder filling material, with an amorphous nature. Several images were collected, showing the nature of the fracture filling material (Figure 22).

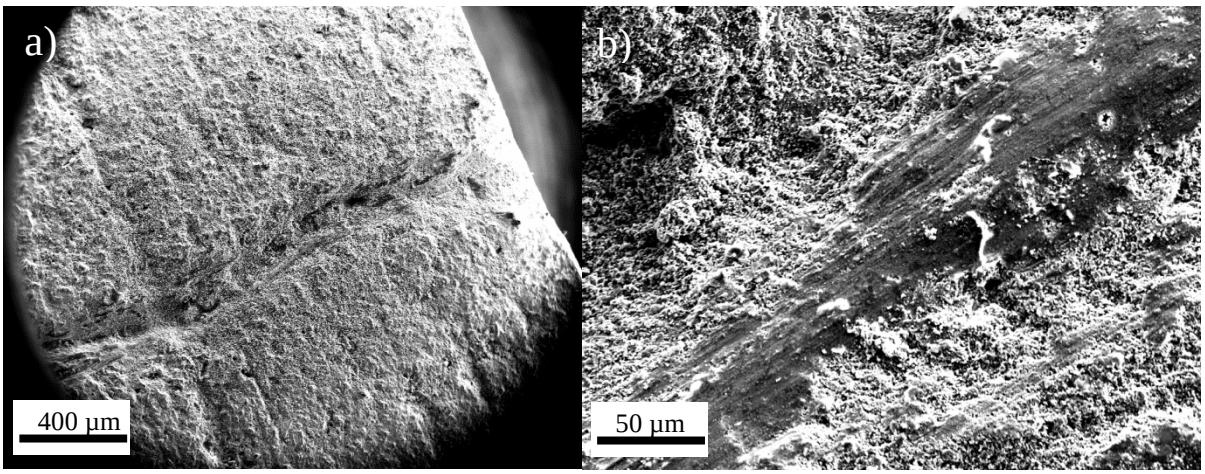

Figure 22. SE-SEM overview micrographs of the natural fracture (a) and close-up of the filling material (b) in slice 5, showing the nature of the fracture filling at the exterior of the core

The filling have lineation which run along the flooding direction of the core. EDS spectra were collected to gain more information of the constituents of the fracture filling.

In Figure 23 we see that the fracture, to the left in the micrograph, has a more cemented and amorphous or possibly finer grained nature that the material outside the fracture, to the right.

EDS spectra were collected in both areas to identify variation in compositions between the two (Figure 24 and Figure 25).

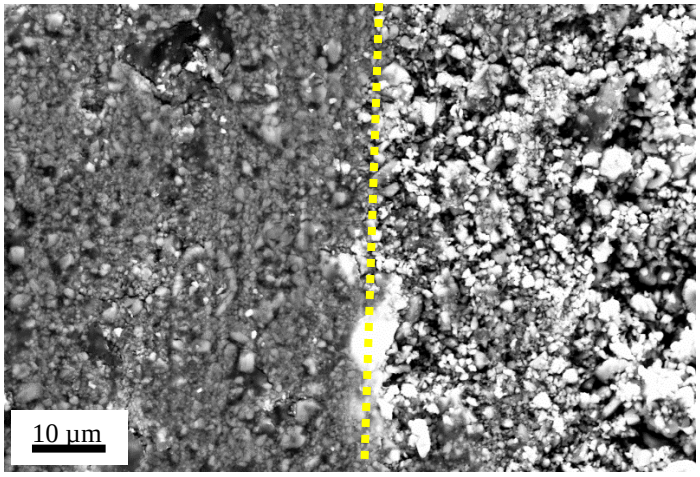

Figure 23. SE-SEM image of the natural fracture in slice 5 to the left of the yellow line and the un-fractured core material to the right. Imaged on the exterior of the core

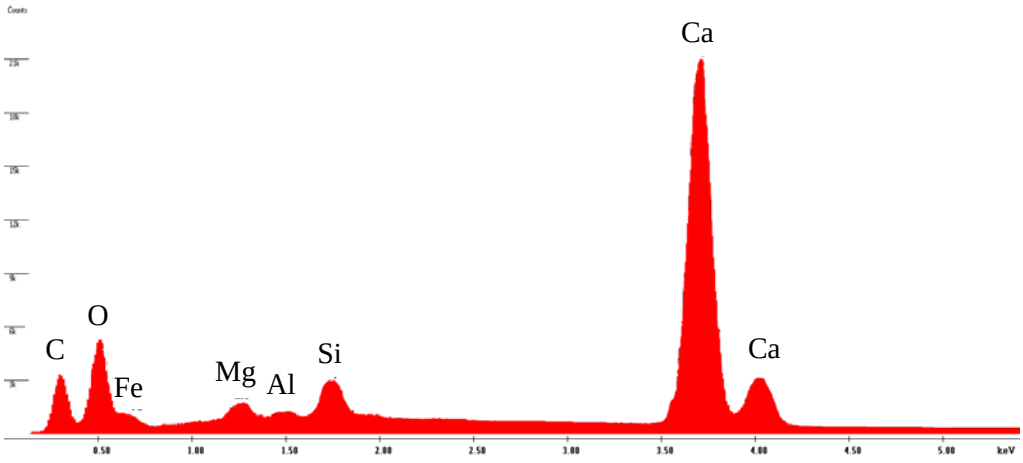

Figure 24. EDS spectra from inside the fracture at the exterior of the core in slice 5

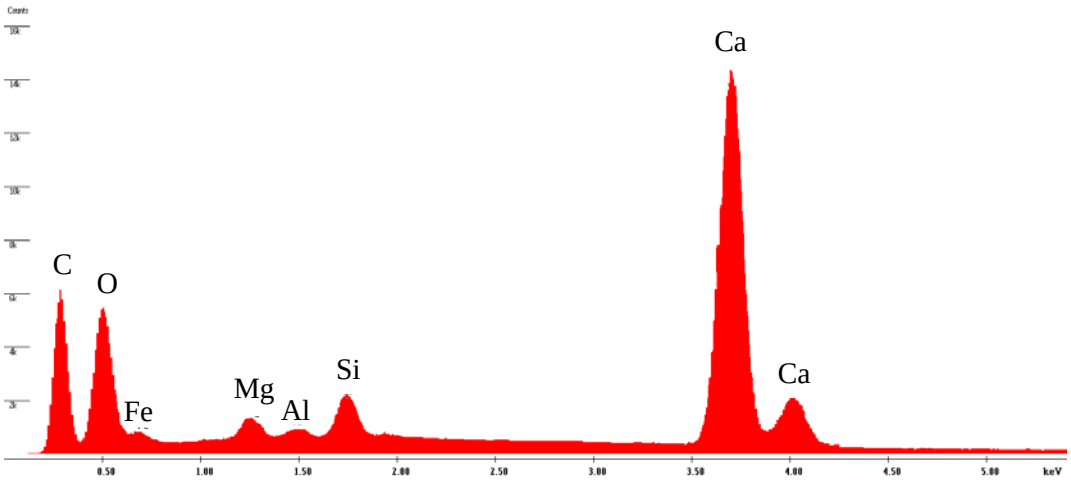

Figure 25. EDS spectra from outside the fracture at the exterior of the core in slice 5

From these spectra, it is not possible to obtain information about chemical differences between the two areas as the semi-quantitative nature of EDS measurements does not allow for differentiating between concentrations with a minimum of variation. This justifies the need to investigate the samples further with methods that offer higher resolution and/or higher quality quantitative results, such as nanoSIMS and MLA.

After finished MLA and nanoSIMS analyses, the sample for slice 5 with the natural fracture was spilt into two and re-analysed by FE-SEM. The assumed area of the fracture did not break as the rest of the rock, it seems to have more cemented nature and there is a ridge in the fractured area (Figure 26). This point to a difference in compaction and/or density.

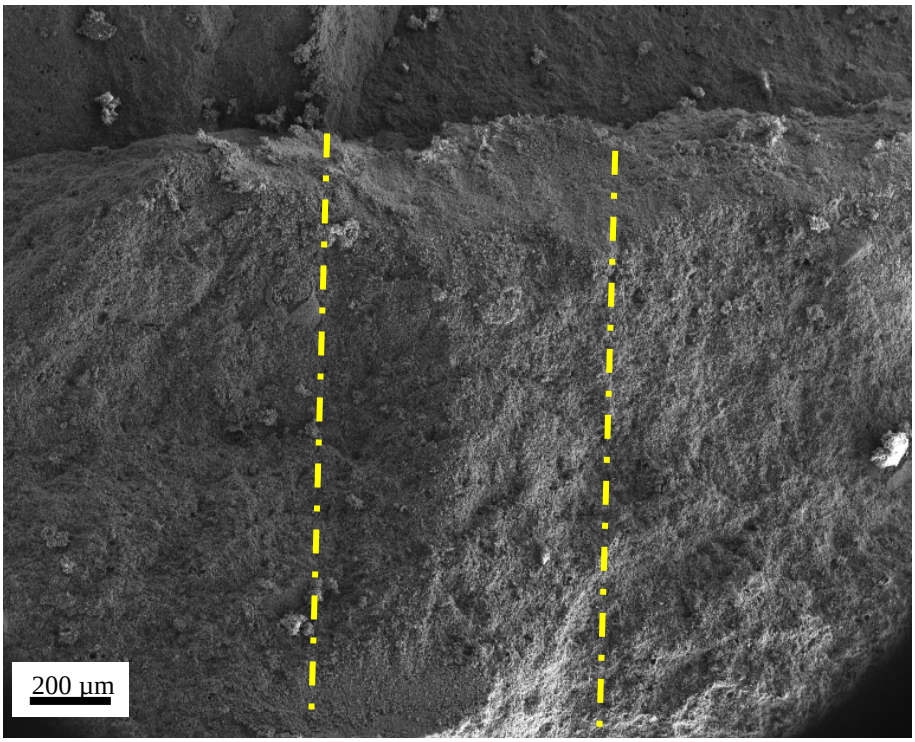

Figure 26. SEM micrograph of the natural fracture in slice 5 (Assumed fracture between yellow lines). The fracture itself seems to break in a different fashion than the un-fractured material. Imaging done on a freshly broken surface inside the core

The SEM micrographs of the freshly broken surfaces show that the chalk is quite pure in both the areas outside and the areas inside the natural fracture. There seems, however, to be slightly more clay in the fractured area (right image, Figure 27).

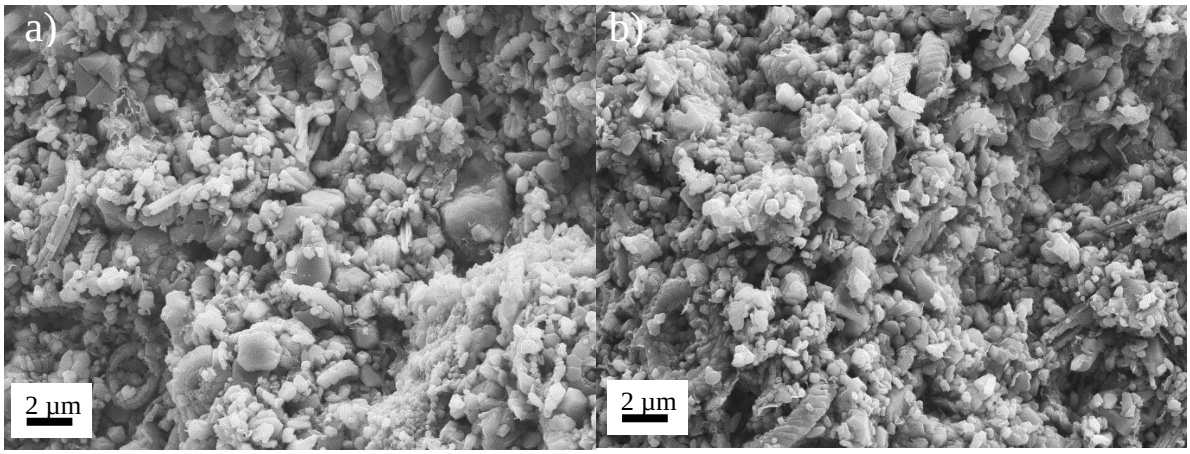

Figure 27. SEM micrograph of the area outside (a) and inside (b) the natural fracture in slice 5. The area inside the fracture seems to contain more clay flakes. Imaging done on a freshly broken surface inside the core

This coincides with the EDS measurements done in the corresponding areas (Figure 28) where there is enrichment of the silicon content in the fracture. It is not possible to identify a

sharp transition from the un-fractured area to the fractured area, as is in the artificial fracture in slice 4 (Figure 21).

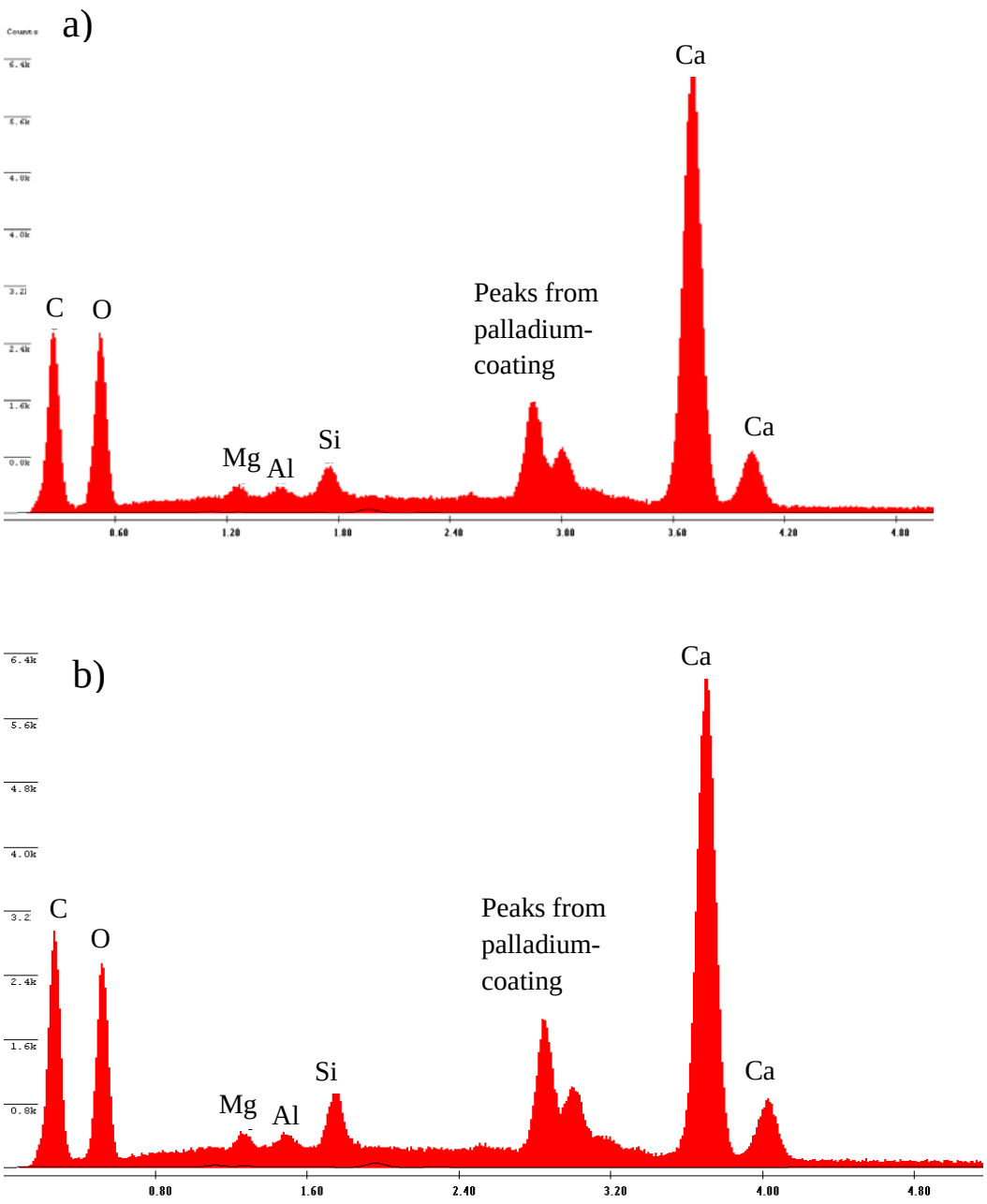

Figure 28. EDS-spectra of the un-fractured area (a) and the fractured area (b) in slice 5. Notice increased Si and Mg content in the fractured area (b)

4.3 Mineral Liberation Analyzer and Backscattered electron images

As backscattered electron images were acquired together with MLA-scans, the results from these analyses will be presented together in this chapter.

4.3.1 Artificial fracture

By the use of SEM-BSE imaging, the fracture was studied along the entire surface. In Figure 29, SEM-BSE images of the fracture have been assembled to give a complete overview of the texture and variation in grayscale, i.e. average atom number (AAN) and mineralogy.

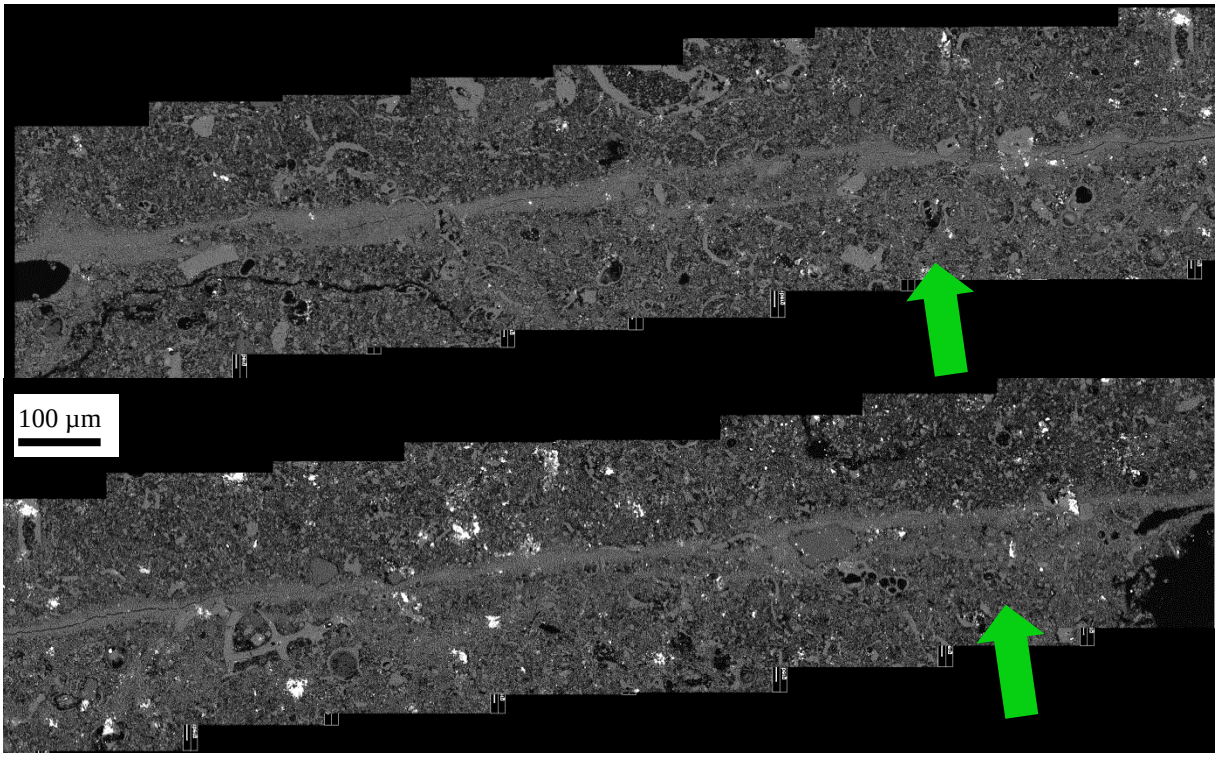

Figure 29. SEM-BSE image of the artificial fracture in slice 4 (green arrow indicating flooding direction). Top image showing left side of fracture, bottom the right side

Based on the BSE images it does not seem to be high contrasts in the composition between the two sides of the fracture. The fracture itself, show a more compact or dense nature. Together with the shells of microfossils, foraminifera, and remnants of macrofossils, bivalves and gastropods, the fracture displays a brighter shade of grey than the surrounding matrix. In BSE micrographs, the average atomic number (AAN) in directly related the greyscale-

intensity, where higher AAN is represented by a higher intensity in the image. If we compare calcite, $CaCO_3$, and magnesite, $MgCO_3$, calcite would have a higher AAN, thus representing a brighter area in the BSE-image. The same could apply to certain types of clay minerals.

In Figure 29, several areas of nearly white are observed. These spots represent two heavier elements further up in the periodic table, tin and copper, and are in this case most likely related to slight contamination on top of the surface.

When studying the textural composition of the sample, the larger pores are mostly related to microfossils floating in the more fine-grained matrix (Figure 30). In addition, rare cases of crystals and non-carbonate grains are embedded in the matrix. Examples of this are quartz (Figure 31), glauconite (Figure 31), and muscovite.

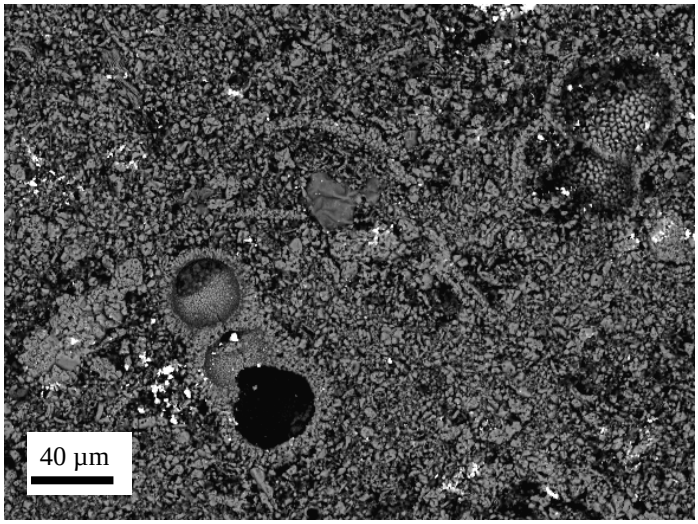

Figure 30. Foraminifera fossils floating in the matrix of slice 4

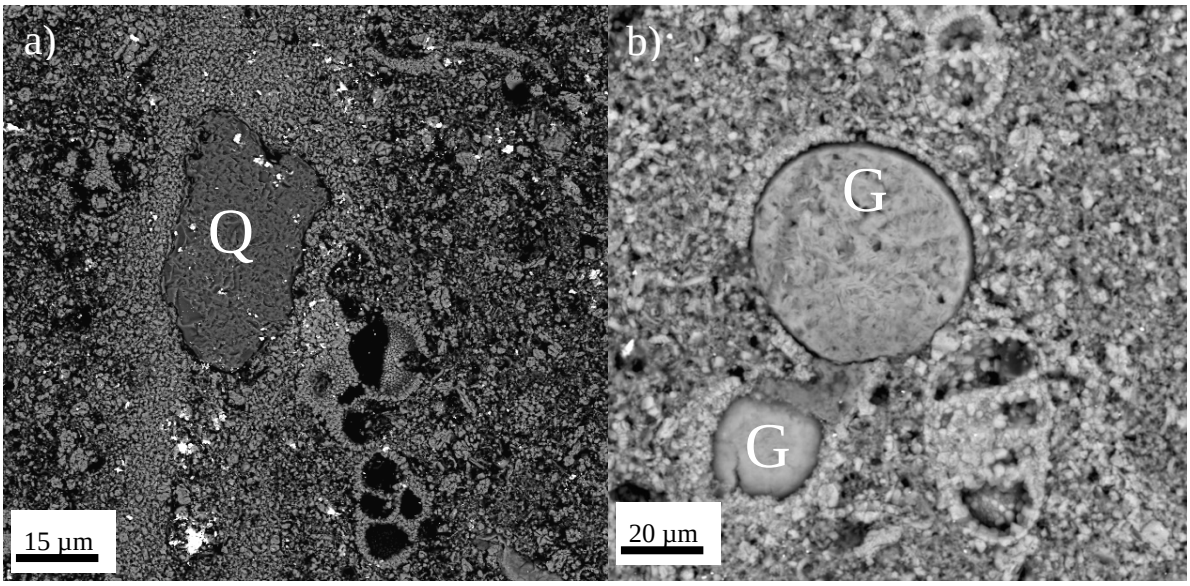

Figure 31. a) Quartz grain (Q) inside the artificial fracture in slice 4. Notice also pore-space inside the skeleton of foraminifera towards the centre bottom of the image. b) Two glauconite (G) grains inside a microfossil

For additional BSE- images, see appendix C.

Classification by MLA was based on a list of spectra used earlier by Dr. Udo Zimmermann on chalk. This list was supplemented by spectra collected from the two samples. In this fine-grained rock, it is not possible to resolve the composition of all minute grains. To be able to discriminate between areas with different concentrations of calcium (Ca), magnesium (Mg), silicon (Si), and aluminium (Al), seven so-called “mixed spectra”, which do not correspond to a specific mineral, rather a mix of minerals, were collected in addition to known minerals such as calcite, magnesite, quartz, glauconite, clay minerals, and feldspars (Figure 32). The names of the mixed spectra are denoted to reflect the content of each element present. The two listings Magnesite_Ca and Magnesite-mix, are spectra with very high concentrations of magnesium, which were not found in the samples of this study.

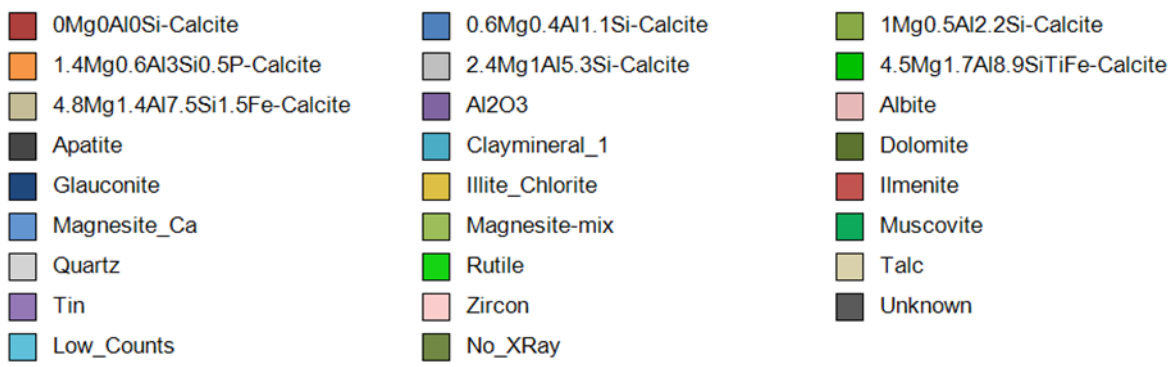

Figure 32. List of all spectra used for classification in MLA maps

Along the fracture, three areas of approximately 1000 by 1500 µm were scanned over approximately four hours per scanned image. The images are 1431 by 743 pixels, resulting in a resolution between 1 and 1.4 µm per pixel.

As an attempt to enhance the differences in composition throughout the sample, the mixed spectra were grouped by the use of the software "Dataview". Different groupings proved to display the chemical and textural differences in different ways. In the best one, the seven mixed spectra were divided into two groups of high and low magnesium content (Figure 33). Silicon- and aluminium-content corresponds in most of the spectra to the magnesium content. For ungrouped MLA images and EDS spectra see Appendix D.

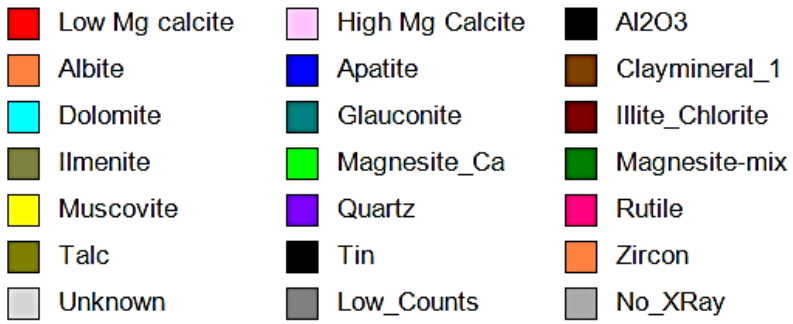

Figure 33. Legend for MLA images with grouping between high and low Mg content, where spectra containing less than 1 wt.% is grouped as Low Mg calcite and all above 1wt.% as High Mg calicte

Colours were chosen so that red includes all spectra with Mg content of 1 wt.% and below, including pure calcite. Pink was chosen to represent all spectra with Mg content over 1 wt.%.

White colour shows areas of unknown composition and represents in most cases pore-space. In the three images in Figure 34 the magnesium content has a higher value inside the fracture itself than the surrounding matrix. There is also a distinct difference in magnesium, silicon and aluminium content between the area below the fracture, with high concentrations, and the area above, with lower concentrations.

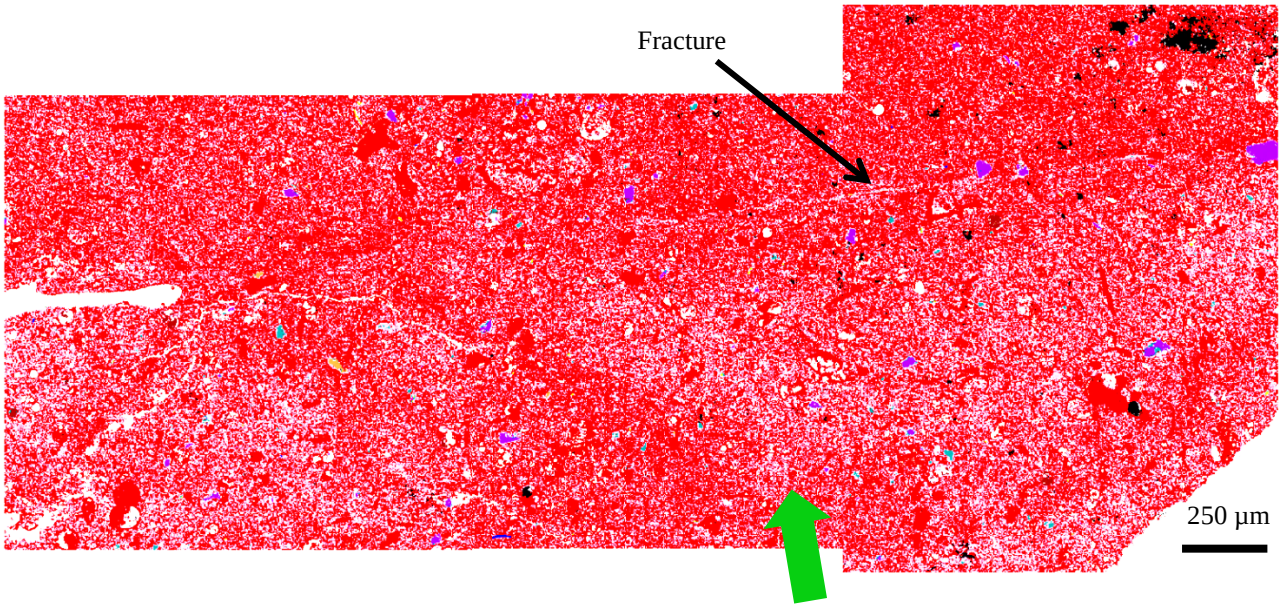

Figure 34. MLA image of the artificial fracture in slice 4 with focus on different magnesium concentration. Notice how the Mg content is higher (pink) below the fracture compared to above (red). Green arrow indicates flow direction. For legend please see Figure 33

4.3.2 Natural fracture

The natural fracture, running along with the fluid flow, was approached in the same way as the artificial fracture when studied with SEM-BSE and MLA. BSE-micrographs were taken of the fracture along the length of the sample, measuring approximately 1 cm, and joined to create a continuous image of the fracture (Figure 35).

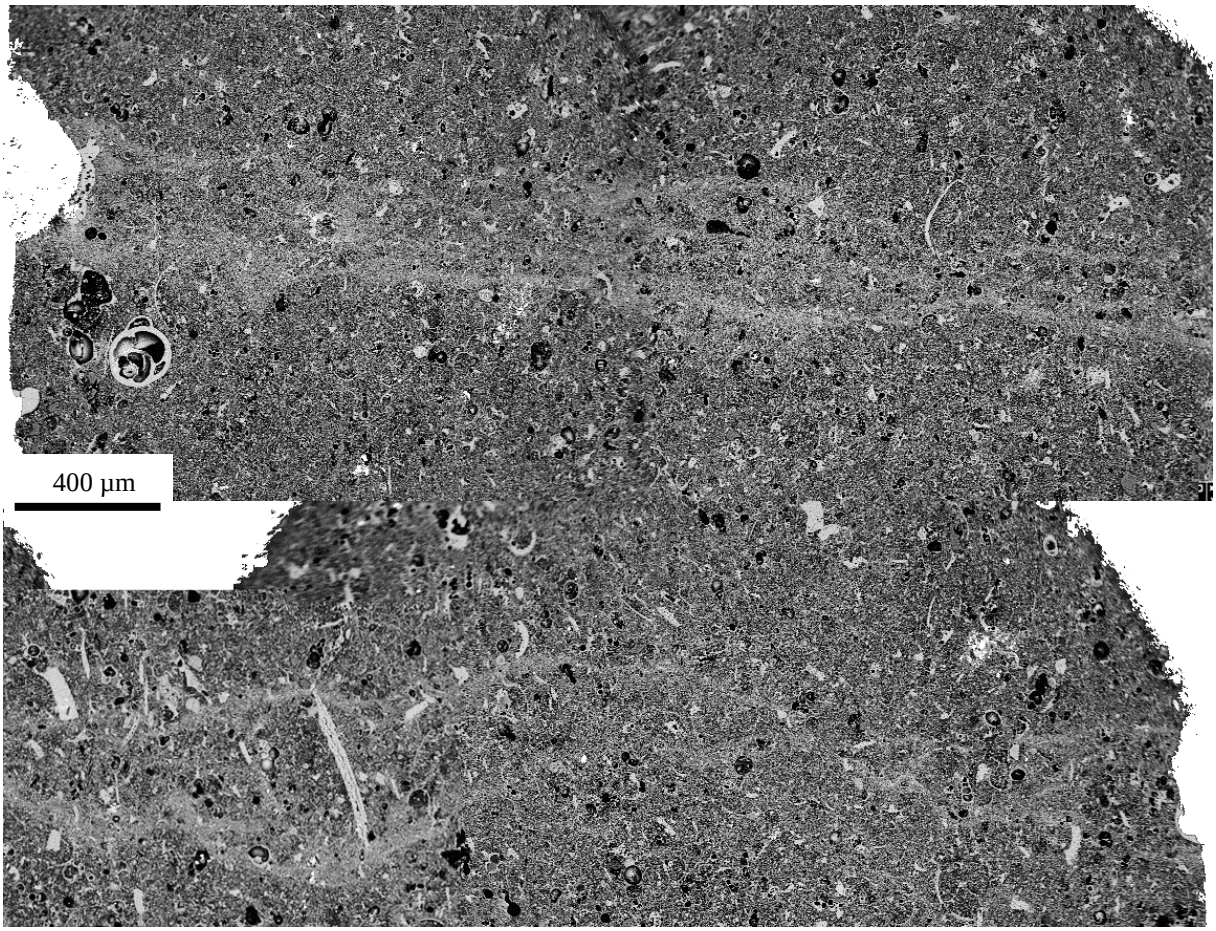

Figure 35. SEM-BSE micrograph of the natural fracture in slice 5. Upper image showing the bottom of the study area in Figure 19, below; top of the study area

As in slice four, shells of macrofossils and microfossils stand out from the image with a higher intensity, representing a higher AAN or lower porosity. The fracture itself, is not as visible as the artificial fracture, and, does not show the same abrupt change in greyscale. In the natural fracture, it can be observed that variations in grayscale and hence mineralogy have a more transitional nature (Figure 35). The rim of the fracture has a brighter shade of grey, compared to the centre of the fracture (Figure 35). As observed with SEM-SE micrographs of the unpolished surface (Figure 22), this fracture has "healed" in a very different manner than the artificial fracture.

In the sample, there are several large foraminifera as well as small and large fragments of shells from macrofossils floating the fine-grained matrix (Figure 36). In addition, there are

clastic grains present in the sample, such as quartz (Figure 36) and muscovite. The quartz or chert grain seems to have grown inside a shell of a foraminifera, or embedded there after the death of the organism.

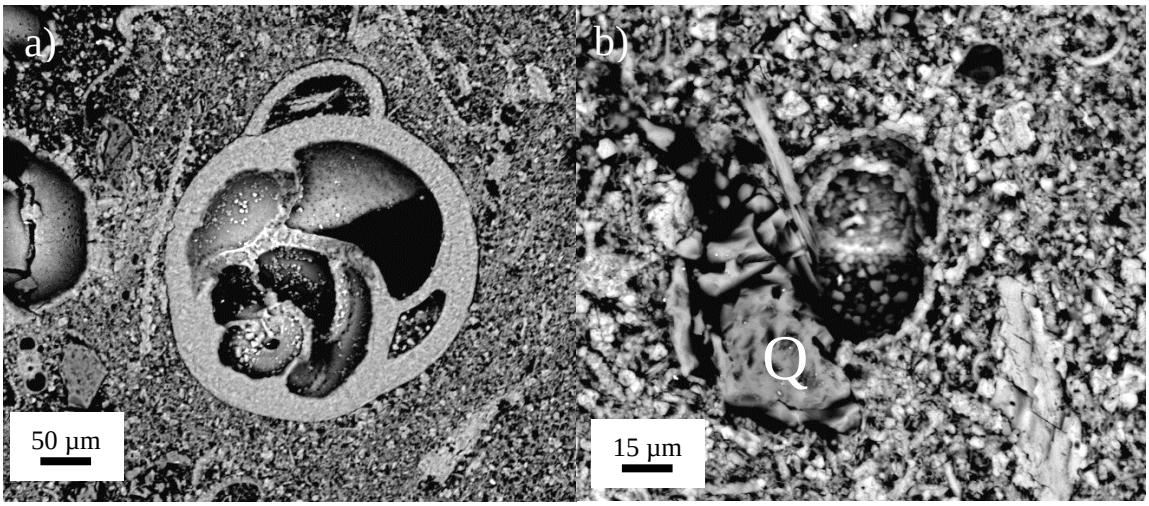

Figure 36. a) An over 100 µm in diameter foraminifera shell and parts of marcrofossils floating in the matrix and b) Quartz grain (Q) inside a foraminifer fossil of slice 5

For additional BSE- images, see appendix C.

Classification by MLA scanning was done using the same database as for slice 4. In all, six images were scanned along the fracture, each for approximately four hours. The size of each image is 1431 by 743 pixels, where the area scanned is 1764 by 1470 µm. This results a resolution between 1.2 and 2 µm per pixel.

To enhance the differences in magnesium content, MLA images were grouped in the same manner as with the artificial fracture, showing the three lowermost values of magnesium content in the spectra in red, while the three spectra with highest content of magnesium is coded in pink (Figure 37).

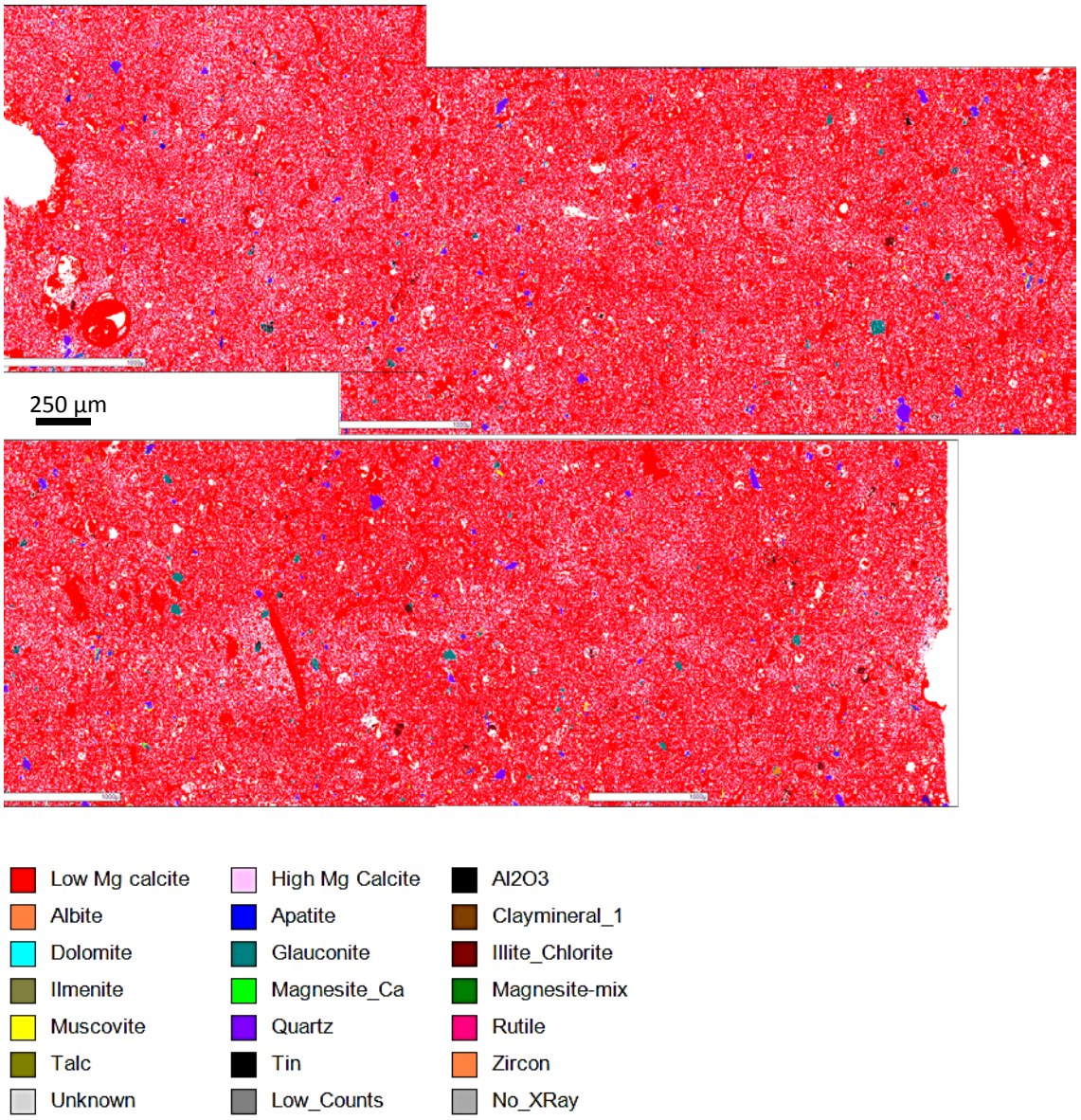

Figure 37. MLA-images of the natural fracture in slice 5 with focus on magnesium content. Notice how the fracture itself has a higher Mg-content (pink) than the surrounding matrix (red)

The MLA-images of the natural fracture shows, naturally, the same pattern as the BSE images. The fracture is not as noticeable as the artificial fracture, and the contrast in magnesium content are not as high. The high- and low-magnesium spectra blend together in more transitional fashion. However, it is possible to see some clear patterns. As in slice 4, shells of micro- and macro-fossils stand out as to have very low magnesium content. Even pure calcite is common in some areas, while the matrix of the rock has a mixture of high and low magnesium content.

The fracture itself does not stand out in all the images, but by careful examination, it is possible to see that the core of the fracture has higher magnesium content, while the rim of the fracture seems to be enriched in calcium. This is quite clear when comparing the images with the SEM-BSE micrographs (Figure 38 a), where the denser area with a higher grey-level in the SEM-BSE micrograph coincides with the higher calcite/lower magnesium concentration in the MLA scan (Figure 38 b).

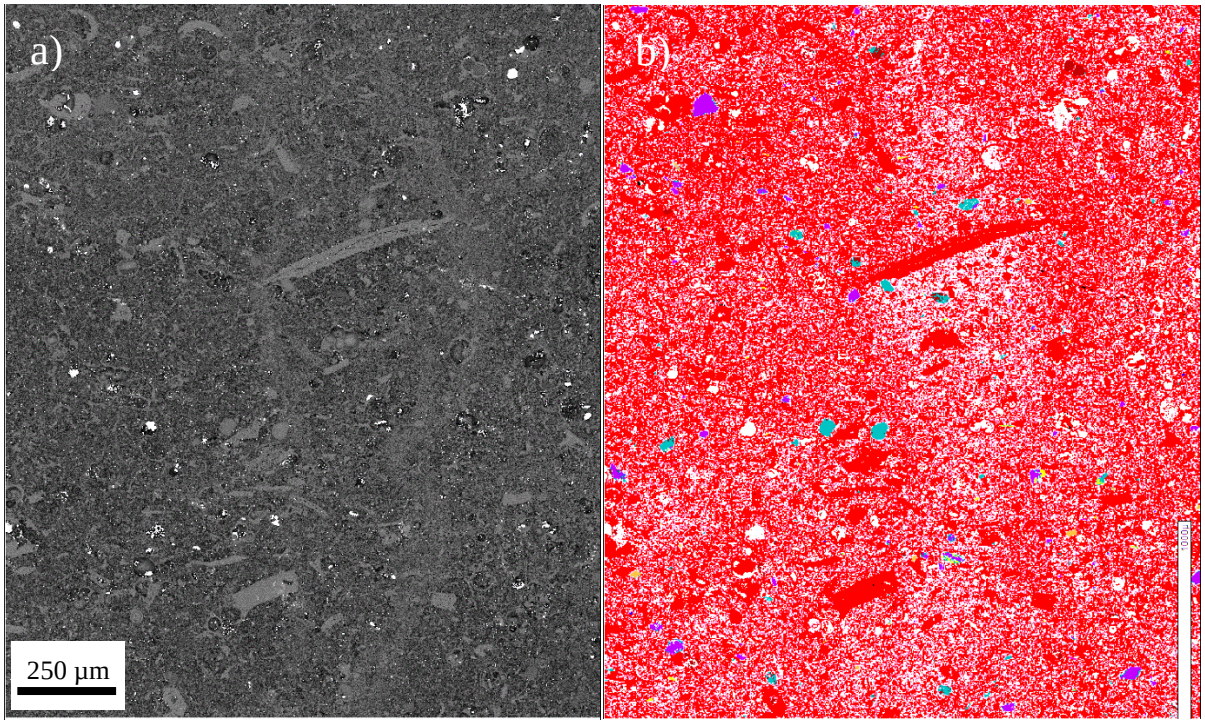

Figure 38. SEM-BSE micrograph (a) and MLA scan (b) of the same area of the natural fracture in slice 5. The Mg-content is higher on on the concave side (below) of the shell than on the convex side (above). For legend, see Figure 37

In the middle of the fracture in Figure 38 a shell from a macrofossil is embedded. There is a clear difference in the magnesium content between the concave (below), with higher magnesium content, and the convex (above) side of the shell.

4.4 Nano Secondary Ion Mass Spectrometry (nanoSIMS)

After MLA scans analyses of both fractures, the samples were further analysed by nanoSIMS. Areas interpreted to be of highest interest were chosen to be studied at a higher resolution

than what is possible to obtain with MLA scanning and SEM analyses. As analyses by nanoSIMS are a time consuming process, analysis of the complete fractures was not an option. In nanoSIMS analyses, different ions react differently when sputtered by the ion beam and counts per pixel are not directly related to the amount present of the element at that spot. Intensity of nanoSIMS images should therefore not be compared between the elements measured, rather than looking at the relative differences within one element-image.

4.4.1 Artificial fracture

The goal to study this sample was to investigate the possible variation in element concentration below, inside, and above the fracture. Three areas along the fracture were chosen (Figure 39). For each of these areas, three scans of 55 by 55 µm were performed, one below, one inside and one above the fracture. Attempts were made to scan areas which partly image the fracture and partly image the surrounding matrix. Several images were obtained, however, only selected images and elements with informative data will be shown here. When referring to elements with regards to nanoSIMS analyses, the author refers to the measured ions as listed in section 3.6, page 27 (e.g. Ca and calcium refers to $^{40}Ca^{16}O$).

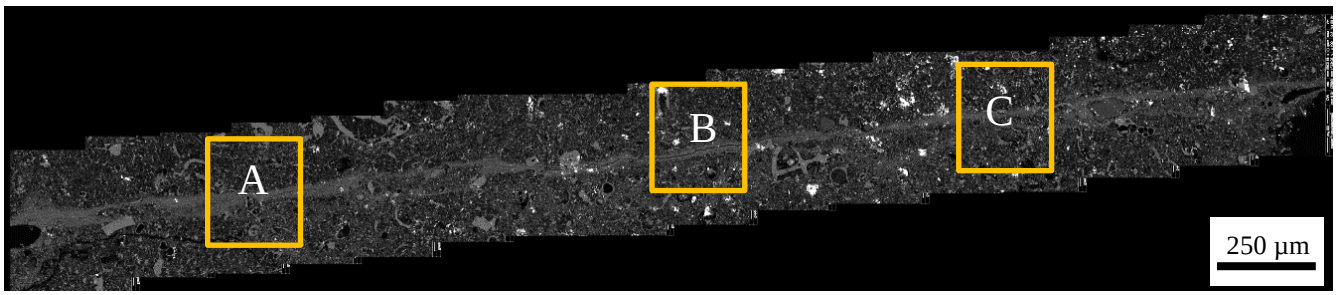

Figure 39. SEM-BSE image of the three areas along the artificial fracture in slice 4 chosen for further investigation

Figure 40 shows the content of Si, Mg and Ca in the fracture in area A (Figure 39). For two of the elements, Si and Mg, there seems to be a higher concentration of the element inside the fracture itself. However, this trend is most visible for magnesium (Figure 40 b).

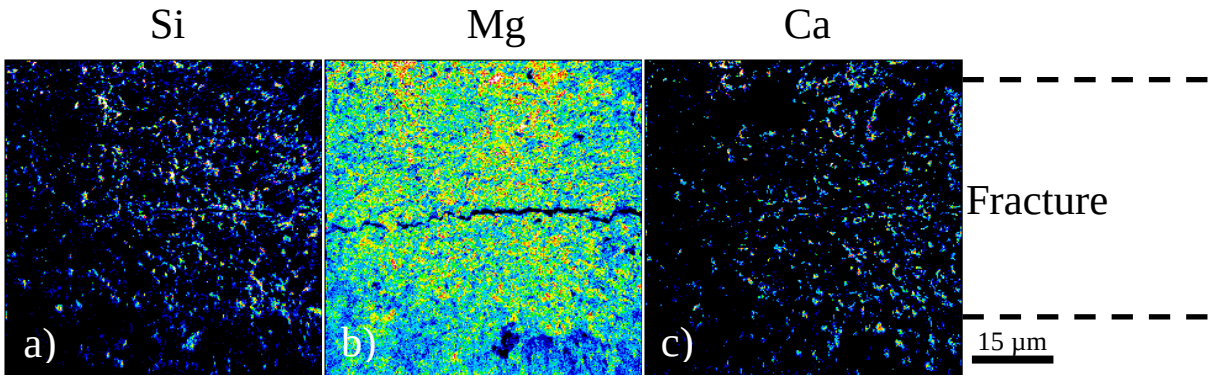

Figure 40. 55 by 55 µm nanoSIMS images of area A, Figure 39, displaying a) Si-, b) Mg- and c) Ca-concentrations inside the fracture. There is an increased concentration of Si and Mg in the fracture.

In area A, a 12 hour non-stop depth scan of 10 x 10 x 1 µm was made inside the fracture (Figure 41). In the top layer (Figure 41 a-d) we see the empty fracture running in the middle of each image. In the middle top, circled in red, there is a circular area with none of the elements present. This is interpreted as a pore. Further down, encircled in yellow, there are two circular objects of approximately 2 to 3 µm in diameter. These have a high amount of calcium (Figure 41 c) and magnesium (Figure 41 b), and resemble the image of two coccolith rings. It is to be observed that they contain no silicon (Figure 41 a). When studying Figure 41 d, the composite image, it is observable that the magnesium (green) is placed inside the calcite in the coccolith ring (red). After sputtering approximately 100 nm deeper into the sample (lower row of images Figure 41 e-h), there is no longer magnesium present in the two rings, only calcium. Only a small spot inside the right ring still contain magnesium.

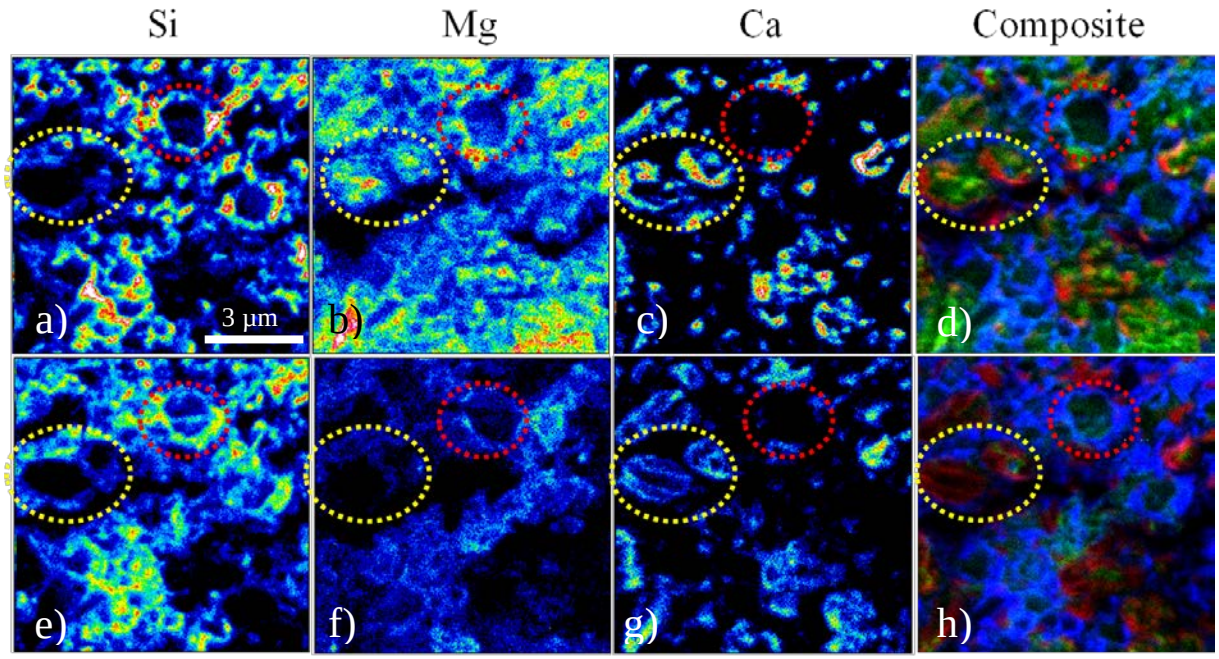

Figure 41. NanoSIMS-depth-scan of the artificial fracture in slice 4. Images d and h; composite images showing: Red; Ca, green; Mg and blue; Si. Top row: first layer, bottom row: approximately 100 nm into the sample. Elements displayed: a and e; Si, b and f; Mg, c and g; Ca

When studying the other end of the fracture (Area C, Figure 39), it may be observed that the fracture itself has a higher content of Si, Mg, and Al compared to the surrounding matrix (Figure 42).

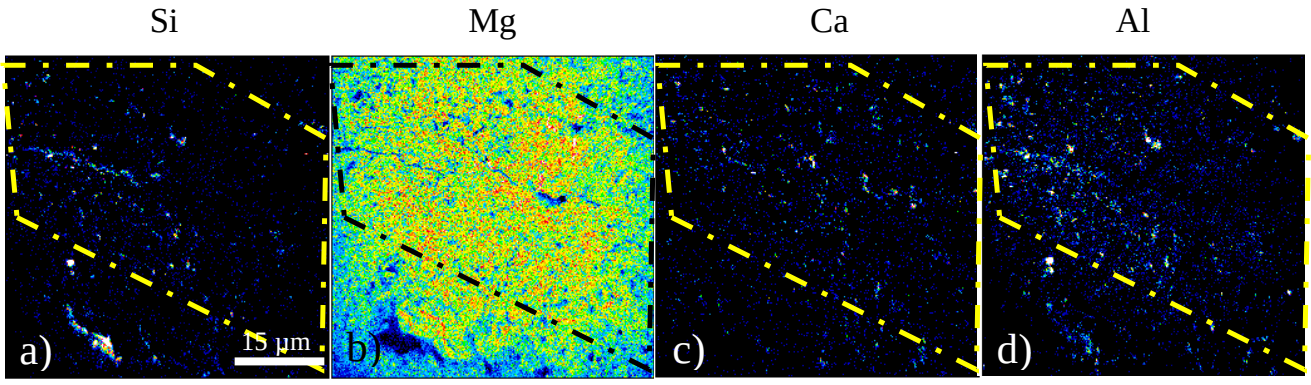

Figure 42. 55 by 55 µm nanoSIMS-scans of the fracture in area C. Showing a) Si, b) Mg, c) Ca, and d) Al. Yellow/black line indicating the fracture with increased concentrations of Si, Mg and Al

Another area of the same size was scanned above the fracture. In this image (Figure 43), we do not see any particular trends with regards to changes in relative element concentration, but it is possible to identify one grain which stands out from the matrix surrounding it. This grain

has a higher concentration of silicon, sodium, and aluminium compared to other phases of the image, and is interpreted as a feldspar grain.

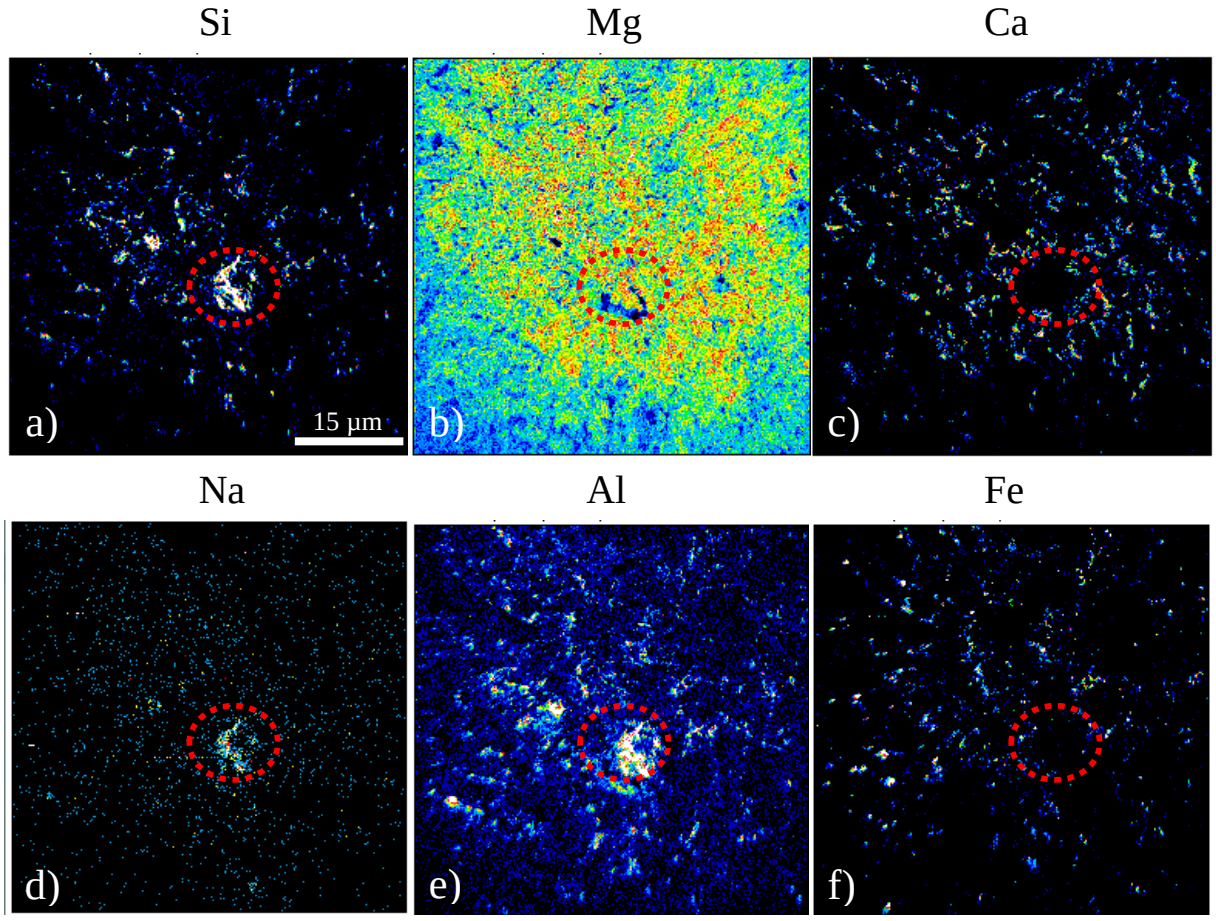

Figure 43. 55 by 55 µm area scanned by nanoSIMS above the fracture in area C. Elements displayed: a) Si, b) Mg, c) Ca, d) Na, e) Al and f) Fe. The combination of elements present inside red circle is interpreted as a feldspar grain

4.4.2 Natural fracture

Based on the observations from MLA analyses, the most interesting areas of the natural fracture was found to be the area in the vicinity of the shell embedded in the fracture with different ratios of magnesium vs calcium on the two sides of the fluid flow. In addition, analyses were taken on the edge of the fracture in an attempt to study the concentrations of the relevant elements inside and outside the fracture. Area D, E and F, were selected for investigation (Figure 44)

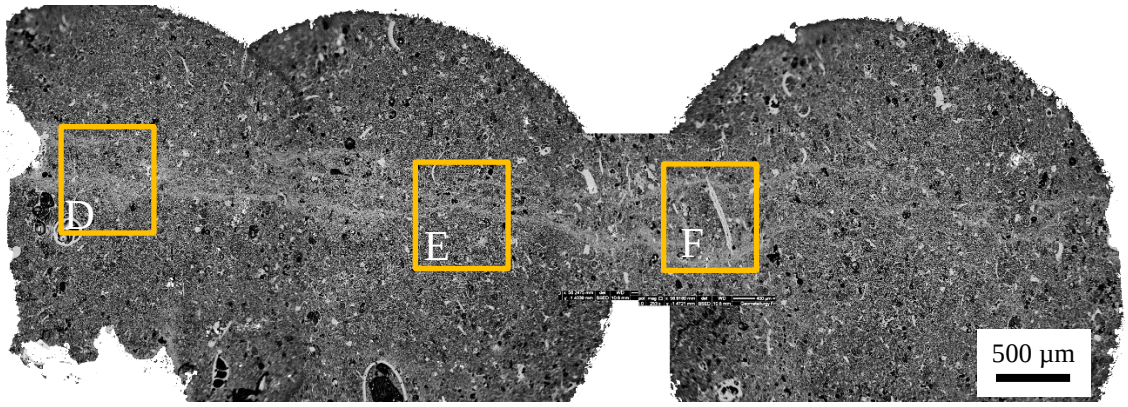

Figure 44. SEM-BSE image of the three areas chosen for further analyses in natural fracture in slice 5

In Figure 45 we see a close-up of the first area of interest in slice 5 (Figure 44 F). Scans were made in four areas at the edge of the shell to study the differences in elemental concentration between the shell and the matrix surrounding it, as well as differences in contrast between the concave and the convex side of the shell as seen in the MLA analyses.

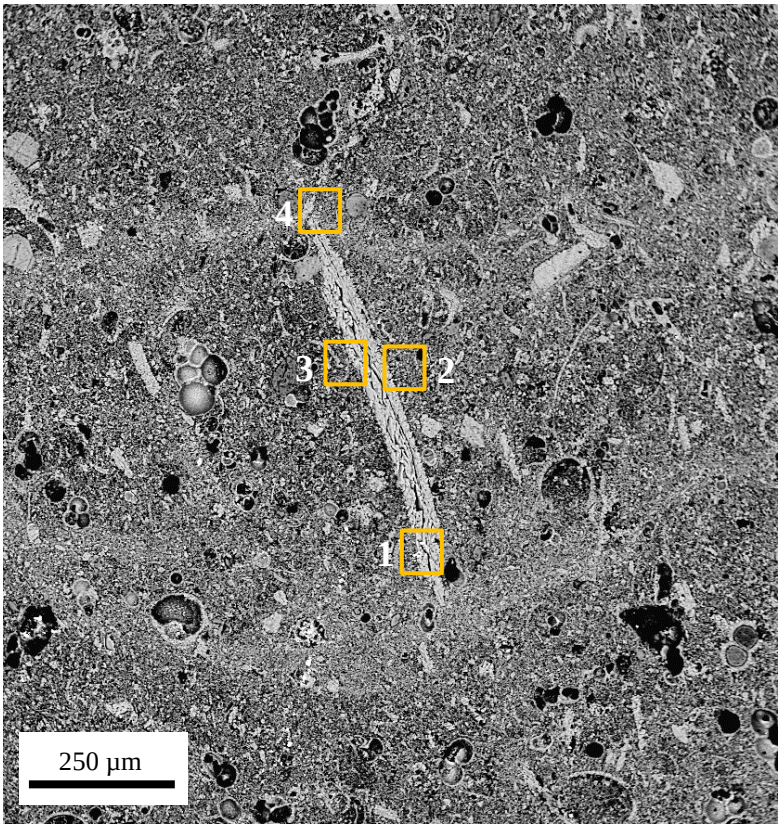

Figure 45. Close-up of SEM-BSE image of area F in slice 5. Squares 1-4 indicating areas of investigation

At the bottom tip of the shell (Figure 45, square 1) , it can be observed that there is still a high content of calcium in the shell itself, followed by depletion in silicon, sulphur, and aluminium levels (Figure 46). Phosphorous is close to absent in the shell. In the middle of the shell, there is a void filled with a higher concentration of calcium as well as silicon.

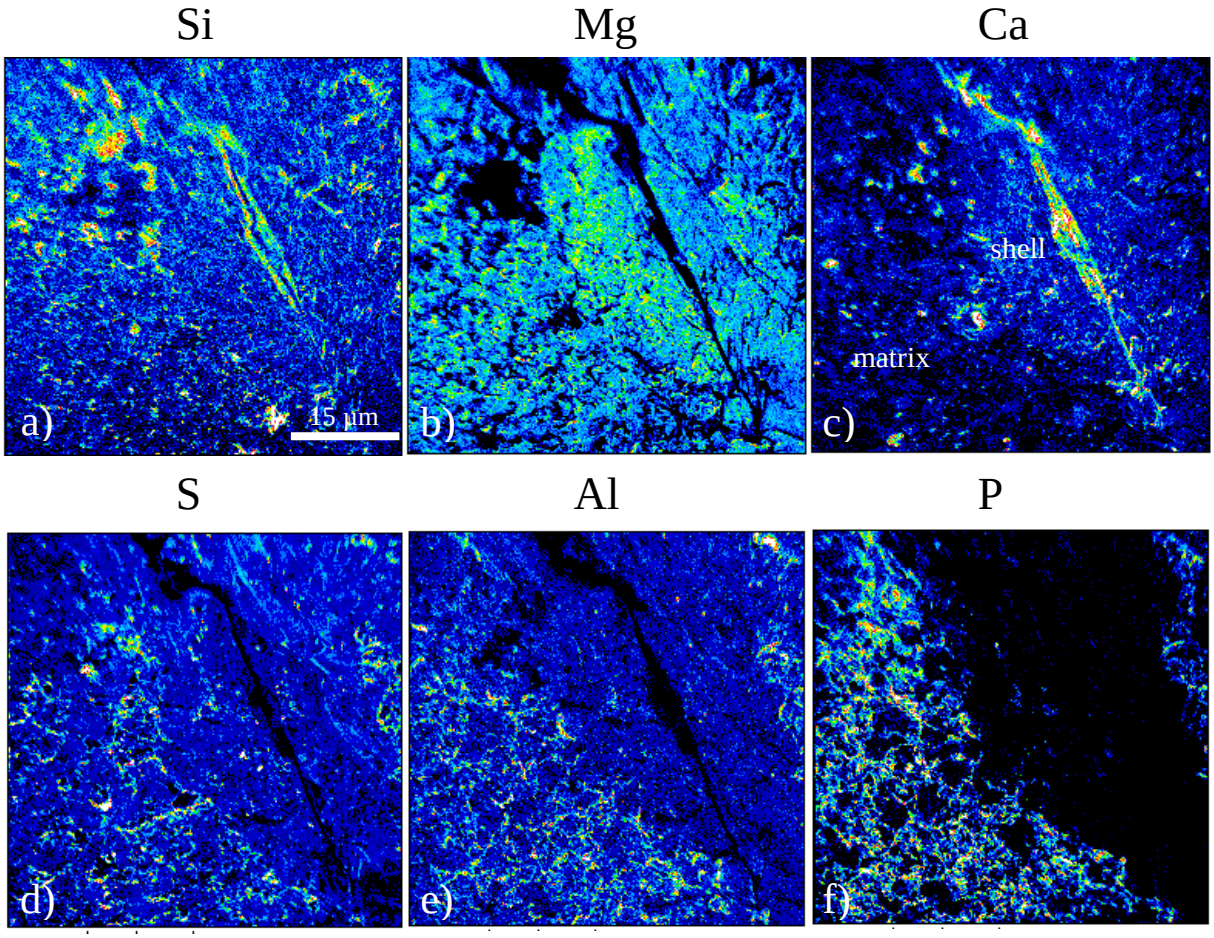

Figure 46. NanoSIMS images of the elemental composition for the top of the shell in Figure 45. a) Si, b) Mg, c) Ca, d) S, e) Al and f) P. All elements show depleted values inside shell except for Ca (c)

Along on the shell, two areas were scanned, one on the convex side (Figure 45, square 2) and one of the concave side (Figure 45, square 3) of the shell. The images contain part of the shell together with the matrix, both inside the fracture centre.

On the convex side of the shell (Figure 45, square 2), it is immediately visible that there are differences in the relative elemental concentration. There is a higher content of calcium in the shell, while the other measured elements are generally depleted (Figure 47). In addition, in the

top right corner, there is a mineral filling part of a pore. The pore contains both magnesium and calcium, but no silicon, aluminium or phosphorous. In the composite image (Figure 47 f), combining the images of Ca (red) and Si (blue), it can be observed that the Si is only distributed in the open space of calcite in the matrix, and not present in the shell.

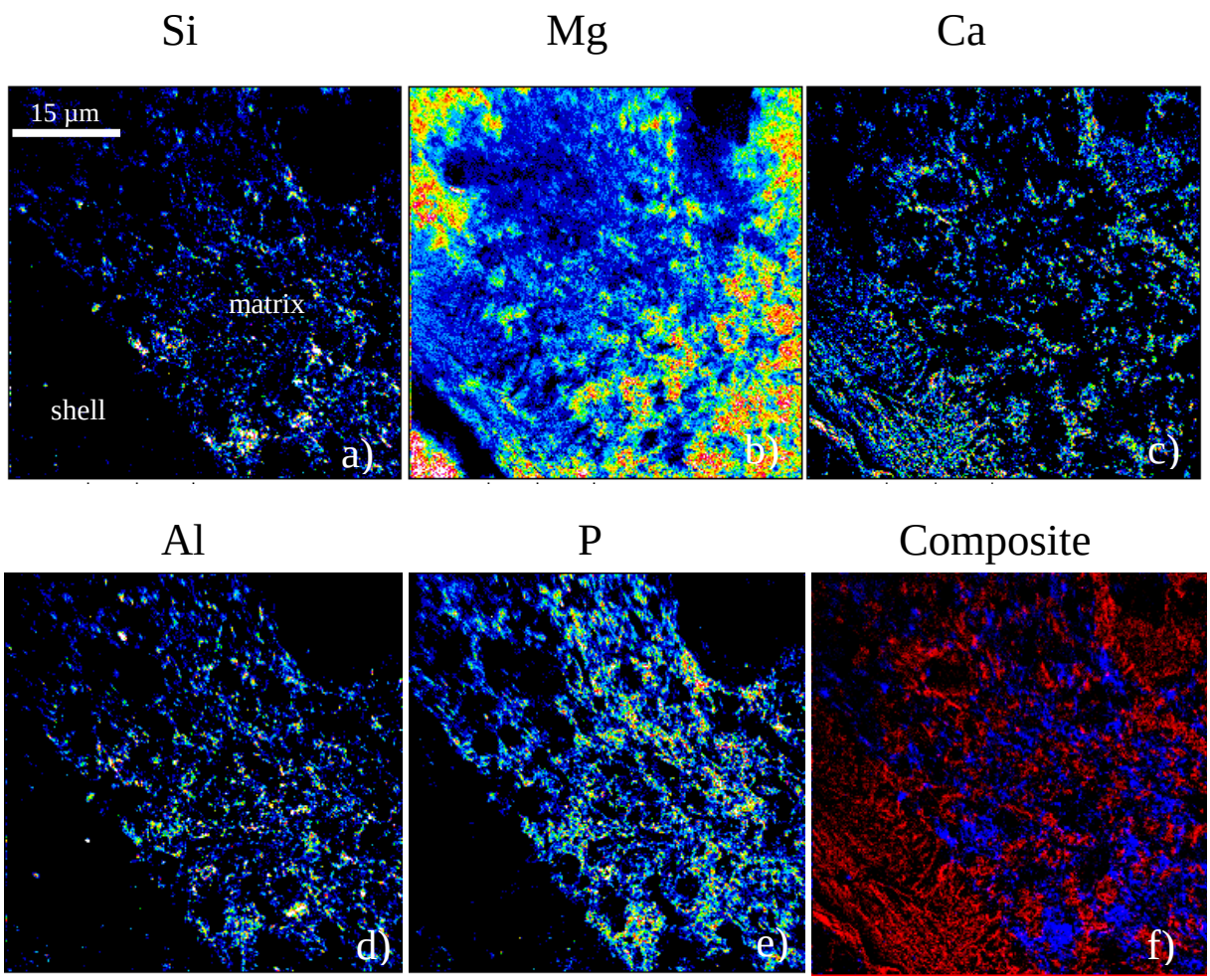

Figure 47. NanoSIMS images of the shell and matrix on the convex side of the shell. Elements: a) Si, b) Mg, c) Ca, d) Al, e) P and f) composite image showing red: Ca and blue: Si. Notice the absence of Si, Al and P inside the shell

In the area of the concave side (Figure 45, square 3), it is difficult to substantiate any changes in element values between the shell itself and the matrix below and to the left. In Figure 48 it can be observed that for all elements, except for silicon and phosphorous, there is no significant difference between the shell and the matrix in relative elemental concentration.

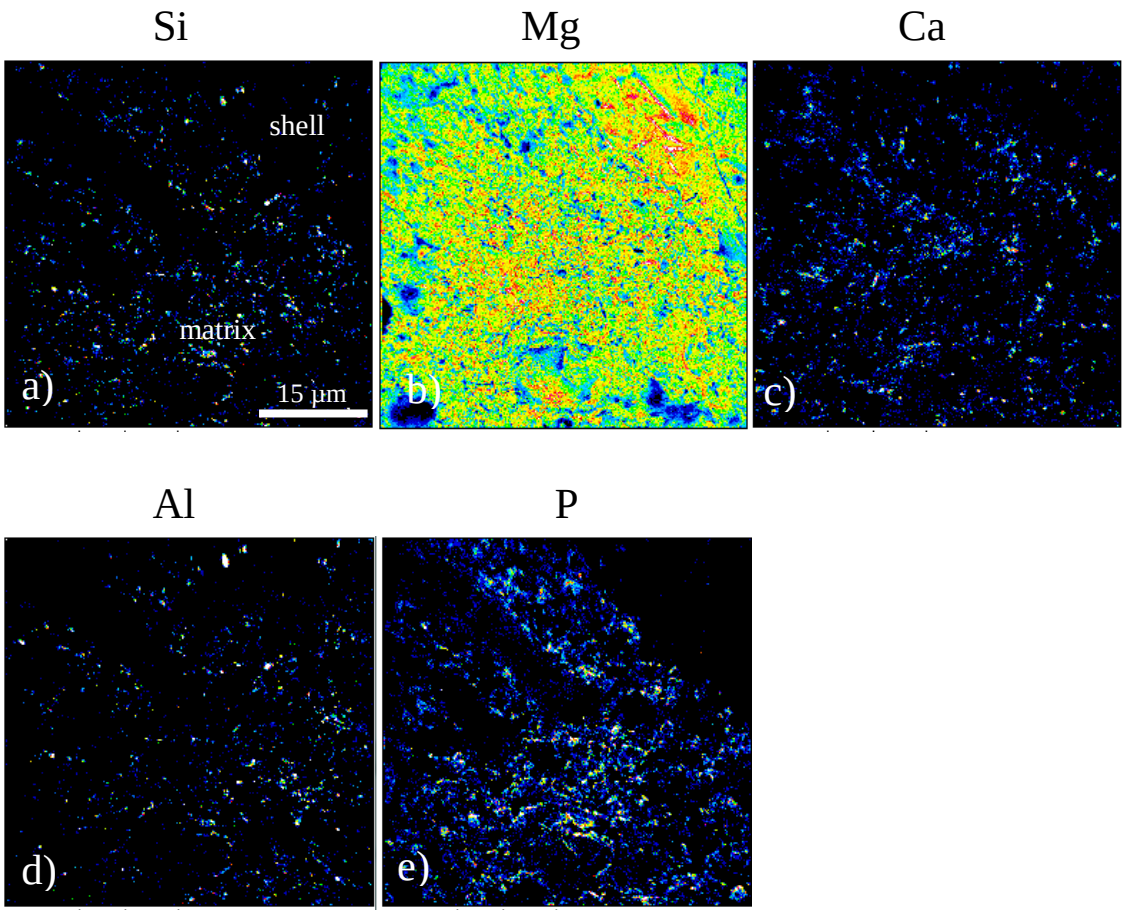

Figure 48. NanoSIMS images of part of the shell and the matrix on the concave side of the shell. Elements: a) Si, b) Mg, c) Ca, d) Al and f) P. It is for this image difficult to observe any elemental differences between the shell and the matrix, except for Si and P

Two more areas showed interesting results from nanoSIMS analyses. Both are made in area E, Figure 44, one inside (Figure 49) and one outside (Figure 50) the fracture. Both images show a clear contrast in composition between the shells of micro and macrofossils to the matrix. It is clear that in both examples, the shells constitute of nearly only calcium and oxygen (in regard of the elements scanned). Together with carbon, this would correspond to pure calcite. In the skeleton of the foraminifera in Figure 49 the absence of all other scanned elements, such as Si, Mg, Fe and Al, is remarkable. The same is the case for the piece of shell from a macrofossil in Figure 50. However, the contrast of magnesium between the shell and the matrix seems to be much lower outside (Figure 50) the fracture than inside (Figure 49), pointing to a higher magnesium concentration in the matrix inside the fracture compared to the outside.

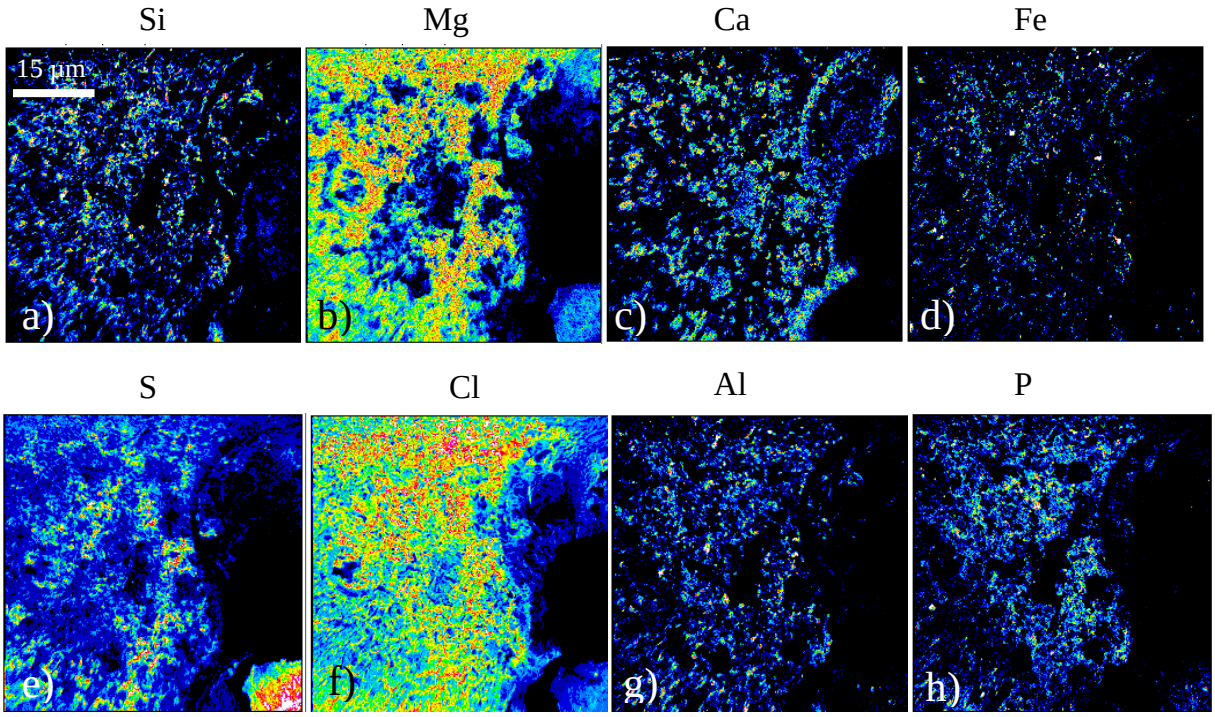

Figure 49. NanoSIMS images of area E, scanned in the matrix inside the fracture in slice 5. Elements: a) Si, b) Mg, c) Ca, d) Fe, e) S, f) Cl, g) Al and h) P, showing the absence of all elements scanned except for Ca in the shell of a foraminifera

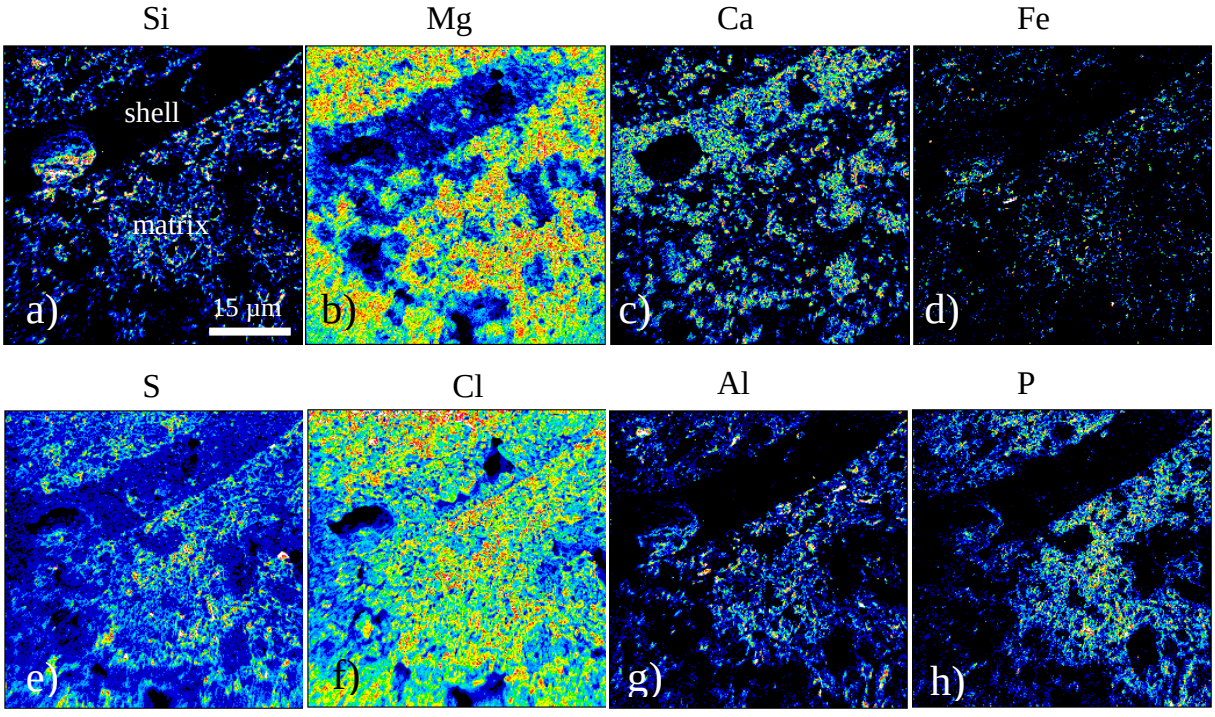

Figure 50. Matrix scanned by nanoSIMS outside the fractured area in slice 5. Elements: a) Si, b) Mg, c) Ca, d) Fe, e) S, f) Cl, g) Al and h) P, showing the depletion of all elements except Ca inside the shell

In Figure 50, there is also visible a grain assumingly made of silicon and oxygen, inside the shell at the top of the image, most likely quartz.

Inside the fracture, next to the embedded shell (Figure 44, area F), another 12 hour non-stop scan of an area of 10 x 10 x 1 µm was done (Figure 51). In this image it is easily observed how Ca is present on some areas, while other areas have a combination of at least Si and Mg. In the composite image, Figure 51 d, it seems like in some areas there is calcite grains (red), while in the other areas (blue and green) a mix of Si and Mg is found, possibly representing clay minerals.

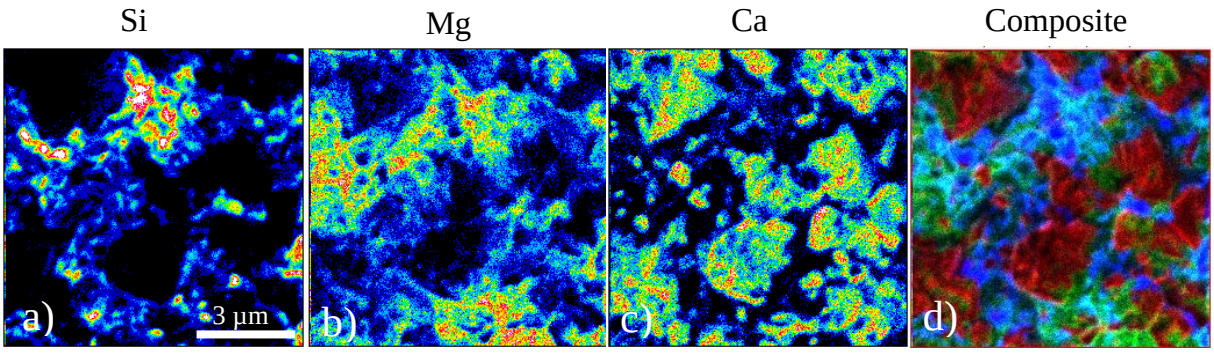

Figure 51. 10 x 10 µm scan inside the fracture in slice 5. Elements: a) Si, b) Mg, c) Ca, d) composite; red: Ca, Green: Mg, and blue: Si displaying the distribution of Mg and Si vs Ca, indicating possibly clay minerals in the pore-space between calcite grains

5 Discussion

5.1 Precipitation of minerals

SEM micrographs clearly show an increase in clay-minerals present in the artificial fracture. In the same images, individual nano- and micro-fossils are no longer distinguishable in the fracture. This may indicate that the fracture consists of newly grown crystals of calcite or Mg-rich carbonates together with precipitated clay. The increase in clay-minerals seems also to be true for the natural fracture, however it is not beyond doubt. These former observations are verified by the increase of Si and Al measured by EDS. Unpublished work at UiS shows that in chalk core flooded with synthetic seawater (SSW), with a hole drilled through the centre, parallel to fluid flow, clay precipitates at the wall of the hole. The area nearest to the hole has a brighter colour, a corona surrounding the hole. This area has next to none visible clay-flakes present. The same study also shows presence of Mg-bearing grains in the drilled hole, possibly magnesite or Mg-rich carbonate. These observations point to dissolution of primary silicates (clay) and calcite, coupled with precipitation of clay minerals and Mg-rich carbonate.

Together with the above-mentioned study, the observations of **this** study indicate that when flooding with SSW, dissolution and precipitation processes plays an important role. The enrichment of clay minerals in the fractures show that formation of clay minerals occur, and preferentially in favoured areas such as fractures, where the stress-regime is different from the un-fractured part of the core. Opened fractures leave room for new-growing material. In fractures, the concentration of ions in the fluid may be altered, possibly to a state further away from equilibrium, thus enhancing precipitation. This may be comparable to the natural occurring formation of stylolites through pressure dissolution, commonly found in chalk. This process may not be fully understood in detail, but as open space is created by dissolution of minerals, precipitation and accumulation of insoluble minerals such as clay minerals and silicates take place in the void. The process is controlled by the effective burial stress and

precipitation of minerals is linked to temperature. The initial non-carbonate content of the chalk and the previous diagenesis is also believed to play a major part (Fabricius & Borre, 2007).

Another possibility would be transport of clay-flakes within the core; however, this seems unlikely, as the clay in some cases have a size larger than the pore-throats of the rock and cannot be identified in these abundances further into the core towards the outlet.

Due to the size of the clay flakes, it is not possible to identify what type of clay or nano-sized-silicates grows in the fracture. Grain-sizes of one µm and below are too small to be resolved by both SEM- and MLA-analyses. NanoSIMS possess this resolution, but as this method is a qualitative method it is not able to quantify the element present in a grain, such that two types of clay-minerals may be distinguished from each other. Possible candidates for the clay-minerals present may be talc ($Mg_6[Si_8O_{20}](OH)_4$) or Kaolinite ($Al_4[SI_4O_{10}](OH)_8$), according to semi-quantitative data of the EDS. Interestingly enough, no anhydrite ($CaSO_4$) was observed in these samples of the core. This is commonly found when flooding chalk with SSW at high temperatures (Madland, et al., 2011). In 4.4.1, Figure 41, grains containing both Mg and Ca can be observed. The same is also found in 4.4.2, Figure 47. This points to precipitation of Mg-rich carbonate such as dolomite ($MgCa(CO_3)_2$) or Huntite ($Mg_3Ca(CO_3)_4$), as found by Madland et al. (2011), or other Mg-bearing carbonates.

5.2 Accumulation of magnesium, aluminium and silicon in fractures

In MLA-BSE images, the fractures clearly stand out with difference in greyscale compared to the surrounding matrix. The artificial fracture has a brighter shade of grey, representing a higher AAN (Figure 29), and possibly difference in composition. However, the centre of the fracture has a lower grey-level. The relative increase in AAN may be a result of denser

packing of the grains in this area, reducing pore-space, thus reducing the areas represented with low intensity. Recrystallization from high porosity fine-grained chalk to larger crystals or grains would also produce a denser area.

For the natural fracture, there is a “rim” of higher AAN or more dense area on either side of the fracture, varying in thickness and grey-level. Inside the fracture there are areas with lower grey-level representing lower AAN, which may in this case be indicative of a higher magnesium- and silicon-level compared to the surrounding matrix. The areas indicating a higher AAN may also in this case be a result of a denser packing of grains, hence an area of lower porosity. On the exterior of the core, when studying the natural fracture, lineation in the filling material, running along the flooding direction may be observed. This may, however, be results of interplay between the core-holder and the core during flooding, and may not be representative of the rock-fluid interaction inside the core. One may also speculate if this can be a result of soft-sediment deformation due to fluidized grains during flooding under stress (Schneiderhan, et al., 2005).

As an attempt to identify the precipitated silicates as well as spatially map the distribution of elements and minerals in the fractured areas, MLA and nanoSIMS were applied. Zimmermann et al. (2015) show that both MLA and nanoSIMS may be used to identify minerals in flooded chalk cores at high resolution. These are state-of-the-art methods, which have not been used earlier studies on chalk.

When studying the distribution of minerals, by MLA, in and around the fractures, it is clear that the fractures themselves have a different composition than the surrounding matrix. In both, the artificial and the natural fracture, there is an enrichment of magnesium as well as silicon and aluminium. This is compatible with the results from SEM-EDS analyses identifying precipitated clay-minerals and/or Mg-rich carbonate in the fractured areas. As

discussed in section 4.3.1, the resolution of MLA scanning is not high enough to resolve the precise quantitative content of single grains, thus renders it impossible to identify the type of mineral present, beyond doubt. However, the increase in concentrations of Mg, Al and Si would be the typical imprint of an increase in clay precipitates, in addition to possible Mg-rich carbonates or minute particles of magnesite.

In slice 4, as described in section 4.3.1, there is a clear difference in relative elemental concentration of the two sides of the artificial fracture, where the area on the inlet side of the fracture has a higher concentration of Mg, Si and Al (Figure 34). As seen in SEM images, the fracture itself has a much denser grain packing and a high content of precipitated secondary clay minerals. The difference in elemental composition suggests that the fracture running perpendicular to the fluid flow is actually blocking or slowing down the fluid flow or specific, in the here measured, ions in the fluid. This could enrich the concentration of reactive ions and shift the state of equilibrium, and possibly induce enhanced formation of clay-minerals and Mg-rich carbonates. These processes may be important with respect to the mechanical properties of the chalk as well as the effective permeability of the core, as studies have shown relationship between chemical alteration and compaction in flooded chalk cores during non-equilibrium brines (Nermoen, et al., 2015). It also is of importance for modelling of fluid flow in rock material, as the presented results would imply knowledge of the fracturing pattern of the rocks.

The increase in Mg content in the chalk after flooding also agrees with the information gained from similar studies; effluent profiles in chalk-flooding experiments showing retention of Mg^{2+} and production of Ca^{2+} (Megawati, 2015).

NanoSIMS imaging of the same areas confirms the distribution of the elements as seen with MLA. However, no single grain or flake of clay stands out with an identifiable composition in

any of the fractures. Inside the artificial fracture in slice 4 (Figure 41), we are able to see what looks like individual coccolith rings inside the fracture. This contradicts the observation from SEM micrographs that the filling material of the fracture is newly crystalized carbonate. The same nanoSIMS depth-scan, reveals that the coccolith rings contain magnesium in the first layers, but when sputtering approximately 100 nm into the grains, they become pure calcitic. This could point to a partial transition towards magnesium bearing carbonate, preferentially through solid-state diffusion, i.e. ion exchange. Another possibility is that there is magnesium overgrowth on the calcite surface. Such overgrowth has not been observed in SEM micrographs. However, when studying the top slice of Figure 41, one may see what looks like a nucleus of magnesium in the centre of each of the two coccolith-rings. This rather points to an overgrowth model, more than a diffusion process, coinciding with what Hiorth et al. (2008) proposed; dissolution and subsequent precipitation is the most likely controlling process in these type of flooding experiments. In addition, in Figure 41 d, it seems that the outer part of the grain or coccolith contains calcium, while the centre or overgrowth contains calcium and magnesium. This observation is not in agreement with a solid-state diffusion process, where one would expect the opposite.

In many of the nanoSIMS images contrasts in phosphorous and iron content as well as sulphur and chlorine levels can be observed. These elements are in all examples not present in the micro- and macro-fossils placed inside the matrix. It is important to remember that the nanoSIMS images show only the relative variations within one element, and even though there may be observed differences in concentration, the real values may be very minute. These elements are to very little extent measured by MLA; proving their low abundances. Some of these elements are easily mobilized, and is not initially present in the SSW of which the core was flooded. These traces of elements may therefore be due to small amounts of particles mobilized within the core.

5.3 Flow patterns and significance of texture in fractures

Maybe the most remarkable observation made in this study is how the concentration of Mg and Si vary between the concave and the convex side of the shell-fragment perpendicular to fluid flow in Figure 38. The flow is clearly obstructed by the shell, visible in both SEM-BSE images as well as in MLA-scans. This proves the significance of the composition and texture of the rock in the microscopic rock-fluid interaction. In nearly all larger microfossils and fragments of macrofossils, the shell itself has preserved a close to pure calcitic composition. Although most of the surrounding matrix seems to be affected by the flooding of SSW, the shells seem inert to the flooding agent and more resistant to mineralogical changes. There may be several reasons for this differentiation.

- The size of the carbonaceous particle matters for the chemical stability of the grain. Smaller particles may be more prone to alteration than larger.
- The initial composition of these fossils is different from the finer grained matrix, such as a different Mg/Ca ratio produced by the organism depending on e.g. age, seawater composition and temperature.
- Curvature and surface properties affect the dissolution rates of the initial grains and fossils (Levenson & Emmanuel, 2013).
- The increase in Mg- and Si-concnetration may be due to precipitation of smaller crystals/grains in the pore-space of the matrix or in the fracture where there is more space and the stress state is different.

If all these possibilities would be deciding factors than the composition of chalk is paramount for the fluid movement in chalk. Without the knowledge of the micro-facies, fluid flow is barely predictable even on core scale. It might be possible that over time these criteria are not of significance when massive fluid flow affects the rocks over the span of millions of years. On the other hand, those compositional and textural variations might also be one of several

factors why even rather simple processes like dolomitisation are difficult to model or predict in geological examples, and in such a perspective, it may be possible that texture and facies plays a role at larger scales than the micro-scale observed here.

Furthermore, what seems to be important is that these more competent components (shells) influence the fluid flow through the core and may play an important role to understand the fluid flow and rock-fluid interaction in fractures and chalk in general. As the rock-fluid interaction is one of the key components controlling compaction in chalk during flooding, this observation suggests that depositional facies and fossil composition is an important factor when studying the geo-mechanical behaviour of chalk. Obstruction of fluids may also cause unpredicted high concentrations of elements, which in turn change the equilibrium in the rock and induce rock-fluid processes, as discussed in 5.2.

Not all observations by nanoSIMS match the results from MLA analyses. When analysing the relative elemental composition on either side of the large shell fragment inside the fracture in slice 5 (Figure 38), one cannot observe the same elemental pattern as seen in MLA scans. Based on the MLA analyses it was expected to see a larger contrast in magnesium content between the shell and the matrix on the concave side of the shell compared to the convex side. This is not observable and is most likely due to the scale of observations. To be able to see the differences in mineralogical distribution in MLA scans, one has to zoom out to a smaller scale to see the pattern. At the scale the nanoSIMS operates, local variations of the heterogeneous chalk may produce more detailed results.

5.4 Sealing of fractures

The fractures in this core were both open at the start of the experiment. At the end of the flooding process, they were both healed, and the natural fracture was nearly impossible to

locate. It seems that the sealing minerals mainly consists of magnesium-rich carbonates and clay, but no anhydrite was found, as might have been expected. When discussing permeability of chalk, there is a great difference in matrix permeability and the effective permeability, which in most cases is higher due to fractures in the chalk. If these fractures are sealed by precipitation of new minerals, this could have large impacts on fluid flow through the rock. In an EOR aspect, reducing or influencing the flow pattern through fractures, could mean a significantly more effective sweep of the reservoir. Being able to imbibe water into the low permeability matrix by blockage of the main fluid pathways, could effectively mobilize some of the immobile oil.

5.5 Methodology

One of the objectives of this study is to investigate how well suited the applied methods are for studying flooded chalk cores with respect to chemical and textural alteration.

For the artificial fracture, one gains a lot of data by the use of FE-SEM-EDS. It can easily be observed an increase in clay-flakes as well as in Mg, Si and Al. It is however, not possible to identify which type of clay is present. For the natural fracture, locating the fracture was problematic with FE-SEM-EDS, because of its indistinct nature, justifying the need for other methods of analyses.

MLA analyses prove very suitable for identifying fluid-flow pattern on µm- and mm-scale. In addition, the significance of micro- and macrofossils for rock-fluid interactions is effectively shown in mineralogical maps produced by the MLA method. Resolution of MLA analyses lie in the range of 1.2 to 2 µm, which is unfortunately not enough to precisely identify the clay minerals. Hence, the need for a tool with higher resolution is obvious.

NanoSIMS is a high-resolution tool to confirm the presence of elements in a material. It is a time-demanding method and navigation to a pre-defined area may be troublesome. However, with targeted use, very useful information may be gathered. NanoSIMS confirms in most cases the information found by MLA analyses, but may in other circumstances not be able to reproduce the same data. This is most likely due to scale-dependencies. Very educational is the data gathered in the depth scanning of the artificial fracture (Figure 41). The scan shows that what appears to be two coccolith rings which consists in the first 100 nm, of magnesium and calcium, with silicon absent. This suggests partial alteration from calcite to magnesium-bearing carbonate or small grains of magnesite. Deeper into the two rings, they nearly only contain calcium and oxygen, and most likely carbon, which is not measured in the process. It is clear how these methods complement each other and have their clear advantages on different scales (as discussed in section 5.3). With the results gained in this study, the author states that they are indeed suitable as state-of-the-art methods to study rock-fluid interactions in fractured chalk cores for EOR purposes.

5.6 Reliability of the data

When working with the described methods, it is important to question the data reliability. One should be aware of any circumstances, which may affect the results. In this study, the certain factors should be assessed for their reliability.

Firstly, it should be acknowledged that all analyses were done post-flooding, and one cannot beyond doubt say that the results are not affected by the heterogeneity of the rock prior to flooding.

The samples were polished to create a flat surface for better quality measurements before MLA and nanoSIMS analyses were carried out. Such preparation processes could in theory

affect the texture and composition of the sample. The data show however, patterns which do not agree with what should be expected from such artefacts, at least not on the larger scale. Another aspect to consider when studying polished surfaces, are how well the machines are able to image the different constituents present in the sample. All larger fossils and coccoliths seem to be preserved, but clay minerals are hard to recognize in a polished surface and are not identifiable like they are when studying freshly broken surfaces by FE-SEM.

When using EDS analyses it is important to remember that there is always a certain error in the measurements. This is related to both resolution and to the nature of electron and x-ray interaction with the sample. EDS is a semi-quantitative method, when done on flat surfaces in properly standardized machines, as done in MLA scans. This leaves room for errors in relative elemental composition; hence, interpretation of spectra may also be erroneous, and for the specific issue of the identification of the existing clay minerals here, it is a problematic situation.

In nanoSIMS analyses different ions reacts differently when sputtered by the ion beam and counts per pixel are not directly related to the amount present of the element at that spot. This may in some measurements lead to different intensities between the elements scanned for, but should not be a problem when using the data with care and considering it as qualitative data, and not quantitative.

The flooding experiment was done at an effective stress of 11.4 MPa. This is not necessarily comparable to the state of stress in a reservoir. As onshore chalk has a different burial history than reservoir chalk, it may yield at a different stress level, hence the experiments cannot be carried out at exact reservoir conditions. The flooding rate of the experiment may also not be comparable to the rate used when injecting water in to a reservoir. These factors need to be incorporated when applying the results of flooding experiments in geo-mechanical simulation

and further work. In addition, this experiment was done on a water-wet chalk core. SSW was flooded through the core and the onshore outcrop core has most likely never seen oil. During flooding reservoir chalk by SSW, reactions and rock-fluid interactions may show different behaviour when grains surfaces are mixed-wet or oil-wet, rather than water-wet.

5.7 Further work

This research project has proven that the use of different methods is very useful for gaining more insight in the alteration produced during flooding experiments. It has also been very educational in such a sense that when analysing data after measurements and merging the gathered data, it is possible to determine a methodology for the study of chalk, despite the mentioned possible issues of the methodologies.

As no precise identifications of the clay minerals and what suggests to be minute grains of magnesite or magnesium-bearing carbonate has been possible, further analyses should be done on the samples, such as by field-emission transmission electron microscopy (FE-TEM), which measures texture and chemical composition at a resolution down to nano-meter or even Ångstrom level. Semi-quantitative EDS-measurements may be done with a spot-size 10 – 20 nm. This method may also offer the possibility to further investigate if the processes that govern the chemical and textural alterations in flooded chalk cores are dominated by magnesium-bearing carbonate overgrowth through precipitation and dissolution rather than ion-exchange and solid state diffusion. *In-situ* isotope measurements may be a method which could answer the question, which crystals are newly grown by displaying disturbed oxygen isotope values. Such measurements could be done by the use of a high resolution FE-TEM.

From this study, it is clear that methods for quantification of mineralogical changes is something the research of EOR could gain on in the future. This may be done by the use of a

so-called electron microprobe analyzer (EMPA), applying a wavelength dispersive system (WDS) for elemental quantification. Even though this type of analysis delivers quantitative results, too large spot-size is also for this method a problem.

As the flooded core was reassembled and already cut into slices before this project was initiated, complete control was missing on slices and flooding direction. To test repeatability and to flood chalk cores with other fracture configurations, running additional similar experiments could verify the findings of this study and may help precisely identify the new-grown minerals in flooded chalk. Chalk is very heterogeneous, at least at core and pore scale. This means that local variations in chalk may influence the results in flooding experiments. Normal procedure when studying flooded chalk cores is to compare un-flooded parts of the core with those parts flooded with brines. Such pieces have not been available for this study, so by running new experiments, it is possible to add these types of analyses as well. A step even further would be to introduce fractures in two-phase experiments, where chalk cores are exposed to both injection brine and oil. This could gain valuable information of imbibition and mobilization of oil from the matrix.

It seems that without the knowledge of the micro-facies fluid flow is difficult to predict at core scale. However, it is of importance to perform long-term tests on fractured samples to prove this. A further step should be a comparison of the flooding with samples of reservoir chalk – if those samples are available. This would test the validity of the statements here made based on the dataset of this study that the composition is a defining parameter and predict better if and how these factors influences fluid-flow on field-scale.

6 Conclusion

The results from this study show clearly that chemical and textural alterations do take place when flooding non-equilibrium synthetic seawater (SSW) through an onshore Liège chalk-core with two fracture systems. This is to be expected; however, more interesting is how these mineralogical changes seem to take place in favoured areas such as fractures. The governing processes of alteration are not entirely clear, but nanoSIMS images suggest overgrowth of minute magnesium-rich carbonate grains on calcite surface. In addition, precipitation of clay minerals seems to take place in the fractures. This suggests dissolution combined with precipitation and new growth of minerals to be the most important processes as opposed to ion-exchange due to solid-state diffusion.

Fluid flow through the core is significantly influenced by the fractures as well as the texture of the rock. These are other very important findings of this study. It is clear that microfossils and the shell debris of macrofossils play an important role in the rock-fluid interplay. Differences in magnesium content on either side of the artificial fracture and a shell embedded inside the natural fracture (both perpendicular to fluid flow), proves that these features manipulate the fluid flow and alteration of the core at micro-scale. This implies that heterogeneity and macro- as well as micro-facies in the chalk are important to keep in mind when modelling these effects with respect to EOR. Even though the flow rate is not necessarily comparable to the injection rate into a reservoir, it is shown that after only a short period, fractures are sealed in the core. Sealing of fractures may be important to create a more efficient sweep of injected water through the matrix of the chalk, sealing the fractures acting as “thief zones”, leading water through open pathways in the reservoir.

Through this study, a lot has been learned about chalk and how it can at best be studied to answer the questions related to EOR research. The applied methods work very well to

complement each other and should be part of a toolbox utilized to study rocks in EOR purposes.

7 References

Andersen, P. Ø., Evje, S., Madland, M. V. & Hiorth, A., 2012. A geochemical model for interpretation of chalk core flooding experiments. *Chemical Engineering Science,* Volum 84, pp. 218 - 241.

Austad, T. et al., 2008. *Seawater in Chalk: An EOR and Compaction Fluid.* Dubai, SPE 2007 International Petroleum Technology conference.

Biot, M. A., 1941. General theory of three-dimensional consolidation. *Journal of Applied Physics,* Volum 12, pp. 155-164.

Claesson, J. & Bohloli, B., 2002. Brazilian test: stress field and tensile strength of anisotropic rocks using an analytical solution. *International Journal of Rock Mechanics & Mining Sciences,* Volum 39, pp. 991 - 1004.

Evje, S. & Hiorth, A., 2011. A model for interpretation of brine-dependent spontaneous imbibition experiments. *Advances in Water Resources,* Volum 34, pp. 1627 - 1642.

Fabricius, I. L. & Borre, M. K., 2007. Stylolites, porosity, depositional texture, and silicates in chalk facies sediments. Ontong Java Plateau – Gorm and Tyra fields, North Sea. *Sedimentology,* Volum 54, pp. 183 - 205.

Fandrich, R., Gu, Y., Burrows, D. & Moeller, K., 2006. Modern SEM-based mineral liberation analysis. *International Journal of mineral processing,* Volum 84, pp. 310 - 320.

Felder, W. M., 1975. Lithostratigrafie van het Boven-Krijt en Dano-Montien in Zuid Limburg en het aangrenzende gebied. I: O. S. Kuyl, red. *Toelichting bij de Geologische Overzichtskaarten van Nederland.* Harlem: Rijks Geologische Dienst, pp. 63 - 72.

Garrison, T., 2010. *Oceanography - An Invitation to Marine Science, 7th edition.* Belmont, USA: Brooks/Cole.

Griffiths, J., 2008. Secondary Ion Mass Spectromerty. *Analytical Chemistry,* Volum 80, pp. 7194 - 7197.

Halleux, L. et al., 1985. Mechanical behavoiur of chalk. *North Sea Chalk Symposium May 1985,* Volum 3, pp. 152 - 178.

Handley, J., 2002. Secondary Ion Mass Spectrometry. *Analytical chemistry,* Volum June 1, pp. 335-341.

Heggheim, T., Madland, M. V., Risnes, R. & Austad, T., 2005. A chemical induced enhanced weakening of chalk by seawater. *Journal of Petroleum Science and Engineering,* Volum 46, pp. 171 - 184.

Hiorth, A., Cathles, L. M. & Madland, M. V., 2008. The Impact of Pore Water Chemistry on Carbonate Surface charge and Oil Wettability. *Transport in Porous Media,* Volum 85, pp. 1 - 21.

Hiorth, A., Jettestuen, E., Cathles, L. M. & Madland, M. V., 2013. Precipitation, dissolution, and ion exchange processes coupled with a lattice Boltzmann advection diffusion solver. *Geochimica Et Cosmochimica Acta,* Volum 104, pp. 99-110.

Hirata, K., Saitoh, Y., Chiba, A. & Yamada, T., 2011. Secondary ion counting for surface-sensitive chemical analysis of organic compounds using time-of-flight secondary ion mass spectroscopy with cluster ion impact ionization. *Review of Scientific Instruments,* Vol 82(3), pp. 1 - 5.

Hjelen, J., 1989. *Scanning elektron-mikroskopi.* Trondheim, Norway: Metallurgisk institutt, NTH.

Hjuler, M. L. & Fabricius, I. L., 2009. Engineering properties of chalk related to diagenetic variations of Upper Cretaceous onshore and offshore chalk in the North Sea area. *Journal of Petroleum Science and Engeneering,* Volum 68, pp. 151 - 170.

Johnson, J. P., Rhett, D. W. & Siemers, W. T., 1989. Rock Mechanics of the Ekofisk Reservoir in the Evaluation of Subsidence. *Journal of Petroleum Technology. Offshore Technology Conference,* Volum July, pp. 717 - 722.

Kennedy, W. J., 1985. Sedimentology o the Late Cretaceousand Early Palaeocene Chalk Group, North Central Graben. *North Sea Chalk Symposium May 1985,* Volum 1, pp. 12 - 152.

Korsnes, R. I., 2007. *Chemical induced water weakening of chalk by fluid-rock interaction, PhD thesis.* Stavanger: University of stavanger.

Korsnes, R. I. et al., 2008. The effects of temperature on the water weakening of chalk by seawater. *Journal of Petroleum Science and Engineering,* Volum 60, pp. 183 - 193.

Levenson, Y. & Emmanuel, S., 2013. Pore-scale heterogeneous reaction rates on a dissolving. *Geochimica et Cosmochimica Acta,* Volum 119, pp. 188 - 197.

Madland, M. V., 2005. *Water weakening of chalk : A mechanistic study. PhD thesis.* Stavanger: Universty of Stavanger.

Madland, M. V. et al., 2011. Chemical Alterations Induced by Rock-Fluid Interactions When Injecting Brines in High Porosity Chalks. *Transport Porous Media,* Volum 87, pp. 679 - 702.

Madland, M. V. et al., 2008. *The Effect of Temperature and Brine Composition on the Machanical Strength of Kansas Chalk.* Abu Dhabi, International Symposium of the Society of Core Analysts.

Madsen, H. B., Stemmerik, L. & Surlyk, F., 2010. Diagenesis of Silica-rich mound-bedded chalk, the Coniacian Arnager Limestone, Denmark. *Sedimentary Geology,* Volum 223, pp. 51 - 60.

Megawati, M., 2015. *Geochemical Aspects of Water-Induced Compaction in High-Porosity Chalks, PhD Thesis.* Stavanger: University of Stavanger.

Megawati, M., Hiorth, A. & Madland, M. V., 2013. The Impact of Surface Charge on the Mechanical Behavior of High-Porosity Chalk. *Rock Mechanics and Rock Engineering,* 46(5), pp. 1-18.

Molenaar, N. & Zijlstra, J., 1997. Differential early diagenetic low-Mg calcite cementation and rhythmic hardground development in Campanian-Maastrichtian chalk. *Sedimentary Geology,* Volum 109, pp. 261 - 281.

Monzurul Alam, M., Fabricius, I. L. & Christensen, H. F., 2012. Static and dynamic effective stress coefficient in chalk. *GEOPHYSICS,* 77(NO 2 (March - April 2012)), pp. L1-L11.

Nermoen, A., Korsnes, R. I., Hiorth, A. & Madland, M. V., 2015. Porosity and permeability development in compacting chalks during flooding of non-equlibrium brines - insights from a long term experiment. *Journal of Geophysical Research: Solid Earth,* Volum 120.

Omdal, E., 2010. *The mechanical behavior of chalk under laboratory conditions simulating reservoir operations, PhD thesis.* Stavanger: University of Stavanger.

Puntervold, T. & Austad, T., 2008. Injection of seawater and mixtures with produced water into North Sea chalk formation: Impact of fluid-rock interaction on wettability and scale formation. *Journal of Petroleum Science and Engineering,* Volum 63, pp. 23 - 33.

Risnes, R., 2001. Deformation and Yield in High Porosity Outcrop Chalk. *Physics And Chemistry Of The Earth Part A-Solid Earth And Geodesy,* 26(1 - 2), pp. 53 - 57.

Risnes, R., Haghighi, H., Korsnes, R. I. & Natvik, O., 2003. Chalk - Fluid interactions with glycol and brines. *Tectonophysics,* Volum 370, pp. 213 - 226.

Sarda, J. P., 1985. Porosity and permeability of chalk samples at reservoir temperature under isotropic loading. *North Sea Chalk symposium May 1985,* Volum 1, pp. 534 - 552.

Schneiderhan, E. A., Bhattacharya, H. N., Zimmermann, U. & Gutzmer, J., 2005. Archean seismites of the Ventersdorp Supergroup, South Africa. *South African Journal of Geology,* Volum 108, pp. 345 - 350.

Snow, S. E. & Brownlee, M. H., 1989. *Practical and Theoretical aspects of Well Testing in the Ekofisk Area Chalk Fields.* San Antonio, SPE Annual Technical Conference and Exibition.

Strand, S., Høgensen, E. J. & Austad, T., 2006. Wettability alterations of carbonates - Effects of potential determening ions (Ca2+ and SO42-) and temperature. *Colloids and Surfaces A: Physicochemical and Engineering Aspects,* 275(1-3), pp. 1-10.

Sulak, R. M. & Danielsen, J., 1989. Reservoir aspects of Ekofisk subsidence. *Journal Of Petroleum Technology,* 41(7), pp. 709-716.

Terzaghi, K., 1923. Die Beziehungen zwischen Elastizitat und Innendrück: Sitzungsberichte. *Akademie der Wissenschaften,* K I. IIa(132), pp. 105 - 121.

Wang, W., In press. *Revealing dynamic porosity: Evaluation of porosity during chemo-mechanical compaction in chalk from Liège (Belgium).* London, Geological society of London.

Yu, L. et al., 2009. Spontaneous imbibition of seawater into preferentially oil-wet chalk cores — Experiments and simulations. *Journal of Petroleum Science and Engineering,* 66(3 - 4, June), pp. 171 - 179.

Zhang, P., Tweheyo, M. T. & Austad, T., 2007. Wettability alteration and improved oil recovery by spontaneous imbibition of seawater into chalk: Impact of the potential determining ions Ca2+, Mg2+, and SO42−. *Colloids and Surfaces A: Physicochemical and Engineering Aspects,* Volum 301, pp. 199-208.

Zimmermann, U. et al., 2015. Evaluation of the compositional changes during flooding of reactive fluids using scanning electron microscopy, nano-secondary ion mass spectrometry, x-ray diffraction, and whole-rock geochemistry. *AAPG BULLETIN,* 99(5), pp. 791 - 805.

Appendix

Appendix A

Synthetic Seawater (SSW)

The composition of the synthetic seawater, which the core was flooded with, is given in table Table 1.

Table 1. The composition of the synthetic seawater used for flooding of the fractured chalk core

Synthetic Seawater		
Salt	g/l	mol/l
NaCl	23.38	0.400
Na_2SO_4	3.14	0.024
$NaHCO_3$	0.17	0.002
KCl	0.75	0.010
$MgCl_2$ x $6H_2O$	9.05	0.045
$CaCl_2$ x $2H_2O$	1.91	0.013

Ions		g/l	mol/l
HCO_3^-	1	0.12	0.002
Cl-	1	18.62	0.525
SO_4^{2-}	**2**	**2.31**	**0.0240**
SCN^-	**1**	**0.00**	**0.000**
Mg^{2+}	2	1.08	0.0445
Ca^{2+}	**2**	**0.52**	**0.013**
Na^+	1	10.35	0.450
K^+	1	0.39	0.010
TDS		**33.39**	
Ionic Strength			**0.6567**

Appendix B

Additional optical light microscopy images:

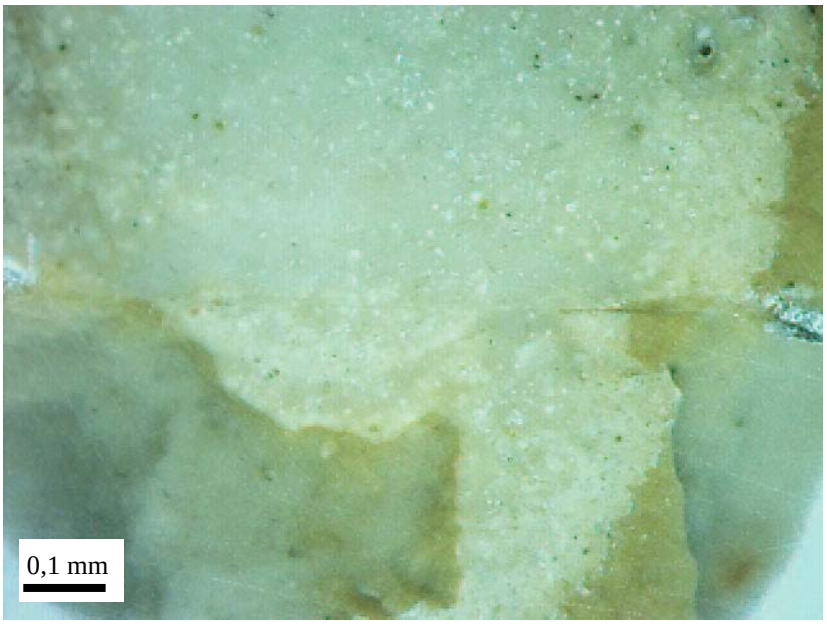

Figure A. OLM image of the artificial fracture in slice 4

Figure B. Close-up of OLM image of the artificial fracture in slice 4

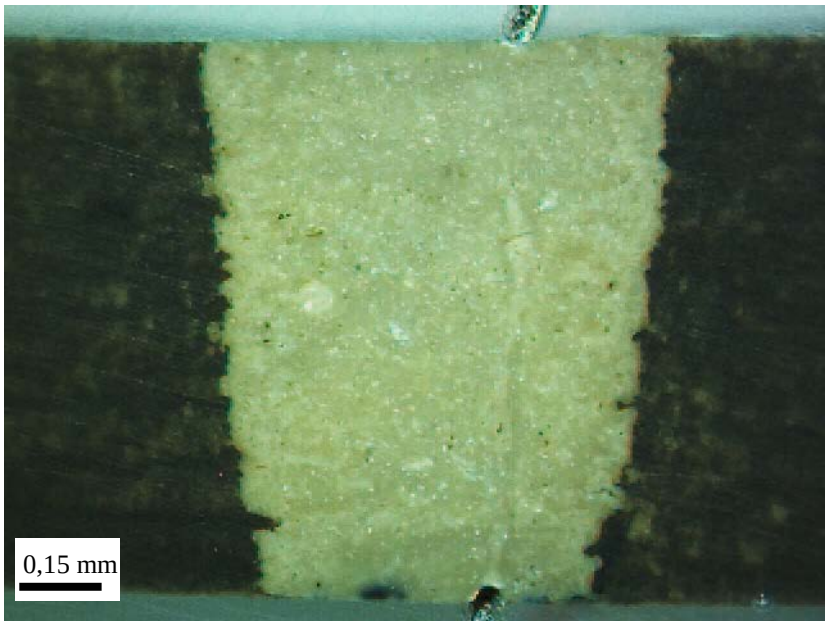

Figure C. OLM image of the natural fracture in slice 5

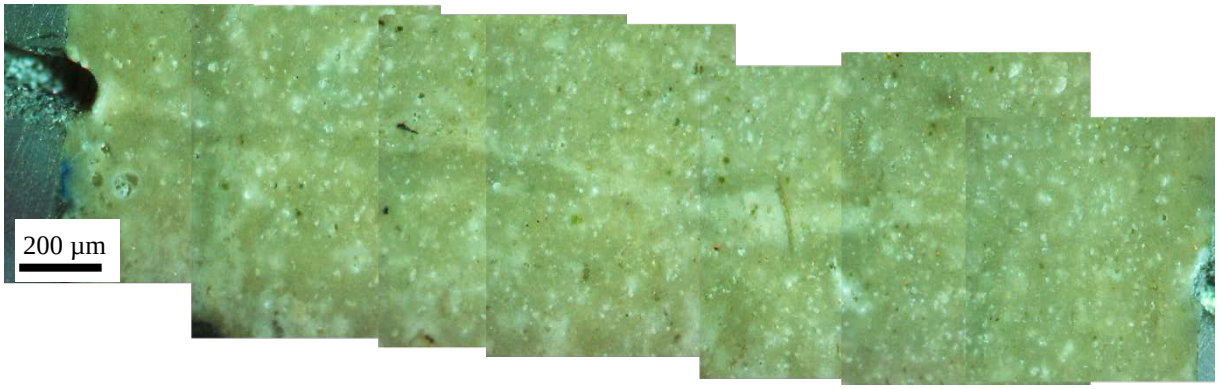

Figure D. Close-up of the OLM image of the natural fracture in slice 5

Appendix C

Additional BSE images.

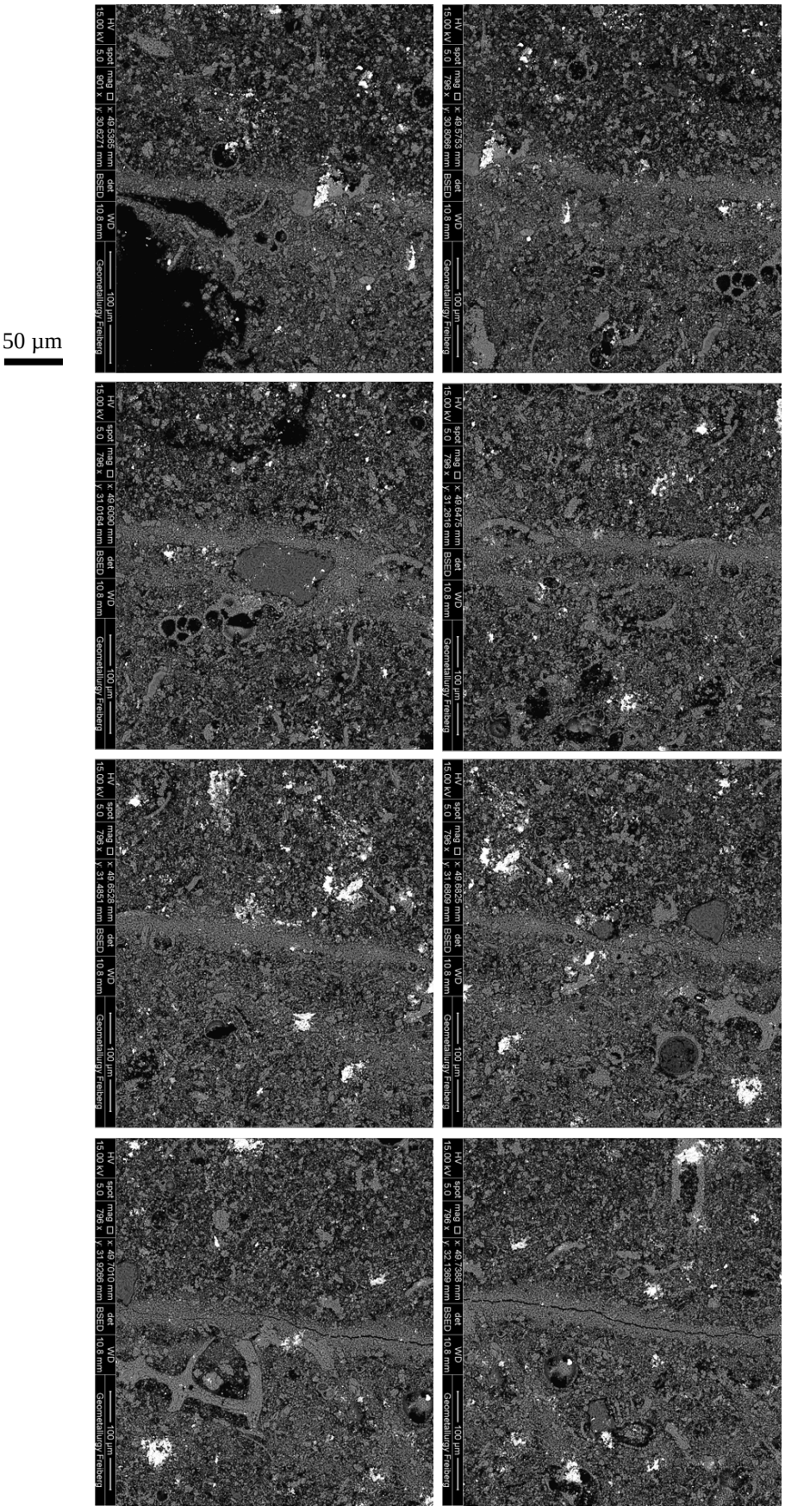

Figure E. BSE images along the artificial fracture. Left part. Same scale for all images

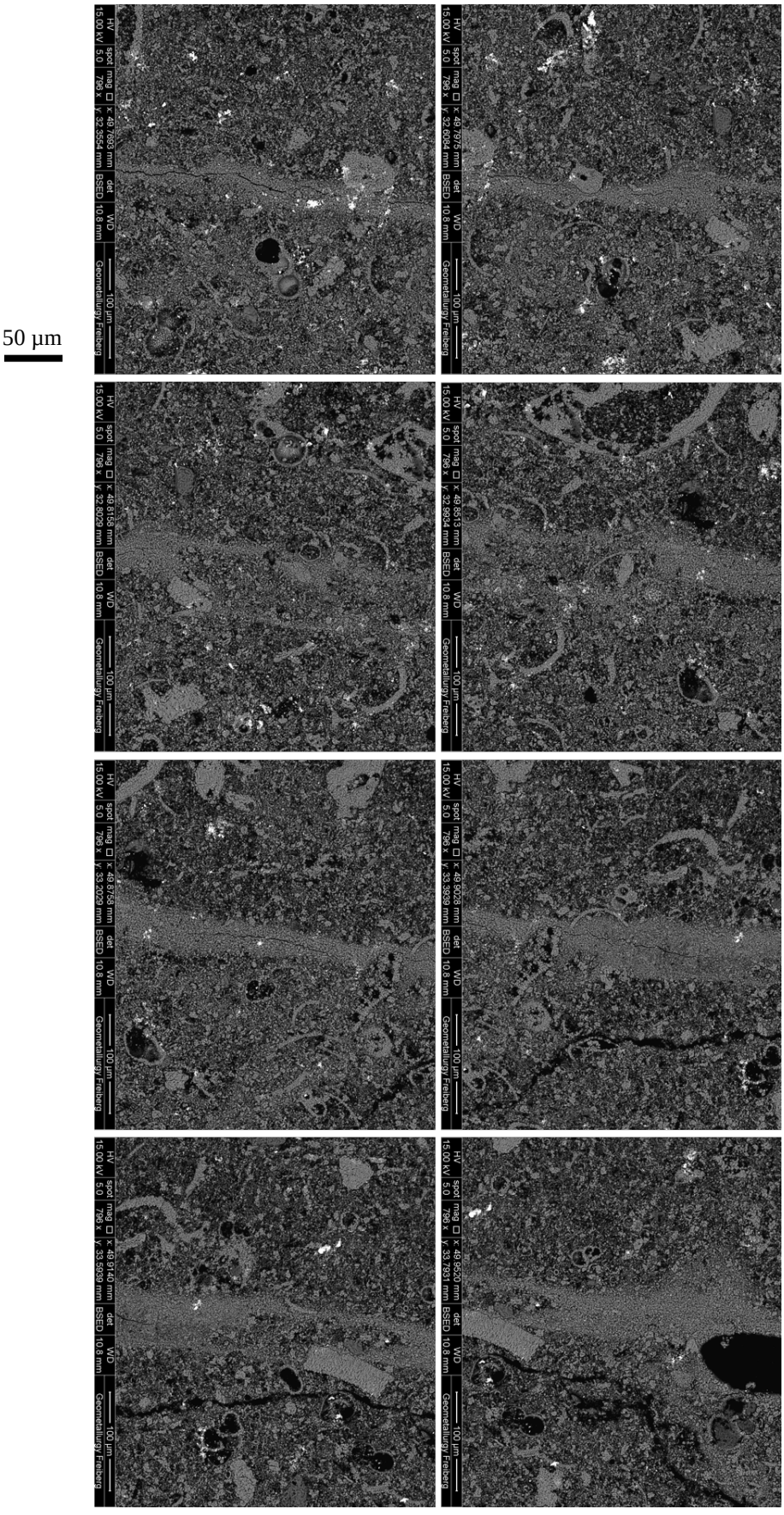

Figure F. BSE images along the artificial fracture. Right part. Same scale for all images

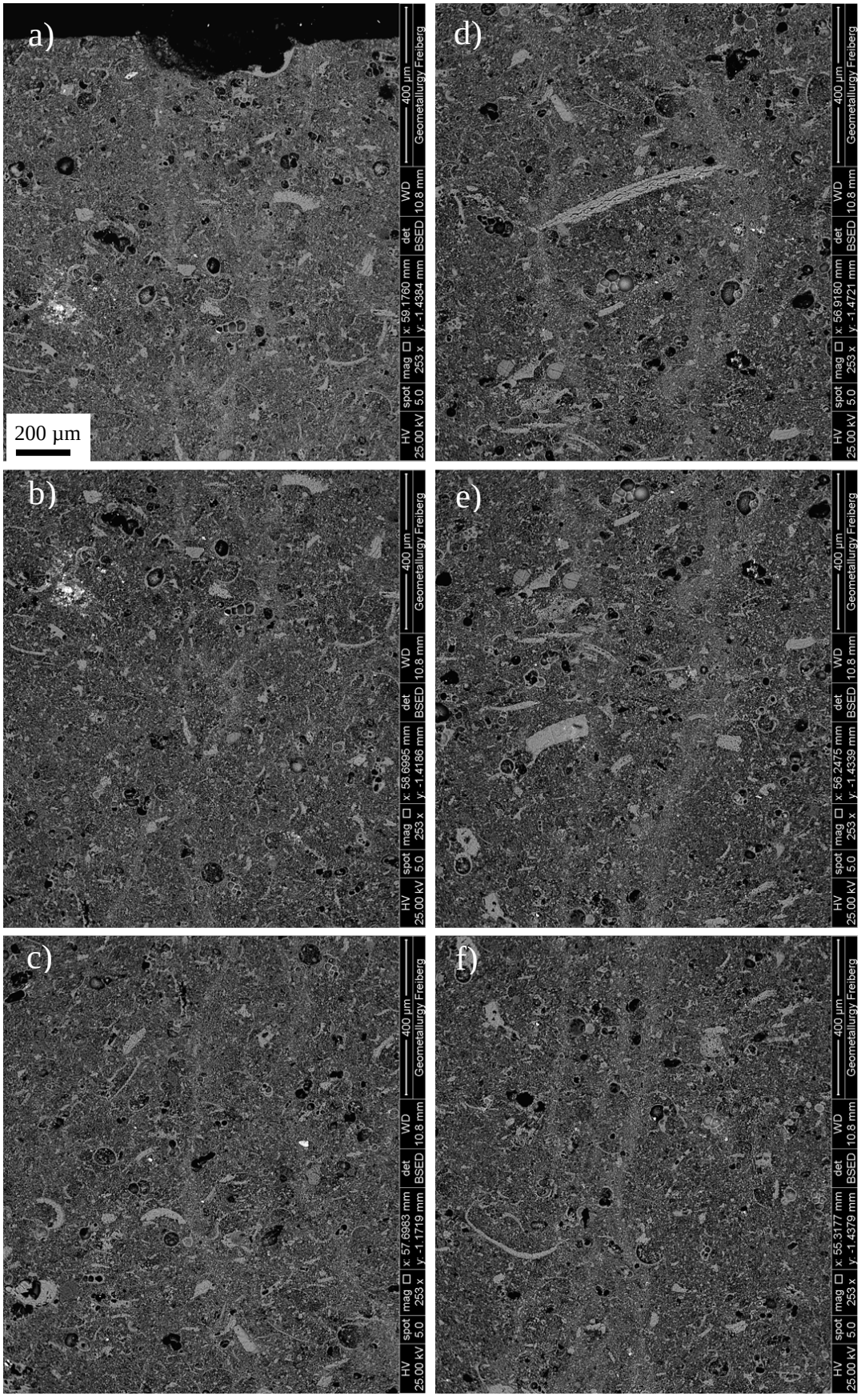

Figure G. BSE images of the natural fracture in slice 5. Order a – f. Same scale for all images as in a)

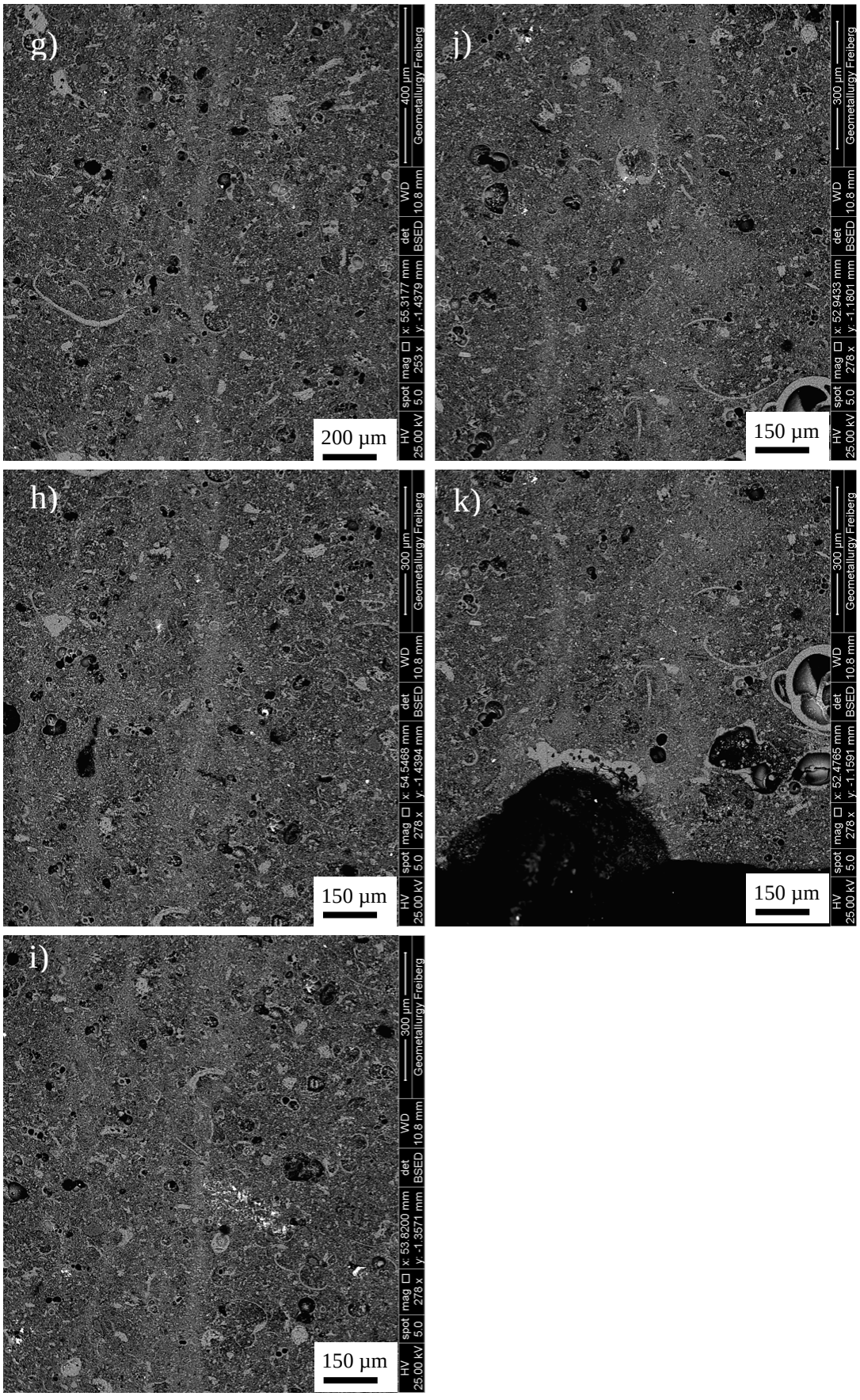

Figure H. Further BSE images of the natural fracture in slice 5. Order g – k

Appendix D

Additional MLA images

Slice 4:

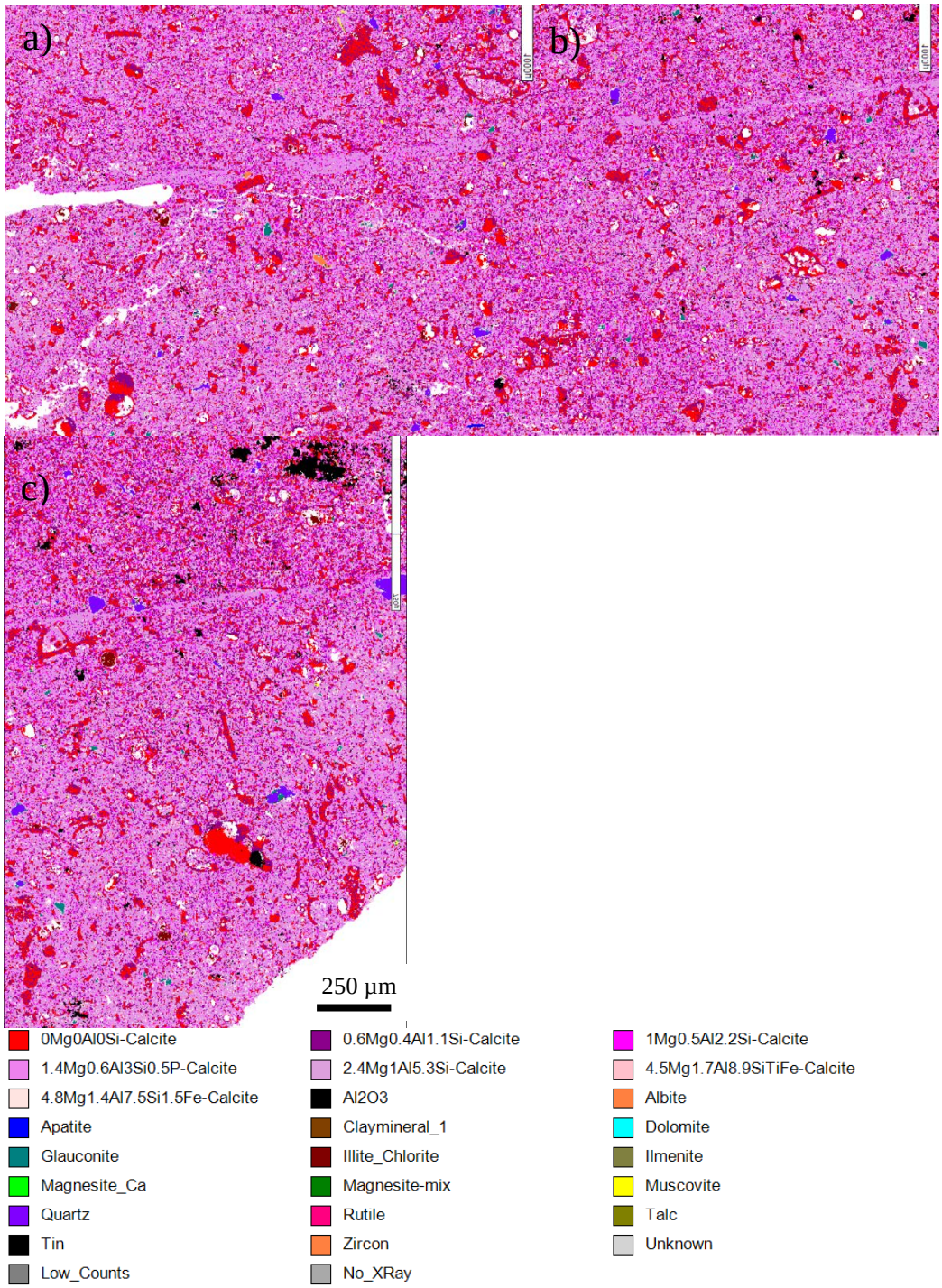

Figure I. MLA images of the artificial fracture in slice 4. Order from left to right a – c

Slice 5:

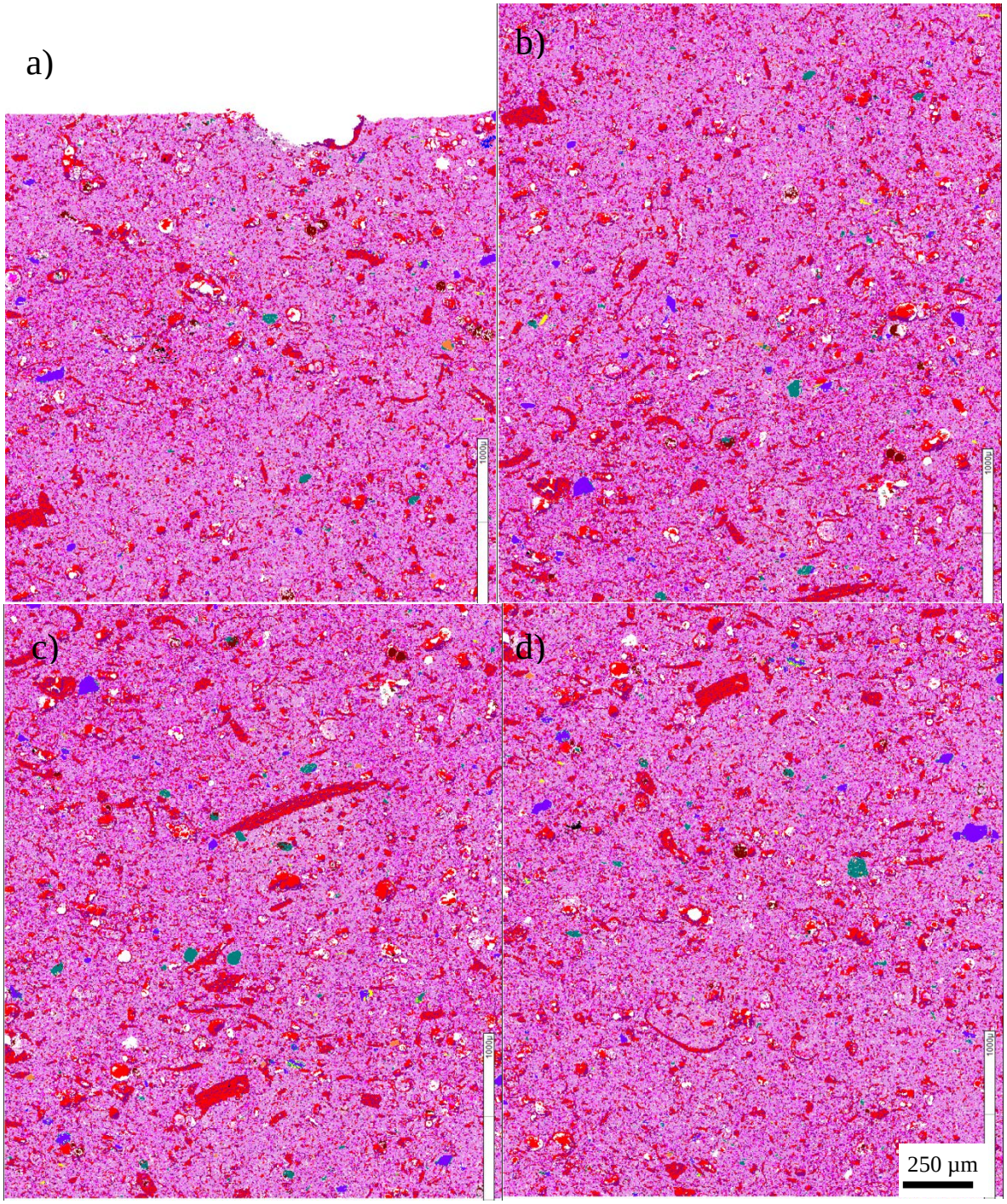

Figure J. MLA images of the natural fracture in slice 5. Order from top to bottom a – d. Same scale on all images. For legend see figure above or below

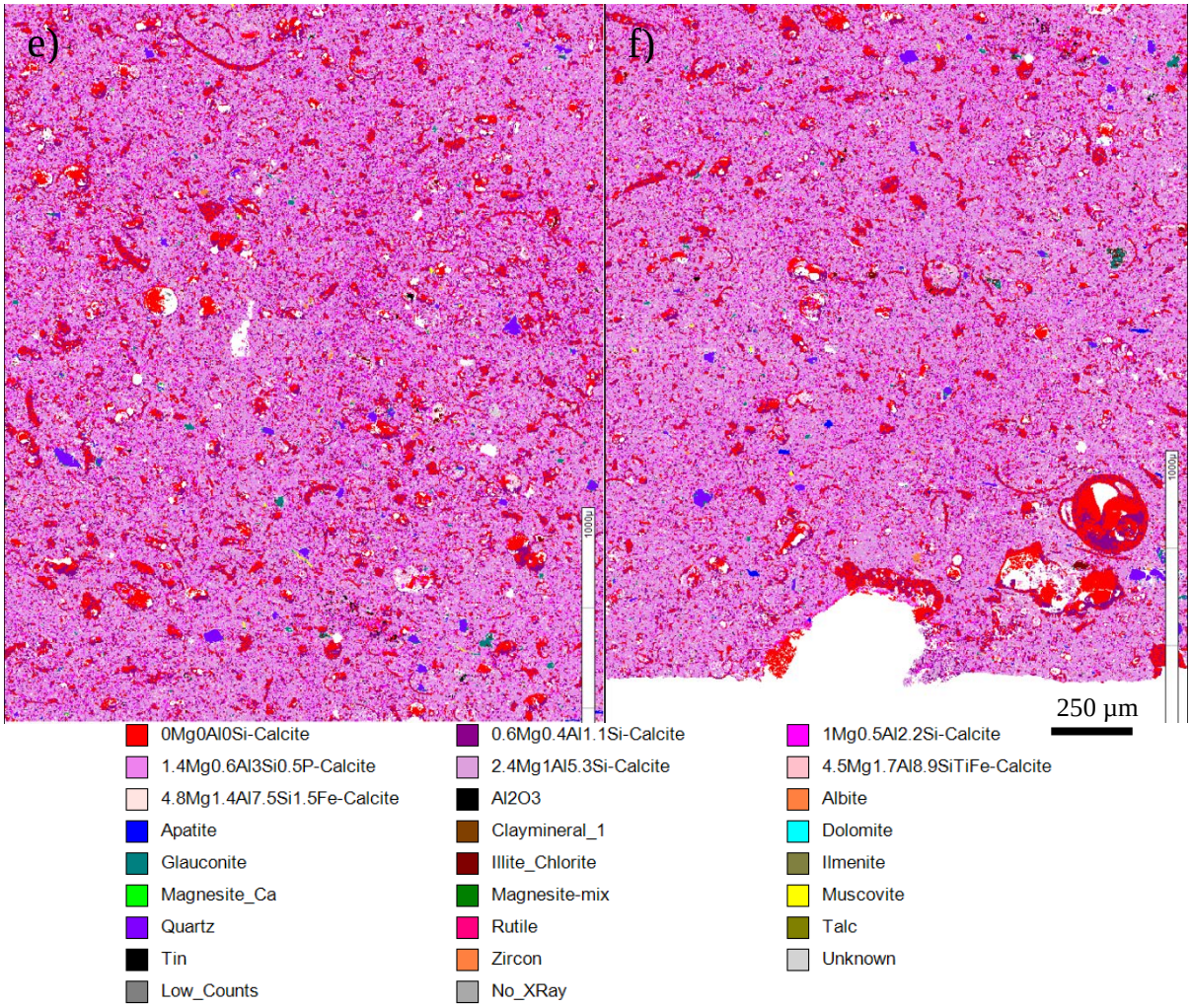

Figure K. MLA images of the natural fracture in slice 5. Order from top to bottom e – f. Same scale on both images

The seven mixed spectra used for MLA classification:

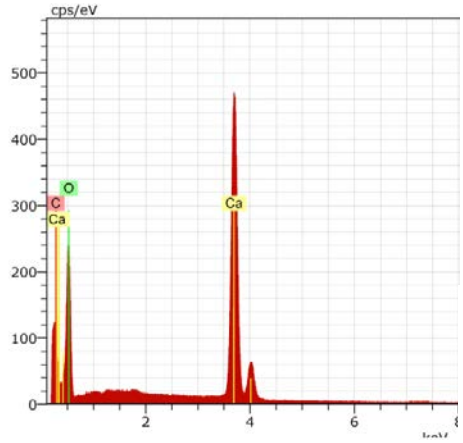

El	OZ	Linie	unn. C [Masse-%]	norm. C [Masse-%]	Atom. C [At.-%]
C	6	K-Serie	8.06	8.98	15.59
Ca	20	K-Serie	39.11	43.60	22.67
O	8	K-Serie	42.53	47.42	61.75
		Summe::	89.7 %		

Figure L. 0Mg0Al0Si-Calcite

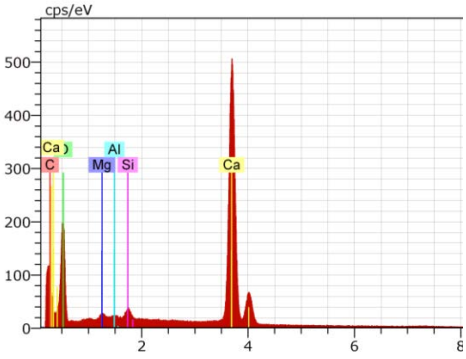

El	OZ	Linie	unn. C [Masse-%]	norm. C [Masse-%]	Atom. C [At.-%]
C	6	K-Serie	7.94	9.13	16.10
Mg	12	K-Serie	0.48	0.55	0.48
Al	13	K-Serie	0.30	0.35	0.27
Si	14	K-Serie	0.94	1.08	0.81
Ca	20	K-Serie	38.61	44.43	23.48
O	8	K-Serie	38.64	44.47	58.86
		Summe::	86.9 %		

Figure M. 0.6Mg0.4Al1.1Si-Calcite

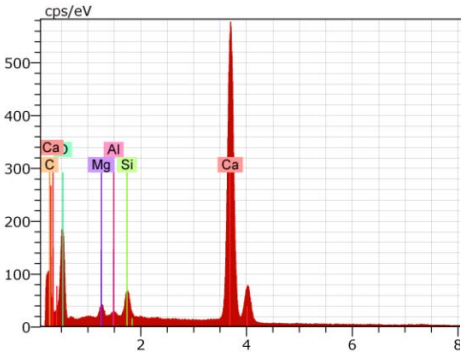

El	OZ	Linie	unn. C [Masse-%]	norm. C [Masse-%]	Atom. C [At.-%]
C	6	K-Serie	7.34	7.94	14.08
Mg	12	K-Serie	0.97	1.05	0.92
Al	13	K-Serie	0.43	0.46	0.36
Si	14	K-Serie	1.99	2.15	1.63
Ca	20	K-Serie	40.13	43.41	23.08
O	8	K-Serie	41.59	44.99	59.92
		Summe::	92.4 %		

Figure N. 1Mg0.5Al2.2Si-Calcite

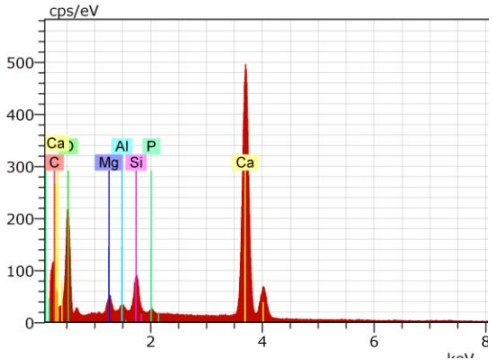

El	OZ	Linie	unn. C [Masse-%]	norm. C [Masse-%]	Atom. C [At.-%]
C	6	K-Serie	7.40	8.81	15.35
Mg	12	K-Serie	1.17	1.39	1.20
Al	13	K-Serie	0.52	0.62	0.48
Si	14	K-Serie	2.55	3.03	2.26
P	15	K-Serie	0.38	0.45	0.31
Ca	20	K-Serie	33.87	40.30	21.04
O	8	K-Serie	38.15	45.39	59.37
		Summe::	84.0 %		

Figure O. 1.4Mg0.6Al3Si0.5P-Calcite

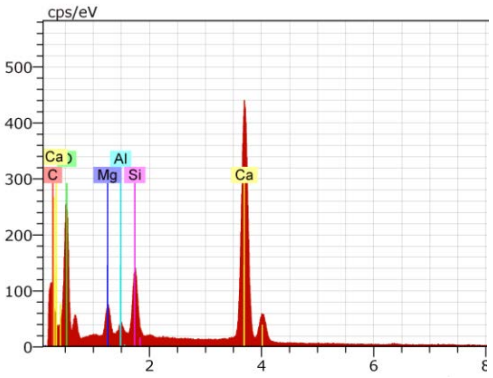

El	OZ	Linie	unn. C [Masse-%]	norm. C [Masse-%]	Atom. C [At.-%]
C	6	K-Serie	7.00	8.32	14.21
Mg	12	K-Serie	2.05	2.44	2.06
Al	13	K-Serie	0.84	1.00	0.76
Si	14	K-Serie	4.42	5.26	3.84
Ca	20	K-Serie	29.70	35.33	18.07
O	8	K-Serie	40.07	47.66	61.07
		Summe::	84.1 %		

Figure P. 2.4Mg1Al5.3Si-Calcite

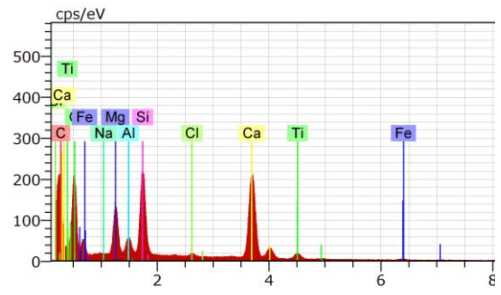

El	OZ	Linie	unn. C [Masse-%]	norm. C [Masse-%]	Atom. C [At.-%]
C	6	K-Serie	15.90	19.49	31.08
Na	11	K-Serie	0.21	0.26	0.22
Mg	12	K-Serie	3.67	4.50	3.55
Al	13	K-Serie	1.36	1.67	1.19
Si	14	K-Serie	7.28	8.93	6.09
Cl	17	K-Serie	0.29	0.35	0.19
Ca	20	K-Serie	18.67	22.89	10.94
Ti	22	K-Serie	1.96	2.40	0.96
Fe	26	K-Serie	1.40	1.72	0.59
O	8	K-Serie	30.80	37.77	45.20
		Summe::	81.6 %		

Figure Q. 4.5Mg1.7Al8.9SiTiFe-Calcite

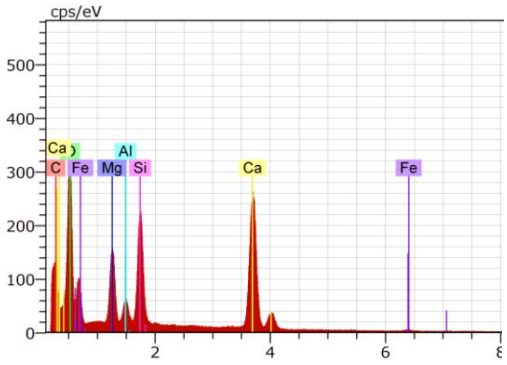

El	OZ	Linie	unn. C [Masse-%]	norm. C [Masse-%]	Atom. C [At.-%]
C	6	K-Serie	9.08	10.93	17.46
Mg	12	K-Serie	4.01	4.83	3.82
Al	13	K-Serie	1.20	1.44	1.02
Si	14	K-Serie	6.26	7.54	5.15
Ca	20	K-Serie	18.97	22.84	10.93
Fe	26	K-Serie	1.21	1.46	0.50
O	8	K-Serie	42.32	50.96	61.12
		Summe::		83.0 %	

Figure R. 4.8Mg1.4Al7.5Si1.5Fe-Calcite